



**National Library
of Canada**

**Bibliothèque nationale
du Canada**

Canadian Theses Service

Service des thèses canadiennes

**Ottawa, Canada
K1A 0N4**

NOTICE

The quality of this microform is heavily dependent upon the quality of the original thesis submitted for microfilming. Every effort has been made to ensure the highest quality of reproduction possible.

If pages are missing, contact the university which granted the degree.

Some pages may have indistinct print especially if the original pages were typed with a poor typewriter ribbon or if the university sent us an inferior photocopy.

Reproduction in full or in part of this microform is governed by the Canadian Copyright Act, R.S.C. 1970, c. C-30, and subsequent amendments.

AVIS

La qualité de cette microforme dépend grandement de la qualité de la thèse soumise au microfilmage. Nous avons tout fait pour assurer une qualité supérieure de reproduction.

S'il manque des pages, veuillez communiquer avec l'université qui a conféré le grade.

La qualité d'impression de certaines pages peut laisser à désirer, surtout si les pages originales ont été dactylographiées à l'aide d'un ruban usé ou si l'université nous a fait parvenir une photocopie de qualité inférieure.

La reproduction, même partielle, de cette microforme est soumise à la Loi canadienne sur le droit d'auteur, SRC 1970, c. C-30, et ses amendements subséquents.

THE UNIVERSITY OF ALBERTA

A FRACTAL ANALYSIS OF HETEROGENEITY
IN MISCIBLE DISPLACEMENT

by



Daniel Joseph Giesbrecht

A THESIS

SUBMITTED TO THE FACULTY OF GRADUATE STUDIES AND RESEARCH
IN PARTIAL FULFILMENT OF THE REQUIREMENTS FOR THE DEGREE
OF MASTER OF SCIENCE
IN
PETROLEUM ENGINEERING

DEPARTMENT OF MINING, METALLURGICAL AND PETROLEUM
ENGINEERING

EDMONTON, ALBERTA

Fall, 1990



**National Library
of Canada**

**Bibliothèque nationale
du Canada**

Canadian Theses Service Service des thèses canadiennes

**Ottawa, Canada
K1A 0N4**

The author has granted an irrevocable non-exclusive licence allowing the National Library of Canada to reproduce, loan, distribute or sell copies of his/her thesis by any means and in any form or format, making this thesis available to interested persons.

The author retains ownership of the copyright in his/her thesis. Neither the thesis nor substantial extracts from it may be printed or otherwise reproduced without his/her permission.

L'auteur a accordé une licence irrévocable et non exclusive permettant à la Bibliothèque nationale du Canada de reproduire, prêter, distribuer ou vendre des copies de sa thèse de quelque manière et sous quelque forme que ce soit pour mettre des exemplaires de cette thèse à la disposition des personnes intéressées.

L'auteur conserve la propriété du droit d'auteur qui protège sa thèse. Ni la thèse ni des extraits substantiels de celle-ci ne doivent être imprimés ou autrement reproduits sans son autorisation.

ISBN 0-315-65081-8



Society of Petroleum Engineers

MAIL ADDRESS: P.O. BOX 833836, RICHARDSON, TX 75083-3836 USA • FACSIMILE: 214/669-0135 TELEX: 730989 SPEDAL
STREET ADDRESS: 222 PALISADES CREEK DRIVE, RICHARDSON, TEXAS 75080 USA • TELEPHONE: 214/669-3377

April 10, 1990

Dan Giesbrecht
#1101-9909 - 104th Street
Edmonton, Alberta
CANADA T5K 2G5

RE: Your copyright request of 13 March 1990

Dear Mr. Giesbrecht:

Thank you for your recent request to use material copyrighted to the Society of Petroleum Engineers. This is to grant one-time permission to use the material identified in your letter for the purpose specified, provided that you include full and proper notice of SPE copyright ownership and acknowledgment of the source.

Your payment of the enclosed invoice within 30 days will activate this permission.

Proper copyright ownership acknowledgment and source attribution for the item(s) that SPE can give you permission to use appear on the enclosed form. Permission to use this is subject to your proper identification of SPE as the copyright holder and source (please see the SPE Copyright Notice information on the enclosed form).

The Society's copyright position encourages the broadest possible distribution of technical material to which it holds copyright, as is consistent with our copyright agreements with authors. Thank you for your cooperation in this matter, which is essential to protect the rights of the many authors who make technical material generally available through the Society.

Sincerely,


Carol Paschetag
Librarian

Enclosure

Research Fee: \$20.00
Copyright Authorization Fee: \$1.00
Total Fee: \$21.00

Research Fee is \$5.00 per item: Copying Authorization Fee is 1.00 to maximum of \$100.00.



PRICE QUOTATION
Prepayment Required

222 PALISADES CREEK DR. RICHARDSON, TEXAS 75080 FACSIMILE (214) 669-0135
P.O. BOX 833836 RICHARDSON, TEXAS 75083-3836 (214) 669-3377 TELEX 730989 SPEDAL

Society of Petroleum Engineers

S • 024255
O Dan Joseph Giesbrecht
L 1101-9909 - 104th Street
D Edmonton Alberta
I CANADA T5K 2G5
T
G

S
H
I
P
T
O

SAME AS SOLD TO UNLESS OTHERWISE SPECIFIED

INVOICE DATE	INVOICE NUMBER	SPE REFERENCE NUMBER	CUSTOMER REFERENCE NUMBER	SHIPPING INSTRUCTIONS
04/06/90	73282	70015987	COPYRIGHT	

QUANTITY	PRODUCT CODE	DESCRIPTION	UNIT PRICE	AMOUNT
4	031662	COPYRIGHT PERMISSION-RESEARCH FEE	5.00	20.00
1	031663	COPYRIGHT-COPYING AUTHORIZATION FEE	1.00	1.00

REMARKS: THANKS FOR YOUR INTEREST IN SPE MATERIAL			TOTAL MERCHANDISE	21.00
			BOOK DEALER DISCOUNT	(.00)
			POSTAGE & HANDLING	.00
			SALES TAX (TEXAS ONLY)	.00
			TOTAL AMOUNT	21.00
			AMOUNT PREPAID	.00
SHIP DATE 00/00/00	TOTAL CARTONS 0	INITIAL	TOTAL BALANCE DUE	
* OUT OF PRINT ** NOT SOLD BY SPE *** ORDERED FROM PRINTER - SHIPPED SEPARATELY			SPE PAPERS NOT SUBJECT TO DISCOUNT RAD: NOT AVAILABLE FOR BOOK DEALER DISCOUNT. MEMBER FLAG M	21.00
PAYMENT OPTIONS ON REVERSE SIDE				

PAYMENT RECEIPT

DAN GIESBRECHT
#1101-9909-104th STREET
EDMONTON, ALBERTA, CANADA.
T5K 2G5.

March 27, 1990.

Publications Manager
Society of Petroleum Engineers
P.O. Box 833836
Richardson, Texas
75083-3836

Dear Sir (or) Madame:

I am writing to inquire into the possibility of obtaining copywrite authorization to include several figures which appeared in SPE journals into a graduate thesis which I am currently writing. The figures would be properly referenced and notice of ownership of copywrite would be prominently displayed. In particular, I would like to reproduce the following figures:

Figure 40K- M.R.J. Wyllie, "Reservoir Mechanics-Stylized Myth or Potential Science?"
JP (June, 1962)

Figure 20K- W.E. Brigham, P.W. Reed and J.N. Dew, "Experiments on Mixing During Miscible Displacements in Porous Media"
SPEJ (March, 1961)

*Figure 5 - T.K. Perkins and O.C. Johnston, "A review of Diffusion and Dispersion in Porous Media"
**Figure 6
Figure 100K- SPEJ (March, 1963)

***Figure 2 No- R.E. Bretz, R.M. Specter and F.M. Orr Jr., "Effect of Pore Structure on Miscible Displacement in Laboratory Cores"
SPERE (August, 1988)

I would appreciate a written reply to this request at your earliest convenience and I thank you in advance for your co-operation.

*Fig.5 - You can either use Ref. 9 as original source or reference this paper and include Ref. 9 in your references. See attached.

**Fig.6 - Reference this paper and also cite where authors obtained data to construct figure - Data from Ref 11, 42, 53 and 59. See attached.

***Fig.2 - SPE does not have copyright on this paper. Contact the author for permission. See attached form for address.

Yours truly,

Dan Giesbrecht

M# 106617

Effect of Pore Structure on Miscible Displacement in Laboratory Cores

R.E. Bretz, SPE, New Mexico Inst. of Mining and Technology
 R.M. Spector,* Arizona State U.
 F.M. Orr Jr., SPE, Stanford U.

Summary. Observations of pore structure in thin-sections are related to the performance of stable, first-contact-miscible displacements in reservoir cores and then to simulations of displacement performance of CO₂ corefloods. Results of effluent composition measurements are reported for miscible displacements in seven core samples—three sandstones and four San Andres carbonates from west Texas or eastern New Mexico. Those displacements are interpreted by fitting the measured effluent compositions to the Coats-Smith (C-S) model, which represents the flow as occurring in flowing and stagnant fractions with mass transfer between them. Observations of thin-sections, including measurements of pore-size distributions and a simple measurement of spatial correlation of pore sizes, are also reported. Comparison of displacement results and thin-section data indicates that wide pore-size distributions and preferential flow paths are characterized in the C-S model by high dispersion coefficients and low flowing fractions. Simulations of the interactions of phase behavior and flow in nonuniform pore structures indicate that wide pore-size distributions and preferential flow paths can significantly increase residual oil saturations (ROS's) in CO₂ floods over those for uniform pore structures. Thus, heterogeneities observable at the scale of a thin-section have significant effects in laboratory core but much smaller effects in displacements at field scale. Large-scale heterogeneities present in field floods, however, probably cause similar increases in residual saturation in some fields.

Introduction

Mixing between injected fluid and that present in a reservoir plays an important role in many EOR processes. In CO₂ floods and other multiple-contact-miscible gas injection processes, for example, it is the transfer of components between phases that leads to high local displacement efficiency.¹⁻³ If the zone in which mixing takes place is confined to a narrow region, as is the case in slim-tube displacements, then the displacement is efficient³⁻⁵ as long as the pressure is high enough that CO₂ extracts hydrocarbons relatively efficiently from the oil.^{6,7} Comparison of numerical simulations of CO₂ floods^{3,5} with Helfferich's analytic solution⁸ of the interactions of phase behavior and flow in the absence of dispersive mixing⁴ indicates that when the transition zone is broad, as when the level of dispersion is high, displacement efficiency is reduced. Gardner and Ypma⁸ argued, on the basis of numerical simulations of the growth of a viscous finger, that mixing between CO₂ in a finger with oil in adjacent unswept regions also reduces local displacement efficiency. Dai and Orr⁹ used simulations of the effects of phase behavior on flow in a porous medium consisting of flowing and stagnant fractions to show that the broadening of the transition zone caused by the presence of the stagnant fraction has a similar effect. They used their model to interpret the CO₂ coreflood experiments performed by Spence and Watkins,¹⁰ who found that cores with a wide pore-size distribution showed higher ROS's after the CO₂ displacements. Thus, there is both experimental and theoretical evidence that mixing effects have a significant impact on CO₂ flood performance at the laboratory scale.

In this paper, we examine the influence of pore structure on the mixing that occurs during miscible displacements in laboratory cores. We present the results of San Andres carbonates. Of those samples, one sandstone and one carbonate are outcrop samples; the remainder are reservoir core samples. The displacements were performed with fluids at matched density and viscosity to eliminate the effects of gravity segregation and viscous instability and hence to isolate the effects of the pore space. We report the displacement results in terms of the parameters of the C-S model,¹¹ which represents the pore space as flowing and stagnant fractions with mass transfer between them.

To characterize the geometry of the pore space, we present pore-size distributions obtained from thin-sections from the same rock samples for which the displacements were performed. We argue

that long transition zones, characterized in the C-S model by flowing fractions less than one, require not only a wide pore-size distribution but also that the pores be connected in such a manner that preferential flow paths are formed. We present a simple method for qualitative detection of the existence of preferential flow paths. The method is based on measurements of the mean size of pores neighboring randomly selected reference pores. Thus, we use the comparison of thin-section observations and coreflood results to argue that features of the pore structure observable at thin-section scale offer clues to the causes of miscible displacement behavior at coreflood scale.

To illustrate the influence of mixing on displacement performance of CO₂ corefloods, we report results of one-dimensional simulations made with the model developed by Dai and Orr.⁹ Results of those calculations confirm that pore structures that lead to preferential paths also produce lower displacement efficiency in laboratory corefloods. Finally, we comment on the problems associated with scaling laboratory coreflood results to field scale.

Displacement Apparatus and Procedure. Fig. 1 is a schematic of the apparatus used for displacement experiments. The fluids used and the apparatus varied slightly over the course of the experiments. In a typical experiment, the positive displacement pump pushes brine [1% NaNO₃, 1% KNO₃, 1% Ca(NO₃)₂, 0.1% NaN₃, CaSO₄ to saturation] through a sample valve, the core, and a differential refractometer and into a collection vessel placed on an electronic balance. Injection of a slug of miscible fluid is achieved by redirecting the flow by means of the sample valve through a sample loop of known volume filled previously with the same brine containing 0.4% sucrose as a tracer. The tracer concentration exiting the core is monitored continuously by the refractometer. Concentration and fluid weight data are acquired automatically with a microcomputer. The smallest available tubing, fittings, end caps, and refractometer cell were used to minimize dead volume in the system. Additional details of the apparatus and procedure may be found in Orr and Taber.¹³

Least-Error Fits to the C-S Model. Effluent composition data were fit to the C-S model, which has the form

$$f \frac{\partial C}{\partial t_D} + \frac{\partial C}{\partial X_D} - \frac{1}{N_{Pe}} \frac{\partial^2 C}{\partial X_D^2} + (1-f) \frac{\partial C^*}{\partial t_D} = 0;$$

*Now with Arizona Board of Regents.

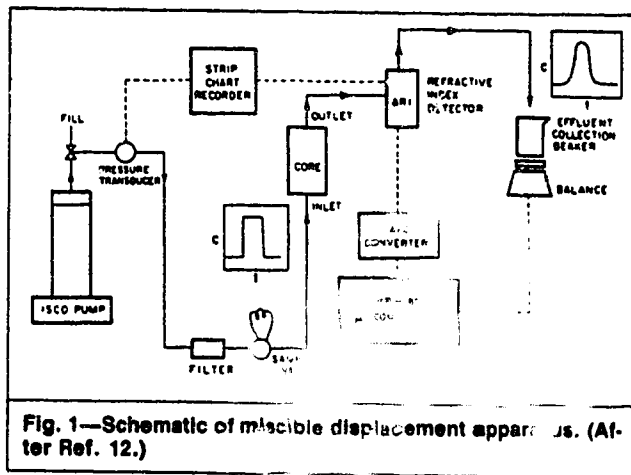


Fig. 1—Schematic of miscible displacement apparatus. (After Ref. 12.)

$$(1-f) \frac{\partial C^*}{\partial t_D} = N_{Da} (C - C^*) \quad (1)$$

In that model, the PV is divided into flowing and stagnant fractions. Thus, the pore space is characterized by three parameters: (1) the flowing fraction, f , the fraction of the pore space that contributes to flow; (2) the Peclet number, $N_{Pe} = vL/K_d$, the ratio of characteristic times for dispersion and flow; and (3) the Damköhler number, $N_{Da} = K_m L/v$, the ratio of characteristic times for mass transfer and flow. Thus, the model represents contributions of convection and dispersion in the flowing fraction and mass transfer between the flowing and stagnant fractions. The composition of fluid at any point within the flowing and stagnant fractions is taken to be uniform, and the rate of mass transfer is assumed to be linear in the difference in concentration between the two fractions.

The appearance of calculated effluent composition curves depends strongly on all three parameters.¹³ For pulse injections of the type used here, reduction of f below 1 causes the injected fluid to appear at the outlet before 1 PV has been injected (see, for example, Figs. 4.16 through 4.18 of Ref. 13). Increasing the Damköhler number above zero causes a long tail on the effluent composition curve, and decreasing the Peclet number broadens the produced peak. If the flowing fraction is 1, the C-S model reduces to the convection-dispersion equation with its single parameter, the Peclet number. In that case, the 50% normalized concentration arrives at 1 PV injected (PVI). The C-S model is the simplest differential model that reflects typical observations of corefloods in which breakthrough occurs before 1 PVI and hence has been used extensively to interpret miscible displacements in laboratory cores.^{10,11,13-17}

The C-S model equations are first order in time and second order in space and hence require one initial condition and two boundary conditions for solution. For the experiments described here, the initial condition is

$$C(X_D, 0) = 0, \quad 0 \leq X_D \leq 1. \quad (2)$$

The inlet boundary condition for a pulse input experiment is

$$C(0, t_D) = C_0 - \frac{1}{N_{Pe}} \frac{\partial C}{\partial X_D} \bigg|_{X_D=0}, \quad t_D > 0, \quad (3a)$$

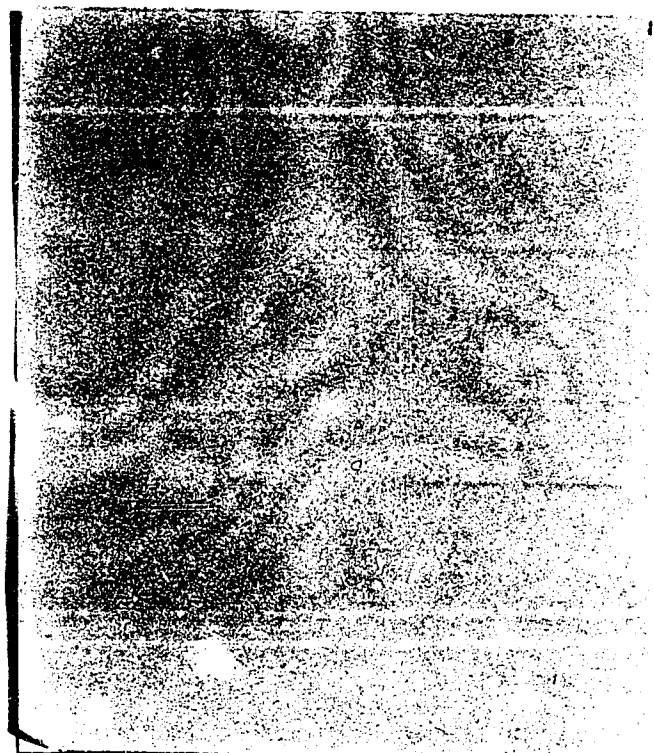
$$C_0 = 1, \quad 0 \leq t_D \leq \beta, \quad (3b)$$

and

$$C_0 = 0, \quad t_D > \beta. \quad (3c)$$

The exit boundary condition is

$$C(X_D \rightarrow \infty, t_D) = 0$$



SPE Does not have
and Copyright - contact author

$$C' = C(1, t_D) - \frac{1}{N_{Pe}} \frac{\partial C}{\partial X_D} \bigg|_{X_D=1}.$$

where C' is the exit concentration.

A discussion concerning the choice of boundary conditions may be found in Ref. 18.

The C-S model was solved numerically with a fully explicit finite-difference algorithm.¹³ The value of physical dispersion used was corrected to account for numerical dispersion caused by truncation errors. The least-error parameter determination was based on a form of Powell's¹⁹ method. The flowing fraction was adjusted first to minimize the sum of the absolute deviations between the calculated solution and data for the leading edge of the effluent pulse. Then, the Peclet number was varied to adjust calculated peak width. Finally, the Damköhler number was adjusted to match data for the tail portion of the peak. For the remainder of the fitting procedure, Powell's method was used to select and minimize along new search vectors until the best fit was achieved. The final result minimized the sum of the absolute deviations.

Thin-Section Analysis. Outcrop core plugs were cut parallel to bedding planes. Reservoir core plugs were cut horizontally from vertical core samples, and where bedding planes were evident, the horizontal plugs were aligned with those planes. A commercial laboratory prepared epoxy-impregnated thin-sections, which were cut parallel to the axis of the plugs. Pore-size distributions were obtained by measuring the pore-body sizes of 300 randomly selected pores. Pore-body size was defined as the smallest-diameter circle that completely circumscribes the pore body. For irregular or elongated pores, that definition exaggerates pore size for pores cut through their longest axis. That exaggeration is partly compensated for by the fact that the plane of the section does not coincide with the longest axis for many pores. In any case, that definition allows comparison between thin-sections, although it does not necessarily produce the same pore-size distribution as might be obtained by other techniques. For additional details of the procedures for measurement of pore sizes and size distributions, see the description given by Specter.²⁰

Several investigators have argued that wide or multimodal pore-size distributions cause the early breakthrough and tailing charac-

- Multiple-Contact Experiment," *SPEJ* (April 1983) 272-80.
8. Gardner, J.W. and Ypma, J.G.J.: "An Investigation of Phase-Behavior/Macroscopic-Bypassing Interaction in CO₂ Flooding," *SPEJ* (Oct. 1984) 508-20.
 9. Dai, K.K. and Orr, F.M. Jr.: "Prediction of CO₂ Flood Performance: Interaction of Phase Behavior with Microscopic Pore Structure Heterogeneity," *SPEJ* (Nov. 1987) 531-42; *Trans., AIME*, 283.
 10. Spence, A.P. and Watkins, R.W.: "The Effect of Microscopic Core Heterogeneity on Miscible Flood Residual Oil Saturation," paper SPE 9229 presented at the 1980 SPE Annual Technical Conference and Exhibition, Dallas, Sept. 21-24.
 11. Coats, K.H. and Smith, B.D.: "Dead-End Pore Volume and Dispersion in Porous Media," *SPEJ* (March 1964) 73-84; *Trans., AIME*, 231.
 12. Bretz, R.E., Specter, R.M., and Orr, F.M. Jr.: "Mixing During Single-Phase Flow in Reservoir Rocks: Models, Effects of Pore Structure and Interpretation of Experiments," *Proc., NIPER Reservoir Characterization Technical Conference*, Dallas (1985).
 13. Orr, F.M. Jr. and Taber, J.J.: "Displacement of Oil by Carbon Dioxide," final report, Contract No. DE-AS19-80-BC10331, U.S. DOE (March 1984).
 14. Stalkup, F.I.: "Displacement of Oil by Solvent at High Water Saturation," *SPEJ* (Dec. 1970) 337-48.
 15. Baker, L.E.: "Effects of Dispersion and Dead-End Pore Volume in Miscible Flooding," *SPEJ* (June 1977) 219-27; *Trans., AIME*, 263.
 16. Batycky, J.P., Maini, B.B., and Fisher, D.B.: "Simulation of Miscible Displacement in Full-Diameter Carbonate Cores," *SPEJ* (Oct. 1982) 647-58.
 17. Salter, S.J. and Mohanty, K.K.: "Multiphase Flow in Porous Media: I. Macroscopic Observations and Modelling," paper SPE 11017 presented at the 1981 SPE Annual Technical Conference and Exhibition, New Orleans, Sept. 26-29.
 18. Bretz, R.E. and Orr, F.M. Jr.: "Comparison of Analytical and Explicit Finite Difference Solutions of the Convection-Dispersion Equation," Report 85-6, New Mexico Petroleum Recovery Research Center (April 1985).
 19. Powell, M.J.D.: "An Efficient Method for Finding the Minimum of a Function of Several Variables Without Calculating Derivatives," *Computer J.* (1964) 7, 155-62.
 20. Specter, R.M.: "Effect of Pore Structure on Mixing in Stable, Single-Phase Miscible Displacement," MS thesis, New Mexico Inst. of Mining and Technology, Socorro (June 1984).
 21. Rao, P.S.C. *et al.*: "Solute Transport in Aggregated Porous Media: Theoretical and Experimental Evaluation," *Soil Sci. Soc. Am. J.* (1980) 44, 1139-46.
 22. Heller, J.P.: "Observations of Mixing and Diffusion in Porous Media," *Proc., Intl. Assn. of Hydraulic Research/Intl. Soc. of Soil Sciences Symposium on Fundamentals of Transport Phenomena in Porous Media*, U. of Guelph, Ont., Canada (1982) 1-26.
 23. Perkins, T.K. and Johnston, O.C.: "A Review of Diffusion and Dispersion in Porous Media," *SPEJ* (March 1963) 70-75; *Trans., AIME*, 228.
 24. Miller, I. and Freund, J.E.: *Probability and Statistics for Engineers*, second edition, Prentice-Hall Inc., Englewood Cliffs, NJ (1977) 322-27.
 25. Bahralolom, I., Bretz, R.E., and Orr, F.M. Jr.: "Experimental Investigation of the Interaction of Phase Behavior with Microscopic Heterogeneity in CO₂ Flood," *SPEJ* (May 1988) 662-72.
 26. Giordano, E.M., Salter, S.J., and Mohanty, K.K.: "The Effects of Permeability Variations on Flow in Porous Media," paper SPE 14365 presented at the 1985 SPE Annual Technical Conference and Exhibition, Las Vegas, Sept. 22-25.
 27. Bretz, R.E. and Orr, F.M. Jr.: "Interpretation of Miscible Displacements in Laboratory Cores," *SPEJ* (Nov. 1987) 492-500.
 28. Ayra, A. *et al.*: "Dispersion and Reservoir Heterogeneity," *SPEJ* (Feb. 1988) 139-48.

SI Metric Conversion Factors

$$\begin{array}{ll} \text{in.} \times 2.54^* & \text{E}+00 = \text{cm} \\ \text{in.}^2 \times 6.451\ 6^* & \text{E}+00 = \text{cm}^2 \end{array}$$

*Conversion factor is exact.

SPEJ

Original SPE manuscript received for review March 13, 1988. Paper accepted for publication July 20, 1987. Revised manuscript received March 11, 1988. Paper (SPE 15017) first presented at the 1988 SPE Permian Basin Oil & Gas Recovery Conference held in Midland, March 13-14.

A Review of Diffusion and Dispersion in Porous Media

T. K. PERKINS
O. C. JOHNSTON
MEMBERS AIME

THE ATLANTIC REFINING CO.
DALLAS, TEX.

ABSTRACT

Because of the influence of dispersion on miscible-displacement processes, diffusion and dispersion phenomena in porous rocks are of current interest in the oil industry. This paper reviews and summarizes a great deal of pertinent information from the literature.

Porous media (both unconsolidated packs and consolidated rocks) can be visualized as a network of flow chambers, having random size and flow conductivity, connected together by openings of smaller size. In such a porous medium, the apparent diffusion coefficient D is less than the molecular diffusion coefficient D_0 , as measured in the absence of a porous medium. For packs of unconsolidated granular material the ratio D/D_0 is about 0.6 to 0.7. For all porous rocks, both cemented and unconsolidated, the ratio of diffusion coefficients can also be represented as $D/D_0 = \frac{1}{F\phi}$, where F is the formation electrical resistivity factor and ϕ is the porosity.

If fluids are flowing through the porous medium, dispersion may be greater than that due to diffusion alone. At moderate flow rates the porous medium will create a slightly asymmetrical mix zone (trailing edge stretched out), with the longitudinal dispersion coefficient approximately proportional to the first power of average fluid velocity (if composition is nearly equalized in pore spaces by diffusion). If the velocity in interstices is large enough, there will be insufficient time for diffusion to equalize concentration within pore spaces. In this region, longitudinal dispersion increases more rapidly than fluid velocity.

At low velocities in interstices, transverse dispersion is characterized by a region in which transverse diffusion dominates. If the fluid velocity gets high enough, there will be a transition into a region where there is stream splitting with mass transfer but with insufficient residence time to completely damp-out concentration variations within pore spaces.

There are several variables that must be con-

trolled to get consistent longitudinal and transverse dispersion results, viz., (1) edge effect in packed tubes, (2) particle size distribution, (3) particle shape, (4) packing or permeability heterogeneities, (5) viscosity ratios, (6) gravity forces, (7) amount of turbulence, and (8) effect of an immobile phase.

INTRODUCTION

Diffusion and dispersion in porous rocks are of current interest to the oil industry. This interest arises because of the influence of dispersion on miscible-displacement processes.

In a recovery process utilizing a zone of miscible fluid, there is the possibility of losing miscibility by dissipating the miscible fluid or by channeling or "fingering" through the miscible zone. Diffusion and dispersion are two of the mechanisms that may lead to mixing and dissipation of the slug. On the other hand, dispersion may tend to damp-out viscous fingers which may be channeling through the miscible slug.⁵⁸ Hence, dispersion may be detrimental or beneficial (if it prevents fingering through the miscible zone). Therefore, it is doubly important that we understand these processes.

In this paper we review, summarize and interpret a great deal of information from the literature. In particular, we will briefly discuss molecular diffusion in miscible fluids. Then we will discuss what differences to expect for diffusion in a porous rock. If there is movement of the fluid through the rock, then there may be an additional mixing or "dispersion". Furthermore, the dispersion longitudinally (in the direction of gross fluid movement) and transverse to the direction of fluid movement will not be equal. We will discuss both types of dispersion as well as several variables which can affect dispersion (viscosity differences, density differences, turbulence, heterogeneity of media, etc.). This group of variables has sometimes led to difficulty when comparing literature data.

DIFFUSION OF MISCIBLE FLUIDS

If two miscible fluids are in contact, with an initially sharp interface, they will slowly diffuse into one another. As time passes, the sharp interface between the two fluids will become a diffuse

⁵⁸References given at end of paper.

Original manuscript received in Society of Petroleum Engineers office Sept. 10, 1962. Revised manuscript received Jan. 15, 1963.

A derivation of this equation has been shown by Fowler and Brown,²⁴ Rifai,⁴⁴ and others.

In the actual case, molecular diffusion will cause mixing along the interface. The net result will be a mixed zone growing at a more rapid rate than would obtain from diffusion alone, but less than the rate predicted by Eq. 8. Taylor⁵² and Aris¹ have studied the case where the time necessary for appreciable concentration changes to appear, owing to convection transport, was long compared with the "time of decay" during which radial variations of concentration were reduced to a fraction of their initial value through the action of molecular diffusion. Theoretical equations derived by these investigators showed that, if one fluid were displaced by another fluid under these conditions where diffusion could nearly damp-out radial concentration variations, then a symmetrical longitudinal mixed zone would be established. The mixed zone would travel with the mean speed of the injected fluid and would be dispersed as if there were a constant dispersion coefficient given by Eq. 9.

$$K_L = D_0 + \frac{U^2 a^2}{48 D_0} \dots \dots \dots (9)$$

where K_L = longitudinal dispersion coefficient, sq cm/sec,

U = average velocity, cm/sec, and

a = radius of the capillary, cm.

The effluent concentration, for the capillary tube, is given by the diffusion equation, Eq. 10.

$$C = \frac{1}{2} \left[1 \pm \operatorname{erf} \left(\frac{0.5}{\sqrt{K_L/UL}} \right) \left(\frac{1-V/V_p}{\sqrt{V/V_p}} \right) \right] \dots \dots (10)$$

Under what conditions will Eqs. 8 or 9 be valid? Taylor has shown that the ratio of time necessary for damping of radial concentration variations to the time to get a significant change in concentration is proportional to the dimensionless group $\frac{ULa^2}{D_0L}$.

Furthermore, he has shown that diffusion effects

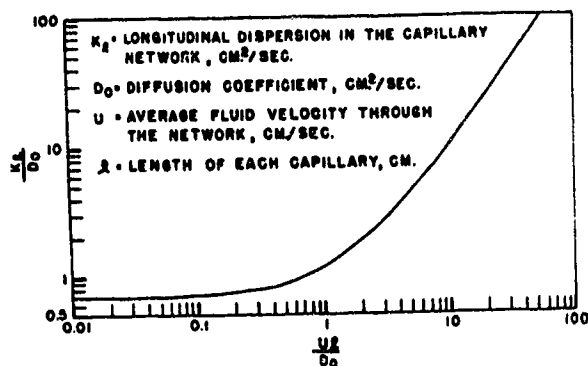


FIG. 4—LONGITUDINAL DISPERSION COEFFICIENTS FOR A RANDOM NETWORK OF CAPILLARIES (FROM SAFFMAN, REF. 45).

are negligible, and therefore Eq. 8 is applicable, if $\frac{Ua^2}{D_0L} > 250$.

An intermediate region where neither Eq. 8 nor Eq. 9 is valid has also been studied by Bosworth⁸ and Van Deemter, *et al*,⁵⁶ but their studies did not result in a quantitative representation of behavior over the full intermediate range. Recently, Bailey and Gogarty⁴ have studied dispersion over the full range by solving the diffusion and flow equations numerically.

Dispersion in a Network of Capillary Tubes

Again we should note that a bundle of straight capillary tubes is not a very good representation of a porous rock. de Jong¹⁷ and Saffman⁴⁵⁻⁴⁷ have studied a random network of capillaries. Their mathematical model is a more accurate description of a porous rock than is a bundle of straight capillaries, but the results are still not quantitatively correct for rock. The analysis is valuable, however, from a conceptual point of view. Saffman's results can be sketched as shown on Fig. 4.

Dispersion in Packs of Granular Material

Let us now proceed to a discussion of longitudinal dispersion in packs of granular material. Most investigators studying this problem have filled a packed column with one fluid, displaced it with another fluid, and measured fluid composition at the exit end of the tube as a function of displacement. Brigham, *et al*,⁹ have shown a convenient method for determining the dispersion coefficient from data of this type. In a slight modification of their method, the function $\frac{V/V_p - 1}{\sqrt{V/V_p}}$ is plotted vs the per cent of displacing fluid (on arithmetic-probability paper) as shown on Fig. 5. The dispersion coefficient can then be calculated with the aid of Eq. 11.

$$K_L = UL \left(\frac{\lambda_{90} - \lambda_{10}}{3.625} \right)^2 \dots \dots \dots (11)$$

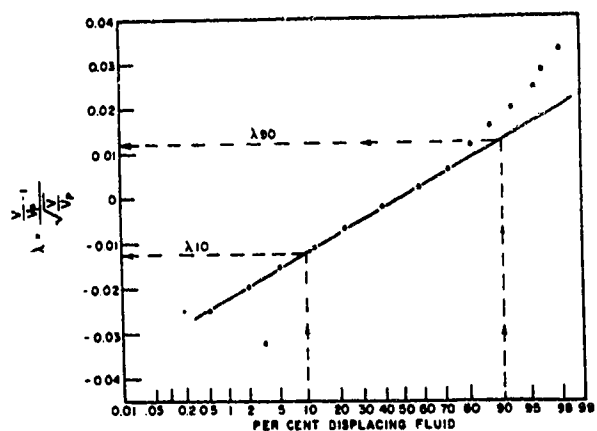


FIG. 5—TYPICAL EFFLUENT-COMPOSITION CURVE FOR MISCIBLE DISPLACEMENT OF A SAND-PACKED COLUMN (ON ARITHMETIC-PROBABILITY PAPER)—FROM BRIGHAM, ET AL (REF. 9).

USE Ref. 9 as original source or
this paper and include Ref 9 in
references

a = radius of a capillary, cm
 C = concentration
 D = apparent diffusion coefficient in a porous medium based on the average area open for diffusion and the over-all length
 D_o = molecular diffusion coefficient, sq cm/sec
 d_p = particle diameter, cm
 d_T = tube diameter, cm
 E = longitudinal convective dispersion coefficient, sq cm/sec
 F = formation electrical resistivity factor
 G = quantity of material diffusing across a plane (see Eq. 1)
 g = acceleration of gravity
 K_l = total longitudinal dispersion coefficient, sq cm/sec
 K_t = total transverse dispersion coefficient, sq cm/sec
 k = permeability
 L = length of a tube or a porous block, cm
 Pe = Peclet number (see Eq. 23)
 S = slope of a log-normal particle size distribution (see Eq. 21)
 t = time, seconds
 U = average interstitial velocity, cm/sec
 V = volume injected, cc
 V_p = total volume of tube or total pore volume
 X = distance, cm
 x = volume fraction of injected fluid in the effluent (see Eq. 8)
 β_t = factor to account for wall effect (see Fig. 14)

$$\lambda = \frac{(V/V_p) - 1}{V/V_p}$$
 μ = fluid viscosity
 ν = turbulence weighting factor (see Fig. 23)
 ρ = fluid density
 σ = a measure of the inhomogeneity of the porous pack
 ϕ = porosity
 ψ = sphericity of a particle (see Fig. 17)

REFERENCES

1. Aris, R.: "On the dispersion of a solute in a fluid flowing through a tube", *Proc., Royal Soc. of London* (1956) Series A, Vol. 235, 67.
2. Aris, R.: "The Longitudinal Diffusion Coefficient in Flow Through a Tube with Stagnant Pockets", *Chem. Eng. Sci.* (1959) Vol. 11, 194.
3. Aris, R. and Amundson, N. R.: "Some Remarks on Longitudinal Mixing or Diffusion in Fixed Beds", *AIChE Jour.* (1957) Vol. 3, 280.
4. Bailey, H. R. and Gogarty, W. B.: "Diffusion Coefficients from Capillary Flow", Paper SPE-302, presented at SPE Production Research Symposium, Tulsa, Okla. (April 12-13, 1962).
5. Baron, Thomas: *Chem. Eng. Prog.* (1952) Vol. 48, 118.
6. Bernard, R. A. and Wilhelm, R. H.: "Turbulent Diffusion in Fixed Beds of Packed Solids", *Chem. Eng. Prog.* (1950) Vol. 46, 233.
7. Blackwell, R. J.: "Laboratory Studies of Microscopic Dispersion Phenomena", *Soc. Pet. Eng. Jour.* (March, 1962) 1.
8. Bosworth, R. C. L.: *Phil. Mag.* (1948) Vol. 39, 847.
9. Brigham, W. E., Read, Philip W. and Dew, John N.: "Experiments on Mixing During Miscible Displacement in Porous Media", *Soc. Pet. Eng. Jour.* (March, 1961) 1.
10. Brown, G. G., et al: *Unit Operations*, John Wiley & Sons, Inc., N. Y. (1950).
11. Carberry, J. J.: "Axial Dispersion of Mass in Flow Through Fixed Beds", D. Eng. Dissertation, Yale U. (1957).
12. Carberry, J. J.: "Axial Dispersion and Void-cell Mixing Efficiency in Fluid Flow in Fixed Beds", *AIChE Jour.* (1958) Vol. 4, No. 1, 13M.
13. Carman, P. C.: "Fluid Flow Through Granular Beds", *Trans., Inst. of Chem. Eng., London* (1937) Vol. 15, 150.
14. Carman, P. C.: "Permeability of Saturated Sands, Soils, and Clays", *Jour. Agri. Sci.* (1939) Vol. 29, 262.
15. Collins, R. E.: *Flow of Fluids through Porous Media*, Reinhold Publishing Co., N. Y. (1961) 201.
16. Crank, J.: *The Mathematics of Diffusion*, Oxford at the Clarendon Press, N. Y. (1957).
17. de Jong, G. de Josselin: "Longitudinal and Transverse Diffusion in Granular Deposits", *Trans., AGU* (1958) Vol. 39, 67.
18. Deans, H. A. and Lapidus, Leon: "A Computational Model for Predicting and Correlating the Behavior of Fixed Bed Reactors: 1. Derivation of Model for Non-reactive Systems", *AIChE Jour.* (Dec., 1960) 656.
19. Ebach, E. A.: "The Mixing of Liquids Flowing Through Beds of Porous Solids", PhD Dissertation, U. of Michigan (1957).
20. Ebach, E. A. and White, R. R.: "Mixing of Fluids Through Beds of Packed Solids", *AIChE Jour.* (1958) Vol. 6, 161.
21. Ergun, S. K.: "Fluid Flow Through Packed Columns", *Chem. Eng. Prog.* (1952) Vol. 48, 89.
22. Fahien, R. W. and Smith, J. M.: "Mass Transfer in Packed Beds", *AIChE Jour.* (1955) Vol. 1, 28.
23. Fatt, I.: "Pore Structure of Sintered Glass From Diffusion and Resistance Measurements", *Jour. Phys. Chem.* (1959) Vol. 63, 751.
24. Fowler, F. C. and Brown, G. G.: "Contamination by Successive Flow in Pipe Lines", *Trans., AIChE* (1943) Vol. 39, 491.
25. Goodknight, R. C., Klikoff, W. A. and Fatt, I.: "Non-

where $\lambda_{90} = \frac{V/V_p - 1}{\sqrt{V/V_p}}$ when effluent contains 90 per cent displacing fluid.

Nearly all literature data show that the longitudinal dispersion coefficients for *unconsolidated* sand or bead packs can be represented as shown by Eq. 12.

$$\frac{E}{D_0} = 1.75 \frac{Ud_p}{D_0} ; \left(2 < \frac{Ud_p}{D_0} < 50 \right) \quad (12)$$

where E = longitudinal convective dispersion coefficient, sq cm/sec, and
 d_p = particle diameter, cm.

Furthermore, in the region where both diffusion and convective dispersion are important, the total dispersion coefficient is the sum of these two coefficients. Hence, the total longitudinal dispersion coefficient in an unconsolidated sand pack can be represented as shown by Eq. 13, and is sketched on Fig. 6.

$$K_L = D + E$$

$$\frac{K_L}{D_0} = \frac{D}{D_0} + \frac{E}{D_0}$$

$$\frac{K_L}{D_0} = \frac{1}{F_\phi} + 1.75 \frac{Ud_p}{D_0} ; \left(\frac{Ud_p}{D_0} < 50 \right) \quad (13)$$

Can the dispersive behavior of granular packs be represented fairly accurately by an "equivalent" bundle of capillary tubes? A comparison of Eqs. 9 and 12 shows that in packed columns the longitudinal dispersion coefficient is proportional to the first power of average velocity (if longitudinal dispersion is large compared to longitudinal molecular diffusion), whereas for capillary tubes the dispersion coefficient is proportional to the second power of average velocity. How can we explain this significant difference in behavior?

A clue is furnished in work reported by Aris and Amundson.³ These investigators have studied the dispersion to be expected in mixing chambers of

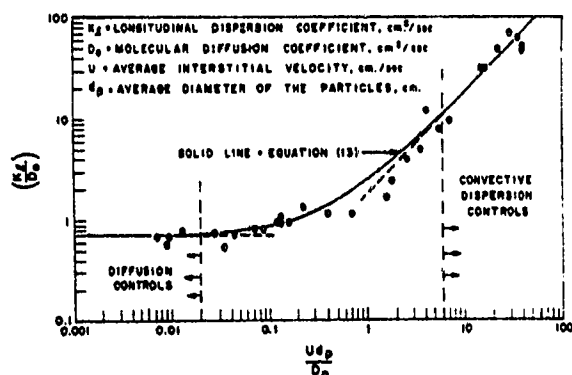


FIG. 6—LONGITUDINAL DISPERSION COEFFICIENTS FOR UNCONSOLIDATED, RANDOM PACKS OF UNIFORM SIZE SAND OR BEADS (DATA FROM REF. 11, 42, 53 AND 59).

7. REF this paper but also cite where authors obtained data to construct figure

uniform size connected in series. The chambers are filled with one fluid and a second fluid is injected at one end at a constant rate. The composition within each chamber is maintained uniform at all times by complete mixing (in the case of granular packs and for some flow conditions, the concentration in each pore space is maintained essentially uniform by diffusion). Eq. 14 gives the concentration of displaced fluid in each cell of a very long series of cells.

$$C_n = 1 - e^{-qt/v} \left[\sum_{n=1}^{\infty} \frac{(qt/v)^n}{n!} + 1 \right] \quad (14)$$

where C_n = concentration of the displaced fluid in the n th cell,
 q = injection rate,
 t = time, and
 v = volume of each cell.

Fig. 7 shows the concentration of displaced fluid calculated from Eq. 14 when a pore volume of 100 cells has been injected (i.e., $qt/v = 100$).

This figure shows that a mixed zone is established which moves with the mean speed of the injected fluid; that is, the 50 per cent point is essentially at the hundredth cell (if the displacement had been piston-like, there would have been an abrupt change in composition after the hundredth cell). Furthermore, the growth of the mix zone, relative to the 50 per cent composition point, can be represented by a constant dispersion coefficient (i.e., plots as an essentially straight line on probability paper). Fig. 7 is equivalent to Fig. 1. The apparent dispersion coefficient can be calculated with Eq. 3. By noting that the time to inject 100 cell volumes is equal to the length of 100 cells divided by the average fluid velocity, it follows that the apparent dispersion coefficient varies as the first power of the mean velocity (the same behavior as exhibited by porous packs, see Eq. 12).

A pack of granular material, of course, can be thought of as a series of chambers or pore spaces connected by smaller openings. This is indicated graphically on Fig. 8, which shows the shapes of void spaces for various types of symmetrical packing of spheres as reported by Graton and Fraser.²⁷

Study of dispersion data from packed columns reveals that the concentration profile in the mixed zone is not typically a perfect S-shaped probability

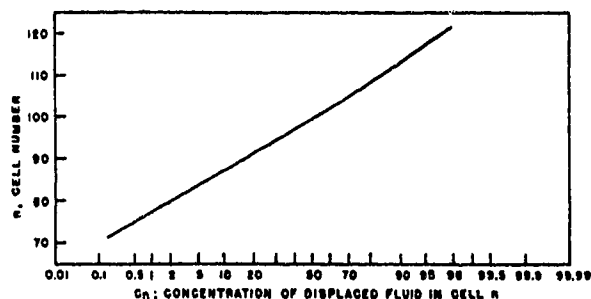


FIG. 7 — DISTRIBUTION OF COMPOSITION ALONG A SERIES OF MIXING CELLS; CALCULATED FROM EQ. 14. (qt/v) = 100.

a = radius of a capillary, cm
 C = concentration
 D = apparent diffusion coefficient in a porous medium based on the average area open for diffusion and the over-all length
 D_o = molecular diffusion coefficient, sq cm/sec
 d_p = particle diameter, cm
 d_T = tube diameter, cm
 E = longitudinal convective dispersion coefficient, sq cm/sec
 F = formation electrical resistivity factor
 G = quantity of material diffusing across a plane (see Eq. 1)
 g = acceleration of gravity
 K_l = total longitudinal dispersion coefficient, sq cm/sec
 K_t = total transverse dispersion coefficient, sq cm/sec
 k = permeability
 L = length of a tube or a porous block, cm
 Pe = Peclet number (see Eq. 23)
 S = slope of a log-normal particle size distribution (see Eq. 21)
 t = time, seconds
 U = average interstitial velocity, cm/sec
 V = volume injected, cc
 V_p = total volume of tube or total pore volume
 x = distance, cm
 x = volume fraction of injected fluid in the effluent (see Eq. 8)
 β_t = factor to account for wall effect (see Fig. 14)

$$\lambda = \frac{(V/V_p) - 1}{V/V_p}$$
 μ = fluid viscosity
 ν = turbulence weighting factor (see Fig. 23)
 ρ = fluid density
 σ = a measure of the inhomogeneity of the porous pack
 ϕ = porosity
 ψ = sphericity of a particle (see Fig. 17)

REFERENCES

1. Aris, R.: "On the dispersion of a solute in a fluid flowing through a tube", *Proc., Royal Soc. of London* (1956) Series A, Vol. 235, 67.
2. Aris, R.: "The Longitudinal Diffusion Coefficient in Flow Through a Tube with Stagnant Pockets", *Chem. Eng. Sci.* (1959) Vol. 11, 194.
3. Aris, R. and Amundson, N. R.: "Some Remarks on Longitudinal Mixing or Diffusion in Fixed Beds", *AIChE Jour.* (1957) Vol. 3, 280.
4. Bailey, H. R. and Gogarty, W. B.: "Diffusion Coefficients from Capillary Flow", Paper SPE-302, presented at SPE Production Research Symposium, Tulsa, Okla. (April 12-13, 1962).
5. Baron, Thomas: *Chem. Eng. Prog.* (1952) Vol. 48, 118.
6. Bernard, R. A. and Wilhelm, R. H.: "Turbulent Diffusion in Fixed Beds of Packed Solids", *Chem. Eng. Prog.* (1950) Vol. 46, 233.
7. Blackwell, R. J.: "Laboratory Studies of Microscopic Dispersion Phenomena", *Soc. Pet. Eng. Jour.* (March, 1962) 1.
8. Bosworth, R. C. L.: *Phil. Mag.* (1948) Vol. 39, 847.
9. Brigham, W. E., Reed, Philip W. and Dew, John N.: "Experiments on Mixing During Miscible Displacement in Porous Media", *Soc. Pet. Eng. Jour.* (March, 1961) 1.
10. Brown, G. G., et al.: *Unit Operations*, John Wiley & Sons, Inc., N. Y. (1950).
11. Carberry, J. J.: "Axial Dispersion of Mass in Flow Through Fixed Beds", D. Eng. Dissertation, Yale U. (1957).
12. Carberry, J. J.: "Axial Dispersion and Void-cell Mixing Efficiency in Fluid Flow in Fixed Beds", *AIChE Jour.* (1958) Vol. 4, No. 1, 13M.
13. Carman, P. C.: "Fluid Flow Through Granular Beds", *Trans., Inst. of Chem. Eng., London* (1937) Vol. 15, 150.
14. Carman, P. C.: "Permeability of Saturated Sands, Soils, and Clays", *Jour. Agri. Sci.* (1939) Vol. 29, 262.
15. Collins, R. E.: *Flow of Fluids through Porous Media*, Reinhold Publishing Co., N. Y. (1961) 201.
16. Crank, J.: *The Mathematics of Diffusion*, Oxford at the Clarendon Press, N. Y. (1957).
17. de Jong, G. de Josselin: "Longitudinal and Transverse Diffusion in Granular Deposits", *Trans., AGU* (1958) Vol. 39, 67.
18. Deans, H. A. and Lapidus, Leon: "A Computational Model for Predicting and Correlating the Behavior of Fixed Bed Reactors: 1. Derivation of Model for Non-reactive Systems", *AIChE Jour.* (Dec., 1960) 656.
19. Ebach, E. A.: "The Mixing of Liquids Flowing Through Beds of Porous Solids", PhD Dissertation, U. of Michigan (1957).
20. Ebach, E. A. and White, R. R.: "Mixing of Fluids Through Beds of Packed Solids", *AIChE Jour.* (1958) Vol. 6, 161.
21. Ergun, S. K.: "Fluid Flow Through Packed Columns", *Chem. Eng. Prog.* (1952) Vol. 48, 89.
22. Fahien, R. W. and Smith, J. M.: "Mass Transfer in Packed Beds", *AIChE Jour.* (1955) Vol. 1, 28.
23. Fatt, I.: "Pore Structure of Sintered Glass From Diffusion and Resistance Measurements", *Jour. Phys. Chem.* (1959) Vol. 63, 751.
24. Fowler, F. C. and Brown, G. G.: "Contamination by Successive Flow in Pipe Lines", *Trans., AIChE* (1943) Vol. 39, 491.
25. Goodknight, R. C., Kliikoff, W. A. and Fatt, I.: "Non-

Steady-State Fluid Flow and Diffusion in Porous Media Containing Dead-End Pore Volume", *Jour. Phys. Chem.* (1960) Vol. 64, 1162.

22. Grane, F. E. and Gardner, G. H. F.: "Measurements of Transverse Dispersion in Granular Media", *Jour. Chem. Eng. Data* (1961) Vol. 6, 283.
23. Gratton, L. C. and Fraser, H. J.: "Systematic Packing of Spheres—With Particular Relation to Porosity and Permeability", *Jour. Geol.* (Nov.-Dec., 1935) 785.
24. Handy, L. L.: "An Evaluation of Diffusion Effects in Miscible Displacement", *Trans., AIME* (1959) Vol. 216, 382.
25. Hoogschagen, Jan: "Diffusion in Porous Catalysts and Adsorbents", *Ind. Eng. Chem.* (1955) Vol. 47, 906.
26. Klinkenberg, L. J.: "Analog Between Diffusion and Electrical Conductivity in Porous Rocks", *Bull., GSA* (1951) Vol. 62, 559.
27. Klinkenberg, A. and Sjenitzer, F.: "Holding-time Distributions of the Gaussian Type", *Chem. Eng. Sci.* (1956) Vol. 5, 258.
28. Koump, V.: "Study of the Mechanism of Axial Dispersion in Packed Beds at Low Flow Rates", D. Eng. Dissertation, Yale U. (1959).
29. Latinen, G. A.: "Mechanism of Fluid Phase Mixing of Fixed and Fluidized Beds of Uniformly Sized Spherical Particles", PhD Dissertation, Princeton U. (1951).
30. Liles, A. W. and Geankoplis, C. J.: "Axial Diffusion of Liquids in Packed Beds and End Effects", *AIChE Jour.* (1960) Vol. 6, 591.
31. McHenry, Keith W., Jr.: "Axial Mixing of Binary Gas Mixtures Flowing in a Random Bed of Spheres", PhD Dissertation, Princeton U. (1958).
32. Orlob, G. T. and Radhakrishna, G. N.: "The Effects of Entrapped Gases on the Hydraulic Characteristics of Porous Media", *Trans., AGU* (1958) Vol. 39, 648.
33. Penman, H. L.: "Gas and Vapor Movement in Soil", *Jour. Agri. Sci.* (1940) Vol. 30, 438.
34. Plautz, D. A. and Johnstone, H. F.: "Heat and Mass Transfer in Packed Beds", *AIChE Jour.* (1955) Vol. 1, 193.
35. Pozzi, A. L. and Blackwell, R. J.: "Design of Laboratory Models for Study of Miscible Displacement", *Soc. Pet. Eng. Jour.* (March, 1963).
36. Prausnitz, J. M.: "Longitudinal Dispersion in a Packed Bed", *AIChE Jour.* (1958) Vol. 4, No. 1, 14M.
37. Raimondi, P., Torcaso, M. A. and Henderson, J. H.: "The Effect of Interstitial Water on the Mixing of Hydrocarbons During a Miscible Displacement Process", *Min. Ind. Exp. Station Circ. 61*, The Pennsylvania State U.
38. Raimondi, P., Gardner, G. H. F. and Petrick, C. B.: "Effect of Pore Structure and Molecular Diffusion on the Mixing of Miscible Liquids Flowing in Porous Media", Preprint 43 presented at AIChE-SPE Joint Symposium, San Francisco, Cal. (Dec. 6-9, 1959).
39. Ranz, W. E.: "Friction and Transfer Coefficients for Single Particles and Packed Beds", *Chem. Eng. Prog.* (1952) Vol. 48, 247.
40. Rifai, M. N. E.: "An Investigation of Dispersion Phenomena in Laminar Flow Through Porous Media", PhD Dissertation, U. of California, Berkeley (1956).
41. Saffman, P. G.: "Dispersion in Flow Through a Network of Capillaries", *Chem. Eng. Sci.* (1959) Vol. 11, 125.
42. Saffman, P. G.: "Theory of Dispersion in Porous Media", *Jour. Fluid Mech.* (1959) Vol. 6, 321.
43. Saffman, P. G.: "Dispersion Due to Molecular Diffusion Through a Network of Capillaries", *Jour. Fluid Mech.* (1960) Vol. 7, 194.
44. Scheidegger, A. E. and Larson, V. C.: "Asymmetry of the Concentration Front During Miscible Displacement in Porous Media", *Can. Jour. Phys.* (1958) Vol. 36, 1476.
45. Schwartz, C. E. and Smith, J. M.: "Flow Distribution in Packed Beds", *Ind. Eng. Prog.* (1953) Vol. 45, 1209.
46. Scott, D. S. and Dullien, F. A. L.: "Diffusion of Ideal Gases in Capillaries and Porous Solids", *AIChE Jour.* (1962) Vol. 8, 113.
47. Singer, E. and Wilhelm, R. H.: "Heat Transfer in Packed Beds; Analytical Solution and Design Method; Fluid Flow, Solids Flow and Chemical Reaction", *Chem. Eng. Prog.* (1950) Vol. 46, 343.
48. Taylor, G. I.: "Dispersion of Soluble Matter in Solvent Flowing Slowly Through a Tube", *Proc., Roy. Soc.* (1953) Vol. 219, 186.
49. Terry, W. M., Blackwell, R. J. and Rayne, J. R.: "Factors Influencing the Efficiency of Miscible Displacement", *Trans., AIME* (1959) Vol. 216, 1.
50. Turner, G. A.: "The Flow-Structure in Packed Beds", *Chem. Eng. Sci.* (1957) Vol. 7, 156.
51. van Bavel, C. H. M.: "Gaseous Diffusion and Porosity in Porous Media", *Soil Sci.* (1952) Vol. 74, 91.
52. Van Deemter, J. J., Broeder, J. J. and Lauwerier, H. A.: "Fluid Displacement in Capillaries", *Appl. Scientific Res.* (1956) Vol. 5A, 374.
53. Van Deemter, J. J., Bralder and Lawrence: "Fluid Displacement in Capillaries", *Chem. Eng. Sci.* (1956) Vol. 5, 271.
54. van der Poel, C.: "Effect of Lateral Diffusivity on Miscible Displacement in Horizontal Reservoirs", *Soc. Pet. Eng. Jour.* (Dec., 1962) 317.
55. Von Rosenberg, D. U.: "Mechanics of Steady State Single-phase Fluid Displacement from Porous Media", *AIChE Jour.* (1956) Vol. 2, 55.
56. Zunker, F.: Blanck's *Handbuch der Bodenlehre*, VI, Berlin (1930) 202.
57. ACS-PRF, 450-A Project. ***

THE UNIVERSITY OF ALBERTA

RELEASE FORM

NAME OF AUTHOR DANIEL JOSEPH GIESBRECHT
TITLE OF THESIS A FRACTAL ANALYSIS OF HETEROGENEITY
 IN MISCIBLE DISPLACEMENT
DEGREE MASTER OF SCIENCE
YEAR THIS DEGREE GRANTED FALL, 1990

PERMISSION IS HEREBY GRANTED TO THE UNIVERSITY OF
ALBERTA LIBRARY TO REPRODUCE SINGLE COPIES OF THIS THESIS
AND TO LEND OR SELL SUCH COPIES FOR PRIVATE, SCHOLARLY OR
SCIENTIFIC RESEARCH PURPOSES ONLY.

THE AUTHOR RESERVES OTHER PUBLICATION RIGHTS, AND
NEITHER THE THESIS NOR EXTENSIVE EXTRACTS FROM IT MAY BE
PRINTED OR OTHERWISE REPRODUCED WITHOUT THE AUTHOR'S WRITTEN
PERMISSION.

(SIGNED) ..*Dan. Giesbrecht*.....

PERMANENT ADDRESS:

...*101-333-2nd Ave. N.E.*.....
...*Calgary, Alberta*.....
...*72E QFS*.....

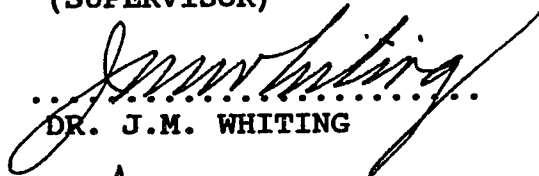
DATE: *June 26, 1990*.....

THE UNIVERSITY OF ALBERTA
FACULTY OF GRADUATE STUDIES AND RESEARCH

THE UNDERSIGNED CERTIFY THAT THEY HAVE READ, AND
RECOMMEND TO THE FACULTY OF GRADUATE STUDIES AND RESEARCH
FOR ACCEPTANCE, A THESIS ENTITLED A FRACTAL ANALYSIS OF
HETEROGENEITY IN MISCIBLE DISPLACEMENT SUBMITTED BY DANIEL
JOSEPH GIESBRECHT IN PARTIAL FULFILLMENT OF THE REQUIREMENTS
FOR THE DEGREE OF MASTER OF SCIENCE IN PETROLEUM
ENGINEERING.



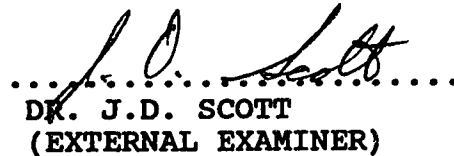
.....
DR. D.L. FLOCK
(SUPERVISOR)



.....
DR. J.M. WHITING



.....
DR. A.K. AMBASTHA



.....
DR. J.D. SCOTT
(EXTERNAL EXAMINER)

DATE: June 18, 1990.....

ABSTRACT

The description of heterogeneity in porous media has always been limited by the impracticality of describing the property in question in complete deterministic detail. The result of this difficulty is that the spatial distribution of the property is often neglected. Recent work has indicated that fractal theory may provide an avenue for the estimation of spatial distribution over many scales of measurement. This knowledge would facilitate the extrapolation of laboratory measured dispersion values to dispersion on a field-wide scale.

The purpose of this investigation was to study the possibility of using the fractal dimension of permeability to describe heterogeneity for a variety of rock types. This study was undertaken by comparing the effluent concentration profiles of first contact miscible displacements in various rock types to the fractal dimensions calculated for permeability, porosity and mean pore throat size. The fractal dimension was calculated through the use of autocorrelation function and variogram techniques using a series of equally spaced permeability, porosity and mean pore throat size values obtained from each core tested.

The fractal dimension for permeability calculated using an autocorrelation function technique provided a valid means

of estimating heterogeneity which compared favorably with other, more traditional heterogeneity indicators. The advantage in this approach is that the fractal dimension describes heterogeneity over all scales it is measured over and provides a means of extrapolating convective dispersion coefficients measured in the laboratory to field scale applications.

ACKNOWLEDGEMENTS

The author is grateful to Dr. D.L. Flock for his encouragement and support in the completion of this study.

Appreciation is extended to the ALBERTA OIL SANDS TECHNOLOGY AND RESEARCH AUTHORITY, CHEVRON CANADA RESOURCES and the DEPARTMENT OF MINING, METALLURGICAL AND PETROLEUM ENGINEERING for financial support over the period of this study.

Appreciation is also extended to Dr. A.K. Ambastha, Dr. P.J. Crickmore and Prof. W.H. Griffin for their advice and helpful discussions.

The author would also like to acknowledge the efforts of Mr. J. Czuroski, Mr. J. Gibeau and Mr. B. Smith in bringing this study to a successful conclusion.

Table of Contents

I. Introduction	1
II. Review of Diffusion and Dispersion	5
A. <u>Introduction</u>	5
B. <u>Convective - Dispersion Model</u>	12
C. <u>Coats - Smith Model</u>	15
D. <u>Other Related Work</u>	19
III. Pore Structure Effects	21
A. <u>Introduction</u>	21
B. <u>Geological Aspects</u>	23
IV. Methods of Spatial Correlation	30
A. <u>Fractal Theory</u>	31
1. Introduction	31
2. Fractal Dimension	32
B. <u>Geostatistical Methods</u>	41
1. Autocorrelation Functions	44
2. Semi-Variogram Analysis	46
V. Experimental Apparatus and Procedure	54
A. <u>Coreflood Studies</u>	54
1. Coreflood Apparatus	55
2. Coreflood Design	57
3. Coreflood Procedure	64

B. <u>Mercury Porosimetry</u>	67
C. <u>Data Analysis</u>	72
VI. Heterogeneity Description	78
A. <u>Dykstra - Parson's V_{Dr}</u>	78
B. <u>Koval's H Parameter</u>	82
VII. Results and Discussion	90
A. <u>Line of Investigation</u>	90
B. <u>Discussion of Results</u>	91
1. Effect of Floodrate and Convective Dispersion on Recovery Efficiency	91
2. Effect of Lithology on K_e and Recovery Efficiency	97
3. Effect of Permeability, Porosity and Mean Pore Throat Size Variance on Dispersion Behavior and Recovery Efficiency	99
4. Relationship Between Fractal Dimension of Permeability, porosity and Mean Pore Throat Size and Dispersion and Recovery Efficiency ..	102
5. Comparison of Dacf with V_{Dr} and Koval's H	109
6. Scale Dependence and Dacf	114
VIII. Conclusions and Recommendations	121

References	124
Appendix A	129
1. Raw Data Listings	130
Appendix B	150
1. ANOVA Calculations	150
2. Semi-Variogram Plots	153
Appendix C	169
1. Calculation of Property Mean and Variance	169
Appendix D	173
1. Sample Calculation of K_p	174
2. Effluent Concentration and λ Data	175
Appendix E	186
1. Program EFFPLOT	186
2. Program ANALYZE	190

List of Tables

Table	Page
IV-1 Semi-Variogram Functional Forms	51
V-1 Properties of Miscible Components	58
V-2 Core Properties	63
VI-1 Dykstra-Parson's Results	82
VI-2 Koval's H Parameter	89
VII-1 Coreflood Results (rate=0.02222 cm/s)	92
VII-2 Coreflood Results (rate=0.01528 cm/s)	92
VII-3 Coreflood Results (rate=0.00972 cm/s)	93
VII-4 Correlation of Variance with K_e and Recovery	101
VII-5 Calculated Fractal Dimensions	103
VII-6 Permeability Fractal Correlations	104
VII-7 Porosity Fractal Correlations	105
VII-8 Pore Throat Size Fractal Correlations	105
A-1 Data Summary - Core A	130

A-2	Data Summary - Core B	132
A-3	Data Summary - Core C	134
A-4	Data Summary - Core D	136
A-5	Data Summary - Core E	138
A-6	Data Summary - Core F	140
A-7	Data Summary - Core G	142
A-8	Data Summary - Core H	144
A-9	Data Summary - Core I	146
A-10	Data Summary - Core J	148
B-1	ANOVA Analysis	152
C-1	Property Mean and Variance	170
D-1	Effluent Concentration Profiles - Core A	176
D-2	Effluent Concentration Profiles - Core B	177
D-3	Effluent Concentration Profiles - Core C	178
D-4	Effluent Concentration Profiles - Core D	179
D-5	Effluent Concentration Profiles - Core E	180

D-6	Effluent Concentration Profiles - Core F	181
D-7	Effluent Concentration Profiles - Core G	182
D-8	Effluent Concentration Profiles - Core H	183
D-9	Effluent Concentration Profiles - Core I	184
D-10	Effluent Concentration Profiles - Core J	185

List of Figures

Figure	Page
II-1 Effluent Concentration Profile for Indiana Limestone Showing a Transition Zone ($M=0.341$)	6
II-2 Convective Dispersion in Porous Media (from Stalkup, 1983)	8
II-3 Mixing by Longitudinal and Transverse Dispersion in a Porous Medium (from Stalkup, 1983)	9
II-4 λ Function Plot (from Brigham et al, 1961)	10
II-5 Effluent Concentration Profile Showing Capacitance	18
III-1 Example of Equivalent Permeability Frequency Distributions but Different Spatial Distributions (from Wyllie, 1962)	22
III-2 Application of Walther's Law to Lateral Depositional Environments (from Blatt et al, 1980)	25
IV-1 Illustration of Structured Walk Technique	36

IV-2	Determination of Fractal Dimension from an ln-ln Plot	37
IV-5	Semi-Variogram Curves Showing Fractal Behavior (Data from Mishra, 1987)	40
IV-6	Definition of Lag Values	42
IV-7	Semi-Variance Calculation Procedure	48
IV-8	Experimental and Theoretical Semi-Variograms ..	49
V-1	Coreflood Apparatus	55
V-2	Behavior of Longitudinal Dispersion Coefficient with Velocity (from Perkins and Johnston, 1963)	60
V-3	Core Sample Locations	68
V-4	Capillary Pressure Cell	71
V-5	Calculation of λ_c , (from Brigham et al, 1961)	73
VI-1	V_{DP} Calculation	80
VI-2	Effluent Concentration Profiles Indiana Limestone	85

VI-3	Effluent Concentration Profiles Berea Sandstone	85
VI-4	Effluent Concentration Profile Swan Hills Limestone	86
VI-5	Effluent Concentration Profile Golden Spike Limestone	86
VI-6	Effluent Concentration Profiles Brown Sandstone	87
VI-7	Effluent Concentration Profiles Tyndle Limestone	87
VII-1	Flood Velocity vs Recovery Factor	94
VII-2	K_r vs Recovery Factor	96
VII-3	K_r vs Recovery Factor with Lithology as a Parameter	98
VII-4	D_{var} Sample Calculation	104
VII-5	D_{acf} vs K_r	108
VII-6	Comparison of D_{acf} , VDP and H vs R.F.	110
VII-7	Comparison of D_{acf} , VDP and H with log K_e	112
VII-8	Comparison of D_{acf} and H	114

VII-9	Growth of Dispersivity with Scale	118
B-1	Permeability Semi-Variograms	154
B-11	Porosity Semi-Variograms	159
B-21	Mean Pore Throat Size Semi-Variograms	164

Nomenclature

A	cross-sectional area cm^2
ANOVA	analysis of variance test.
a	range of semi-variogram (L)
b	scale multiplier.
C	relative solvent concentration.
C_D, C_D^*	dimensionless concentrations in mobile and stagnant fractions ,respectively.
$C_v(x, x+h)$	autocovariance function.
$C(x, x+h)$	autocorrelation function.
D	fractal dimension.
D_{acf}	fractal dimension calculated from autocorrelation functions.
D_{var}	fractal dimension calculated from variogram analysis.
D_a	Damkohler number = $\frac{\kappa L}{v}$
D_l	longitudinal dispersion coefficient (cm^2/s).
D, D_o	molecular diffusion coefficient (cm^2/s).
d	mean pore throat diameter (nm).
d_p	average particle diameter (cm).
E	mathematical expectation operator.
erfc	complementary error function.
F	formation resistivity factor.

F	length of a line.
f	mobile fluid fraction.
G	quantity of solute diffused across a sharp interface (moles).
H	fractal co-dimension = $\eta - D$
H	Koval's heterogeneity factor.
h	lag distance.
K	mass transfer coefficient (cm^2/s).
K_e	effective dispersion coefficient (cm^2/s).
K_l	coefficient of longitudinal dispersion (cm^2/s).
K_t	coefficient of transverse dispersion (cm^2/s).
k	permeability (md).
Ke_{lab}	dispersivity = $\frac{K_e}{v}$.
L	length.
M	mobility ratio.
N	number of measurements.
N(h)	number of data pairs separated by lag value h.
n	number of observations.
P_c	capillary pressure (psi).
P_e	Peclet number = $\frac{vL}{D_l}$.
P.V.	pore volume.
R.F.	recovery factor.

r	correlation coefficient.
S	fraction of porespace invaded by mercury.
t_D	dimensionless time = $\frac{vt}{L}$.
t	time (s).
V	pore volumes of fluid injected.
V_p	pore volume of the core.
V_{DP}	Dykstra-Parson's permeability variation.
X_D	dimensionless distance = $\frac{x}{L}$.
x	distance.
$Z(x)$	variable value at location x .
$Z(x+h)$	variable value at location $x+h$.
$\gamma(h)$	semi-variance.
η	dimension in euclidean space.
θ	contact angle (degrees).
λ	lambda function.
λ_L	lithology factor.
μ	viscosity (cp).
$\bar{\mu}_x$	mean value.
v, U	Darcian velocity (cm/s).
ξ	length of a measurement.
σ	heterogeneity coefficient.
σ^2	variance.

I. Introduction

A major focus in petroleum engineering since its inception has been an attempt to maximize oil recovery in the most economical manner possible. Primary depletion, using natural reservoir energy as the driving force, will typically recover only a few percent of the original oil in place. Secondary recovery methods utilizing voidage replacement techniques have been successful in raising overall recovery to 50% in favorable cases. Despite these advances, a large percentage of the original oil in place remains unrecoverable due, in part, to the effects of interfacial tension and capillary forces which exist between phases within the porous media.

Tertiary recovery methods were developed in an attempt to increase recovery by minimizing or eliminating the effects of interfacial tension and capillary forces. Commonly, a displacing fluid which is completely miscible with the resident oil under reservoir conditions is injected into the formation. The choice of the solvent used is dictated by economic and operational considerations.

The efficiency of the miscible flooding process depends on two main groups of factors.

1.) Flood Instabilities

An unstable miscible front is detrimental to the efficiency of the displacement process. Factors important to the attainment of a stable front include the velocity of the front, the production rate of fluids from the wellbore as well as the effect of geological heterogeneities within the porous media.

2.) Fluid Mixing

Fluid mixing is an important factor in the maintenance of miscibility conditions. Factors such as molecular diffusion and convective dispersion have been quantified on a microscopic and macroscopic scale by many investigators. These phenomena affect the efficiency of the displacement process.

It has long been recognized that the severely unstable behavior of a miscible displacement front is a result of both microscopic and macroscopic heterogeneities within the porous media. A number of investigators have attempted to quantify the effect on a microscopic level by using either a Koval heterogeneity factor (H), or a Dykstra-Parsons V_D , variance factor. While these studies tend to be based upon porous media having a relatively homogeneous pore structure, little work has been directed toward quantifying the relationship between flood front instabilities and the more

heterogeneous pore structures which exist in carbonate rocks.

The primary objective of this study was to further investigate flood front mixing processes as influenced by heterogeneous pore systems. Any estimator of the degree of heterogeneity in a porous medium must account for the following factors (Warren and Price, 1961).

1. The nature of the property variation
(frequency distribution).
2. The spatial distribution of the property.
3. The inherent stability of the mechanism under study.

While many estimators of heterogeneity have been developed which account for factors one and three, the spatial distribution of properties as they relate to mixing processes is often ignored. The difficulty in quantifying the spatial correlation structure is that the properties of interest seem to exhibit different patterns of variability over different scales of measurement. Recently, many of these apparently random variations at different scales of measurement have been found to display characteristics of similarity across different scales of measurement (Gleick, 1987; Hewett, 1986). The concept of this apparent "order within chaos" is the basis for the emerging study of fractal theory and its application to processes in nature. In the

current study, an examination was carried out of the distribution of porosity, permeability and pore throat sizes using mercury porosimetry techniques. Spatial correlation of these properties were examined using fractal methods and an attempt was made to provide an improved estimator of heterogeneity which incorporated a fractal component to account for spatial distribution. Specifically, the following topics were investigated:

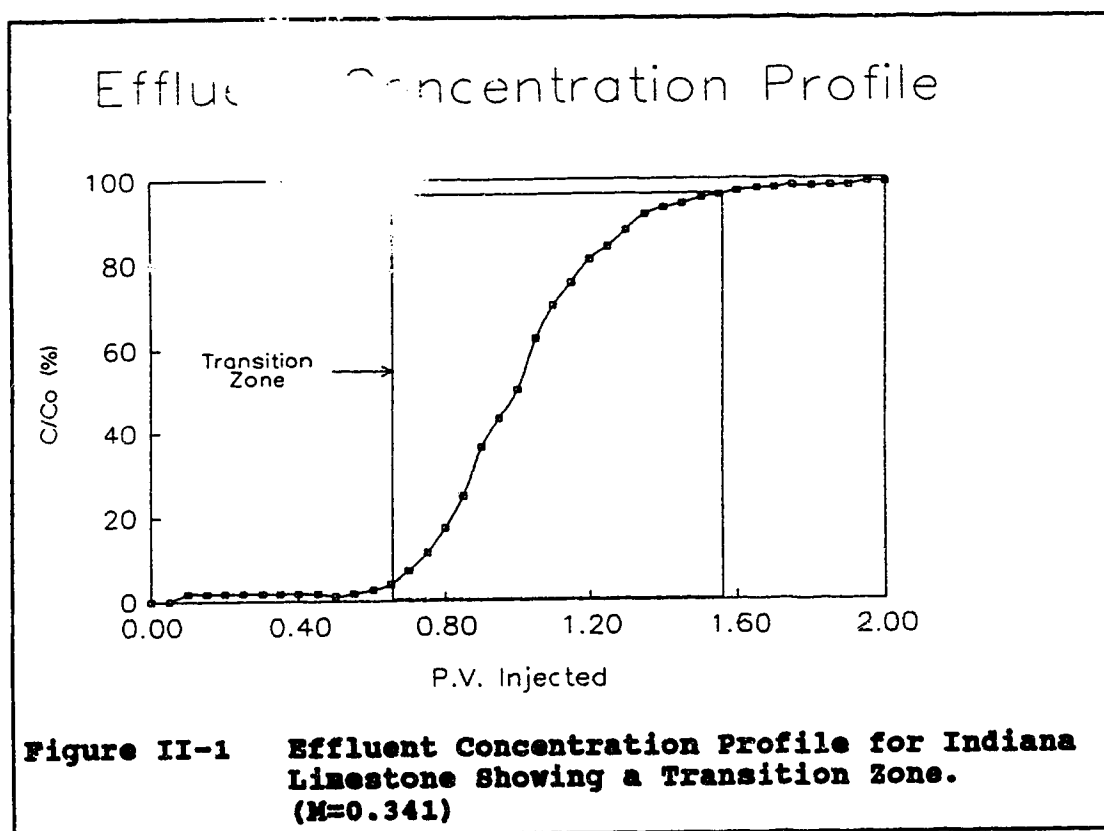
1. Relationship between floodrate, convective dispersion (K_c) and recovery factor.
2. Effect of lithology on convective dispersion (K_c) and recovery efficiency.
3. Effect of permeability, porosity and mean pore throat size variances on convective dispersion and recovery efficiency.
4. Relationship between fractal dimension of permeability, porosity and mean pore throat size and dispersion and recovery behavior.
5. Comparison of V_{Dr} , Koval's H factor and a fractal estimator of heterogeneity (D_{acf}) with dispersion and recovery factor.
6. Scale dependent dispersivity and the fractal heterogeneity estimator D_{acf} .

II. Review of Diffusion and Dispersion

A. Introduction

Factors affecting the mixing of fluids at the flood front can have a profound effect upon the efficiency of the displacement process. In this context, mixing may be considered to be a microscopic process arising from velocity contrasts within the porous medium (convective dispersion) as well as the effects of molecular diffusion (Blackwell, 1962). Studies by Spence and Watkins (1980), among others, have found that there is an inverse relationship between the magnitude of convective dispersion and displacement efficiency. This finding has important implications not only for the oil industry, but in the area of groundwater hydrology as well. A large amount of research has been conducted in both fields aimed at quantifying the mechanisms associated with dispersion. Of particular interest has been the study of the effect of spatial arrangement of pore space as it relates to convective dispersion.

Figure II-1 illustrates a typical effluent concentration profile obtained in the current study for a first contact miscible displacement in Indiana limestone.



In this case, the mobility ratio was favorable and the porous medium relatively homogeneous. Typically, mixing between the solvent and the resident fluid results in the formation of a transition zone of finite thickness which separates 100% solvent from 100% resident fluid. Under conditions of favorable mobility ratio, eg. no viscous fingering, the thickness of this transition zone is the result of three main processes:

1. Molecular Diffusion
2. Convective Dispersion
3. Channeling

Convective dispersion as described by the effective dispersion coefficient K , used in this study is a function of these processes to varying degrees. It is possible to vary the parameters of the miscible displacement in order to emphasize the effect of individual processes. This aspect will be discussed further in Chapter V.

Mixing caused by molecular diffusion in a porous medium is often represented by a modification of the Fick diffusion equation (Stalkup, 1983).

$$\frac{dG}{dt} = -DFA\phi \frac{\partial C}{\partial x} \quad (11-1)$$

Where: G = quantity of solute diffused across a sharp interface.

D = molecular diffusion coefficient.

C = concentration.

A = cross-sectional area.

F = formation resistivity factor.

t = time.

x = distance.

ϕ = porosity.

For miscible fluids flowing in a porous medium, more mixing occurs than can be accounted for by molecular diffusion alone. Convective dispersion and channeling play

a major role in mixing processes at both the laboratory and field scale (Perkins and Johnston, 1963; Coats and Smith, 1964). Variations in the interstitial velocity field at microscopic scales result in a combination of streamlines having markedly different solvent concentrations (Figure II-2).

Figure II-2 illustrates mixing of streamlines 1 and 2 in pore A. The equalized solvent concentration then proceeds to pore C where mixing with streamline 3 takes place. Convective dispersion may occur as longitudinal dispersion parallel to flow and/or as transverse dispersion normal to flow (Figure II-3).

This figure was removed due to the unavailability of copyright authorization. This figure showed a schematic diagram of convective dispersion on a pore scale in a porous medium.

The original reference is fig. 3.3 on pg. 33 of the reference cited below.

**Figure II-2 Convective Dispersion in Porous Media
(from Stalkup, 1983)**

This figure was removed due to the unavailability of copyright authorization. This figure showed a schematic diagram of mixing in longitudinal and transverse directions in a porous medium.

The original reference is fig. 3.2 on pg. 32 of the reference cited below.

**Figure II-3 Mixing by Longitudinal and Transverse Dispersion in a Porous Medium.
(from Stalkup, 1983)**

Based upon a review of published data, Perkins and Johnston (1963) proposed empirical equations for longitudinal and transverse dispersion coefficients. These equations are based on miscible floods using fluids of equal density and viscosity:

$$K_l = D_o \left\{ \frac{1}{F\phi} + 0.50 \frac{v\sigma d_p}{D_o} \right\}, \quad \frac{v\sigma d_p}{D_o} < 50 \quad (\text{II-2})$$

$$K_t = D_o \left\{ \frac{1}{F\phi} + 0.0157 \frac{v\sigma d_p}{D_o} \right\}, \quad \frac{v\sigma d_p}{D_o} < 10^4 \quad (\text{II-3})$$

Where: K_l = coefficient of longitudinal dispersion.

K_t = coefficient of transverse dispersion.

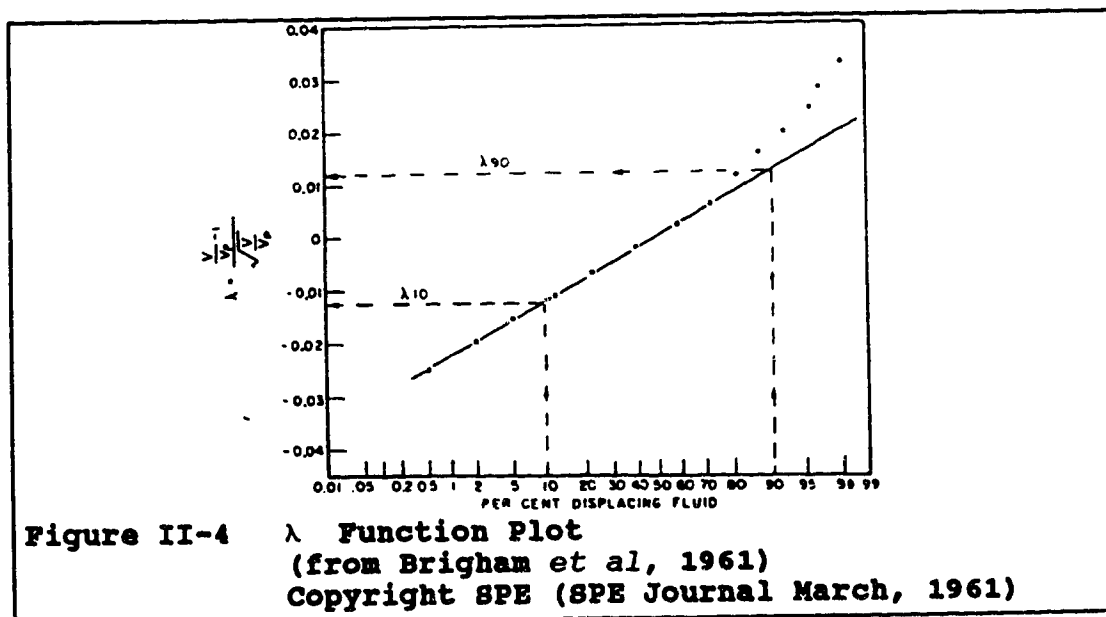
v = average darcian velocity.

D_o = molecular diffusion coefficient.

d_p = average particle diameter.

An examination of these two equations suggests several important results. At low fluid velocities the molecular diffusion term will tend to dominate and $K_t \approx K_d$. Under stable displacement conditions in the absence of gravity effects K_t will tend to dominate the mixing process with increasing fluid velocity. An examination of the dispersion terms of Equations II-2 and II-3 indicates that K_t will increase at a rate approximately 30 times that of K_d under these conditions.

Channeling of solvent through conduits of increased or decreased permeability is not addressed explicitly in the formulation of Equations II-2 and II-3 but is implicitly included in most calculation methods used for determining K_t and K_d .



Brigham (1974) describes a simple method for determining K_L . The λ function method is shown in Figure II-4. The λ function is plotted vs the percent displacing fluid (on an arithmetic probability scale). The dispersion coefficient may then be calculated from Equation II-4:

$$K_L = vL \left\{ \frac{\lambda_{90} - \lambda_{10}}{3.625} \right\}^2 \quad (\text{II-4})$$

$$\text{Where: } \lambda = \frac{\frac{V}{V_p} - 1}{\sqrt{\frac{V}{V_p}}}$$

$$\frac{V}{V_p} = \text{pore volumes injected.}$$

$$v = \text{darcian velocity.}$$

$$L = \text{length of the core.}$$

$$K_L = \text{longitudinal dispersion coefficient.}$$

Equation II-4 uses the width of the transition zone $(\lambda_{90} - \lambda_{10})$ as an indicator of K_L . The transition zone length will be significantly influenced by channeling or viscous fingering if it occurs. As a result, K_L will be a function of other factors in addition to the irregularity of the pore space under consideration. In general, as K_L increases, the recovery factor associated with the miscible flood will decrease. This result has been reported by several workers and occurs as a direct result of the adverse effect of heterogeneity upon the thickness of the transition zone (Koval, 1963; Spence and Watkins, 1980).

For the purposes of the current study, only the effects of longitudinal dispersion and channeling will be examined in detail.

A review of the literature reveals numerous attempts to model miscible mixing behavior through the use of mathematical models (Aronofsky and Heller, 1957; Coats and Smith, 1964). These models were developed by solving second order differential equations describing mass transport by dispersion within a porous medium. The following discussion will center on several models used to describe miscible flooding behavior.

B. Convective - Dispersion Model

The generalized form of the convective-dispersion (C-D) equation is given by Equation II-5 (Brigham, 1974).

$$K_l \frac{\partial^2 C}{\partial x^2} - v \frac{\partial C}{\partial x} = \frac{\partial C}{\partial t} \quad (\text{II-5})$$

Where: K_l = longitudinal dispersion coefficient.

x = distance from the inlet end of the core.

v = darcian velocity.

C = relative solvent concentration.

This equation may be solved by Laplace transform techniques under the appropriate boundary conditions. The choice of boundary conditions is not critical when the width of the transition zone is short compared with the

length of the porous medium (Brigham, 1974). Under laboratory coreflood conditions the following boundary conditions and solution result:

$$\begin{aligned} \text{Boundary Conditions:} \quad x = 0, \quad C = 1 \\ x \rightarrow \infty, \quad C \rightarrow 0 \end{aligned}$$

$$C = \frac{1}{2} \operatorname{erfc} \left\{ \frac{x - vt}{2\sqrt{K_l t}} \right\} + \frac{1}{2} e^{\frac{vx}{K_l}} \operatorname{erfc} \left\{ \frac{x + vt}{2\sqrt{K_l t}} \right\} \quad (\text{II-6})$$

Where: C = relative solvent concentration at the outlet.

v = darcian velocity.

t = time.

K_l = longitudinal dispersion coefficient.

erfc = complementary error function.

This equation may be history matched to effluent concentration profiles by setting x equal to L and expanding the second term of Equation II-6 using a Taylor series approach:

$$C = \frac{1}{2} \operatorname{erfc} \left\{ \frac{L - vt}{2\sqrt{K_l t}} \right\} + \frac{1}{2\sqrt{\pi}} e^{-\left\{ \frac{L - vt}{2\sqrt{K_l t}} \right\}^2} \cdot \left\{ \frac{2\sqrt{K_l t}}{x + vt} - \frac{1}{2} \left(\frac{2\sqrt{K_l t}}{x + vt} \right)^3 \right\} \quad (\text{II-7})$$

Where: L = length of the core.

The derivation of this equation makes the following assumptions:

1. One dimensional flow.
2. First contact miscibility.

3. Dispersion is only significant parallel to flow.
4. Incompressible fluids.
5. Favorable mobility ratio.

The mobility ratio referred to in assumption five is simply the ratio of the viscosity of the resident oil divided by the viscosity of the displacing fluid. The preceeding conditions will be met in a properly designed laboratory coreflood. Brigham (1974) found that determination of K_i by the λ factor method (Equation II-4) is valid even under conditions where the boundary conditions applied to the convective-dispersion equation change eg. an infinite length boundary condition is not necessary. This implies that, for all practical purposes, only the first error function term of Equation II-7 is important when determining K_i . This reduces Equation II-7 to:

$$C = \frac{1}{2} \operatorname{erfc} \left\{ \frac{L - vt}{2\sqrt{K_i t}} \right\} \quad (\text{II-8})$$

This result is simply the solution to the C-D equation when an infinite length boundary condition is applied. The C-D model allows for the direct calculation of K_i as all of the other quantities will be available as parameters in a coreflood. The C-D equation described has the disadvantage of not accounting for dead-end pore volume in the porous medium and also does not address the problem of scale

dependence in convective dispersion. In cases where a significant portion of the pore space consists of dead-end pores, a more sophisticated approach will be required (Baker, 1977).

C. Coats - Smith Model

A more sophisticated approach to the modelling of effluent concentration profiles was proposed by Coats and Smith in 1964. In this model, resident oil is assumed to be trapped in dead-end or occluded pore space. This dead-end pore space is only accessible to the flowing solvent at a single point with mass transfer occurring by diffusional processes only. The Coats-Smith model is a modification of the convective-dispersion (C-D) model in which terms accounting for a stagnant volume are added. All assumptions implicit in the development of the convective-dispersion model also apply to the Coats-Smith model. Equation II-9 illustrates the one-dimensional dimensionless form of their equation.

$$\frac{1}{P_*} \frac{\partial^2 C_D}{\partial X_D^2} - \frac{\partial C_D}{\partial X_D} = f \frac{\partial C_D}{\partial t_D} + (1-f) \frac{\partial C_D^*}{\partial t_D} \quad (\text{II-9})$$

$$\text{and: } (1-f) \frac{\partial C_D}{\partial t_D} = D_a (C_D - C_D^*)$$

$$\begin{array}{ll} \text{Boundary conditions: } X_D \rightarrow 0.0 & C_D \rightarrow C_D(t_D) \\ & X_D \rightarrow \infty & C_D \rightarrow 0.0 \end{array}$$

Where: P_e = Peclet number = $\frac{vL}{D_l}$

D_a = Damkohler number = $\frac{KL}{v}$

f = mobile fraction.

C_D, C_D^* = dimensionless concentration in mobile and stagnant fractions, respectively.

t_D = dimensionless time = $\frac{tv}{L}$

X_D = dimensionless distance = $\frac{x}{L}$

K = mass transfer coefficient.

D_l = longitudinal dispersion coefficient.

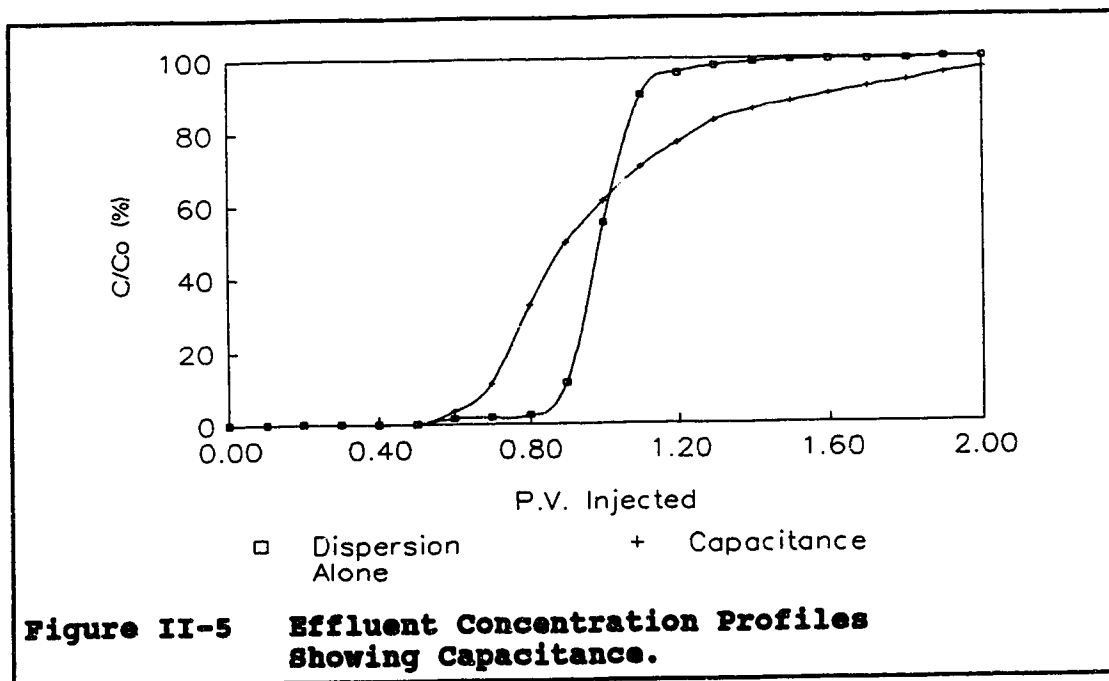
L = core length.

Equation II-9 is represented by three dimensionless parameters, the Damkohler number (D_a), the mobile fraction (f) and the Peclet number (P_e) which control the behavior of the Coats-Smith model and its ability to match effluent concentration profiles. As pointed out by Jasti et al (1987), D_a and P_e are highly velocity dependent. For sufficiently small velocities, D_a will be large and mass transfer by diffusive processes will be essentially instantaneous (Coats and Smith, 1964). Under these conditions, Equation II-9 reduces to the simple C-D equation discussed earlier with $\frac{1}{P_e} \approx \frac{D_l}{L}$. In physical terms, this has the effect of reducing the relative contribution

of convective dispersion and describes a narrower transition zone in the effluent concentration profile. For cases where v is large, D_a becomes insignificant and Equation II-9 once again reduces to the C-D equation. In this case, convective dispersion is dominant over diffusion and $\frac{1}{P_e} \cong \frac{D_l}{v}$. Under these conditions, Perkins and Johnston (1963) show that D_l is approximately proportional to v so that $\frac{1}{P_e} \cong D_l$. The flowing fraction f appears to be relatively insensitive to variations in the Darcian velocity. Studies by Baker (1977) and Jasti et al (1987) suggest that f is a function of the porous medium only. The flowing fraction f has been defined as the break-through pore volume observed in an experiment conducted at high fluid velocities. This method of defining f is conceptually identical to the phenomena of channeling implicitly accounted for in the longitudinal dispersion coefficient D_l , which forms part of the convective-dispersion equation.

The prime advantage afforded by the Coats-Smith model is its ability to fit effluent concentration profiles which exhibit "tailing" of the concentration curve as a result of gradual mass transfer from dead-end pore space by diffusion processes. Figure II-5 shows that in the case of capacitance where dead-end pore space causes stagnant regions within the porous medium, tailing of the

concentration curve is much more pronounced and dispersion alone cannot account for it. This figure uses data from the current study. The curve depicting capacitance was from a miscible flood in Golden Spike limestone while the other curve is the result of a displacement at an equivalent rate in Berea sandstone.



Another advantage is the explicit treatment of the contribution of channeling through the use of the flowing or mobile fraction, f . The major disadvantage to the Coats-Smith model is that it is a multiple parameter model and, as such, encounters the problem of non-uniqueness of parameters. Typically, the parameters (D_a), f and (P_s) are

chosen to provide the best fit to the observed effluent concentration profile from a laboratory coreflood. As Baker (1977) and Stalkup (1983) have pointed out; however, there are different combinations of model parameters which will yield an equally good fit to the experimental data. As a result of this, model parameters estimated solely through best-fit techniques may lack practical significance.

D. Other Related Work

Most related work in the area of miscible displacement modeling has centered on refinements to the original C-D and Coats-Smith models. Brigham (1974) correctly recognized that the original analytical solutions obtained for these equations described *in-situ* solvent concentrations and were inappropriate for matching effluent concentration profiles. The use of the original solutions in modelling laboratory data resulted in serious material balance errors and new solutions for the original equations applicable to effluent concentrations were derived.

Baker (1977) provided a means of relating the effective dispersion coefficient, which governs field-scale floods, to the Coats-Smith parameters obtained from laboratory corefloods. Capacitance caused by dead-end pore space tended to increase the length of the transition zone above the length that would be expected from longitudinal

dispersion alone.

In general, neither the convective-dispersion model or the Coats-Smith model are able to account for the effect of viscous fingering. As a result, their use has been confined to miscible displacements with favorable mobility ratios. Vossoughi et al (1984) describe a method of modifying the C-D equation to account for the effect of viscous instabilities. This method was used with success in the modelling of polymer flow by introducing dead-end pore volume and polymer retention terms to the original differential equation.

Correa et al (1987) used simplified solutions to the Coats-Smith, porous sphere and transverse matrix diffusion models to interpret effluent concentration profiles from heterogeneous cores. Using simplified solutions in Laplace space, they developed a means of estimating a unique set of parameters (eg. (D_e) , f , and (P_e)) which apply to any of the three parameter models they studied.

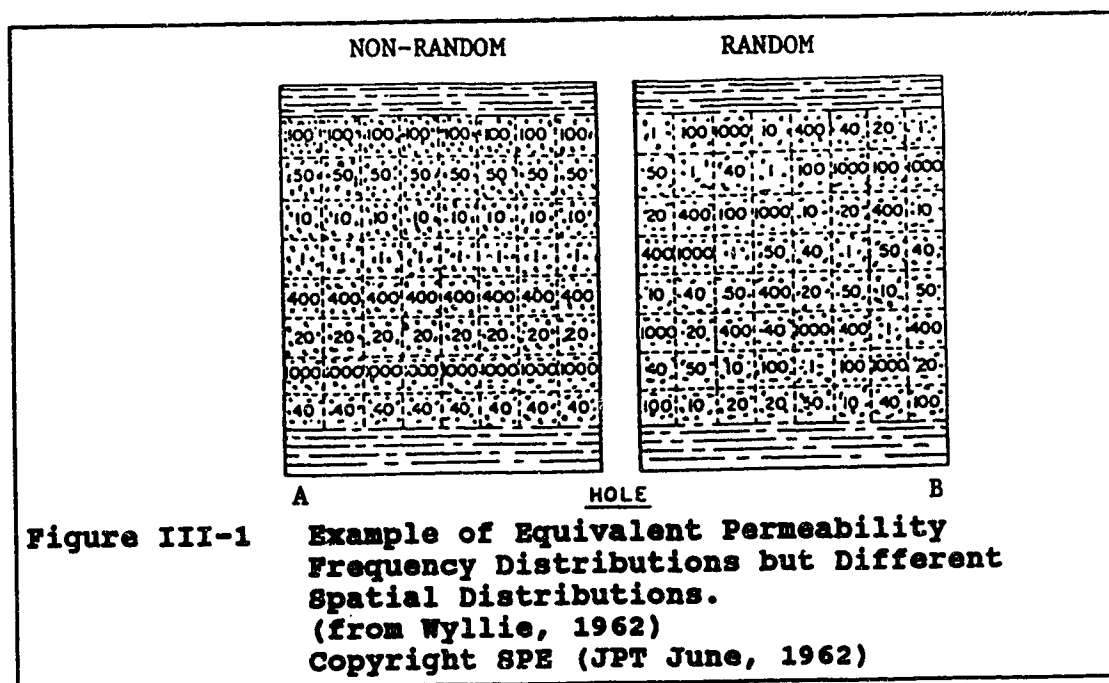
III. Pore Structure Effects

A. Introduction

The most commonly measured properties of a porous medium are porosity and permeability. For the case of immiscible displacement, studies have indicated a positive correlation between porosity and recovery efficiency as well as a lack of correlation between permeability and recovery efficiency (Wardlaw, 1976). Although in common use, recent studies have indicated that porosity and permeability alone may not be good indicators of producibility (Jodry, 1972; Wardlaw, 1976; Bretz et al, 1988). Another approach to this question involved determining the relationship between pore size and recovery efficiency. Wardlaw (1976) found an inverse relationship between pore to throat size ratios and non-wetting phase displacement efficiency. Also recognized was a positive correlation between pore throat to pore coordination number and recovery efficiency. These studies were conducted under conditions of immiscible displacement and may not be valid under miscible conditions.

The relationship between pore structure and dispersion in miscible flooding has been investigated by several workers (Spence and Watkins, 1980; Bretz et al, 1988). A common approach to the problem has been to examine the

relationship between recovery efficiency and permeability distribution (Perkins and Johnston, 1963; Warren and Price, 1961; Warren and Skiba, 1964). This approach, while having the advantage of simplicity, does not address the difficulties inherent in the non-uniqueness of the permeability frequency distribution chosen. Figure III-1 illustrates this effect. Both sides of the figure have "similar frequency distributions" but "different spatial distributions" of permeability.



Bretz et al (1988) interpreted the effect of differing frequency and spatial distributions of pore size in terms of the Coats-Smith model for miscible displacement. While a

broadening of the frequency distribution curve could be correlated with an increase in convective dispersion, the *spatial correlation of the pore sizes* also played a large role in the behavior of the displacement. This finding is not surprising in that spatial correlation of large and small pore sizes will often lead to systematic variations in permeability which can lead to channeling of the solvent and an increase in the apparent dispersion coefficient. Despite the fact that spatial correlation structure is of importance to fluid flow most measures of heterogeneity make the assumption that porosity and permeability are randomly distributed (McCaffery et al, 1978). Porosity and permeability development in nature occurs in response to geological processes which are "non-random" in both a lateral and vertical sense. Thus, the assumption of randomness of porosity and permeability on an areal scale may not be valid.

B. Geological Aspects

Studies of heterogeneity often assume that porosity and permeability are randomly distributed throughout the porous medium (Wyllie, 1962; Warren and Price, 1961). While this assumption may be reasonable on the scale of individual pores, it does not account for the influence of geological processes upon porosity and permeability distributions at

larger scales.

From an areal standpoint, the distribution of porosity and permeability have been shown to be related to the type of reservoir rock present in a given location (McCaffery, 1978; Blatt et al, 1980). Langton and Chin (1968), and McCulloch et al (1969) showed a distinct correlation between porosity and permeability and the occurrence of depositional environments in a carbonate reservoir at Rainbow Lake. The distribution of these depositional environments in space is predictable using current geological methods. In general, the lateral distribution of reservoir rocks is determined by the relationship between sediment supply and the energy level of the depositional environment. Under conditions of a marine transgression, where water depths are gradually increasing, the depositional environments shown in Figure III-2 will gradually prograde inland. The high-energy, shallow-water environments will tend to deposit more coarse-grained and well-sorted sediments which tend to form rocks having high porosity and permeability. Conversely, low-energy, deep-water environments result in the deposition of finer grained clays and mudstones with poor porosity and permeability characteristics.

This figure was removed due to the unavailability of copyright authorization. This figure showed the relationship between the vertical geological record and depositional environments.

The original reference is fig 19-1 on pg. 620 of the reference cited below.

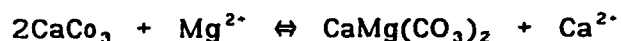
**Figure III-2 Application of Walther's Law
to Lateral Depositional Environments
(from Blatt et al, 1980)**

A fundamental principle in the geological sciences is Walther's law of succession of facies. In it's simplest form, it states that rocks which are deposited in a lateral sequence will also show the same sequence in cross-section (Figure III-2). This principle is valid provided that the depositional record is continuous, eg. subsequent erosion has not removed any of the rock layers. If the vertical succession of rock types is related to areal environments of deposition which obey non-random physical laws, then it is reasonable to assume that vertical rock sequences may also be non-random. Studies by Cant and Walker (1976) used

Markov chain analysis to demonstrate spatial correlation of rock sequences in a vertical sense. Hence, porosity and permeability distributions are non-random if a sufficiently large scale of investigation is applied. Recent studies (Burrough, 1981; Hewett, 1986; Goggin, 1988) suggest that spatial correlation may also exist at smaller scales of measurement and that the behavior of spatial correlation may be fractal in nature. This possibility will be discussed in a later section.

The vast majority of oil bearing reservoirs are composed of either carbonates or sandstones. Both of these rock types develop porosity and permeability distributions characteristic of their environments of deposition, but through different processes. The fact that carbonate reservoirs are organic in nature tends to complicate studies of their patterns of heterogeneity. Modern analogs to ancient carbonate environments indicate that water depth, temperature and salinity are the controlling factors. Carbonate rocks exhibit a much more variable nature than do sandstones. Carbonates exhibit their greatest porosity and permeability immediately after deposition. Subsequent burial and compaction causes a sharp reduction in the original porosity and permeability in response to changes in the subsurface stress field,

temperature and chemistry of meteoric waters. The particles which comprise limestones are primarily biological in origin and may contain a significant amount of intra-particle porosity and permeability. These rocks are; by definition, composed almost exclusively of calcium carbonate and aragonite. These minerals are highly soluble in meteoric waters leading to dissolution of the matrix in some locations and a reprecipitation of carbonate as pore-filling cements in other areas. In addition to dissolution and cementation of pore space, replacement of calcite is also a common occurrence. The circulation of Mg^{2+} -rich groundwaters through the carbonate matrix causes the recrystallization of calcite to form dolomite by the following reaction (Blatt et al, 1980):



This reaction is significant in that dolomitization improves the producibility of the rock due to a transformation of the pore structure and an increase in porosity.

Diagenetic alteration is a complex process related to the geochemical stability of the matrix under local conditions of pressure, temperature and cation saturation

within circulating groundwaters. Interplay of these factors in carbonate rocks results in an extremely heterogeneous pore structure which may greatly increase dispersion and channeling under miscible displacement conditions. Chilinger (1972) states that the effect of diagenetic alteration of carbonates is such that quantitative measures of porosity and permeability may no longer offer a satisfactory indicator of the producibility of the rock. Under these conditions, a study of the pore to pore correlation structure is essential to a proper determination of producibility (Jodry, 1972; Wardlaw, 1976; Wardlaw and Cassem, 1978).

Sandstones are, in general, much more areally continuous than carbonates and display significantly different characteristics. Like carbonates, most sandstones experience a sharp reduction in porosity and permeability upon lithification. Unlike carbonates, however, sandstones are composed of dense, volcanically derived quartz and feldspar particles which contain little or no intra-particle porosity or permeability. As a result porosity and permeability is inter-granular in nature in these rocks. Post-depositional diagenetic alteration of sandstones by circulating meteoric waters has been found to produce only minor alteration of the pore structure (Blatt

et al, 1980). Alteration of grain boundaries through pressure dissolution and mineral cementation will occur under conditions of high temperature and pressure however, the relative insolubility of quartz and feldspar serves to minimize this effect. Hence, the pore structure in sandstones is fairly homogeneous resulting in a fairly direct influence of porosity and permeability upon the producibility of the rock (Jodry, 1972).

IV. Methods of Spatial Correlation

The use of deterministic methods in the assessment of spatial correlation structure requires a complete description of the parameter of interest with respect to space. While this requirement is satisfied for properties which are homogeneous over a given sample space, it is difficult to describe heterogeneous systems in complete deterministic detail (Mishra, 1987). The intermittent nature of sampling in the current study thus rules out deterministic methods in the study of spatial correlation. As a result, a stochastic approach is required whereby the observed properties will be treated as random variables with a known mean and variance (Journel and Huijbregts, 1978).

The current study is concerned with defining an improved estimator for heterogeneity at the core level incorporating a component of spatial correlation. One such component is available through the use of fractal analysis. Fractal analysis is a mathematical technique which is useful in defining the "irregularity" or spatial heterogeneity of a particular property. In this study, the irregularities of permeability, porosity and pore throat size were studied using this technique. Determining spatial heterogeneity in this context requires a determination of the Hausdorff - Besicovitch (fractal) dimension of the data series. Recent

studies (Hewett, 1986; Goggin, 1988) indicate that large scale reservoir properties such as permeability distributions also display fractal characteristics. The remainder of this chapter outlines the basics of fractal theory and describes methods of application employed in the current study.

A. Fractal Theory

1. Introduction

Fractal theory, in it's present form, may be traced to studies conducted by Benoit Mandelbrot two decades ago. Mandelbrot (1971) provided a mathematical framework for the description of irregular and complex shapes found in nature. Fractal geometry has since been used to fit a variety of natural property distributions. Natural phenomena ranging from annual flowrates in rivers and the geometry of blood vessels (Gleick, 1987) to permeability distributions in porous media (Hewett, 1986; Goggin, 1988) have been modeled with fractals. The search for fractal behavior in sedimentary rocks is closely linked to the fractal nature of hydrological cycles. Since most reservoir rocks were deposited under aqueous conditions and were subsequently subjected to diagenetic alteration in response to varying hydrogeological conditions, it would seem reasonable that the distribution of properties

within the rock may also be fractal in nature.

The term "fractal" may be described through the concept of "self-similarity". Self-similarity implies symmetry across scales of measurement. Hewett (1986) provides the following description:

"Fractals are characterized by the fact that they exhibit variations at all scales of observation and have partial correlations over all scales. Every attempt to divide such a geometry into smaller, more uniform regions results in the resolution of even more structure or roughness. The closer you look, the more detail you see."

By way of illustration, consider a coastline. Observed from an orbiting satellite, it appears to be very irregular. Move closer and the scale of observation changes, yet the degree of irregularity does not. Even at a distance of several feet the water is observed to meet the sand in an irregular pattern. The irregularity of the coastline is statistically "self-similar"; the degree of irregularity is the same at any scale of observation (Wheatcraft and Tyler, 1988). This characteristic irregularity may be quantified by a parameter called the fractal dimension.

2. Fractal Dimension

Consider the following simple equation in one dimension:

$$F = N\xi^\eta \quad (\text{IV-1})$$

Where: η = dimension in euclidean space.

($\eta = 1$)

N = number of measurements.

ξ = length of measurement.

F = length of a line.

For the one dimensional example if the length of F is fixed, then ξ is proportional to N . For simple geometrical shapes in η - dimensional euclidean space the above relationship is satisfied. eg.

$$\lim_{\xi \rightarrow 0} (N\xi) = F \quad (\text{IV-2})$$

As the length of the measurement decreases the number of measurements (N) increases accordingly and F remains constant. Under conditions of self-similarity, however, this may not be the case. Returning to the example of the irregular coastline it may be observed that $F \rightarrow \infty$ as $\xi \rightarrow 0$ (Wheatcraft and Tyler, 1988). A three dimensional example of this may be observed for the case of ordinary chalk. As the measurement scale decreases, the surface area rapidly increases. This implies that decreasing the scale at which an observation is made reveals increased irregularity. In general, the following equation describes this scale dependence:

$$F = N\xi^{\eta-D} = \text{constant} \quad (\text{IV-3})$$

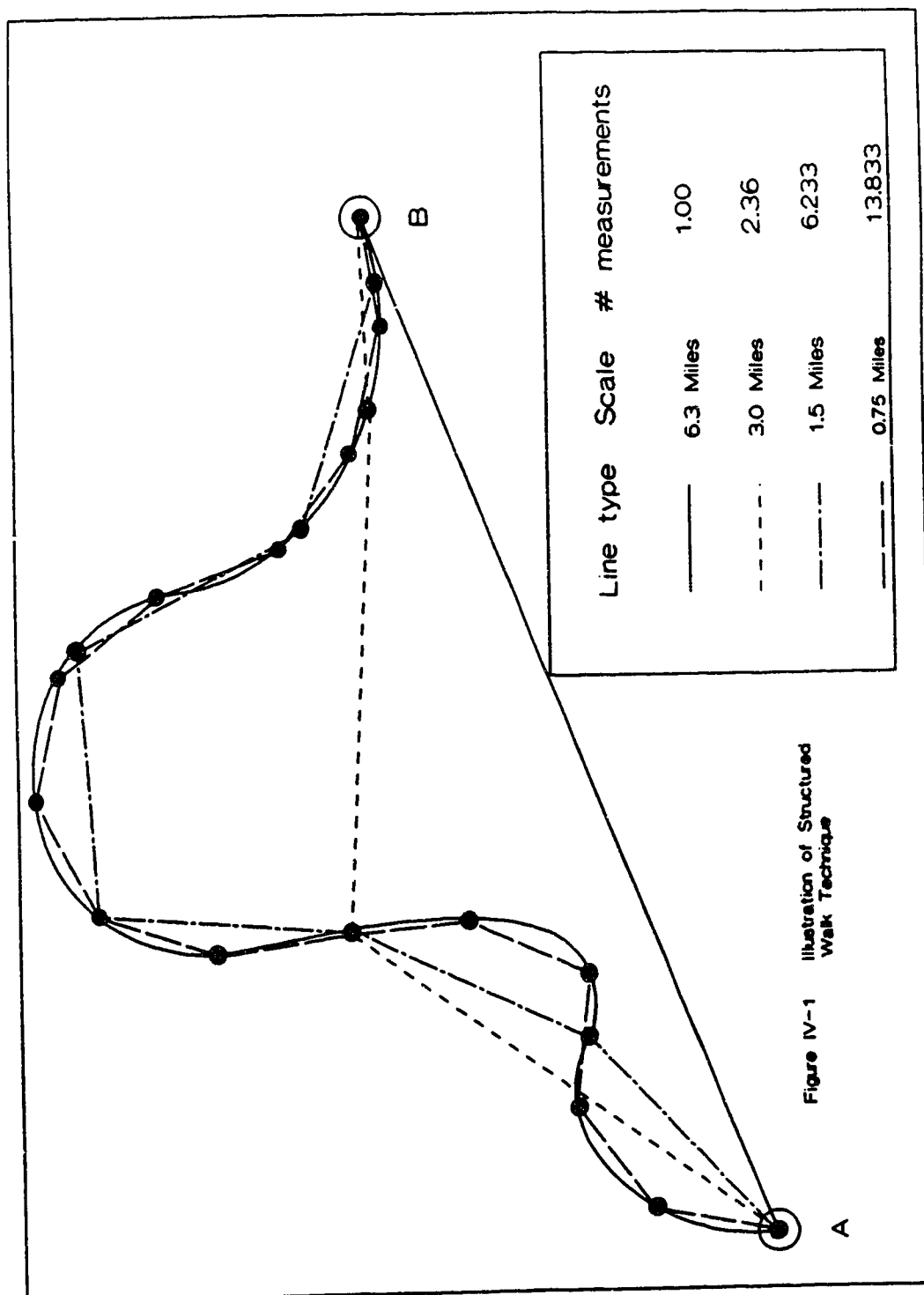
Where: D = fractal dimension and $D \leq \eta$.

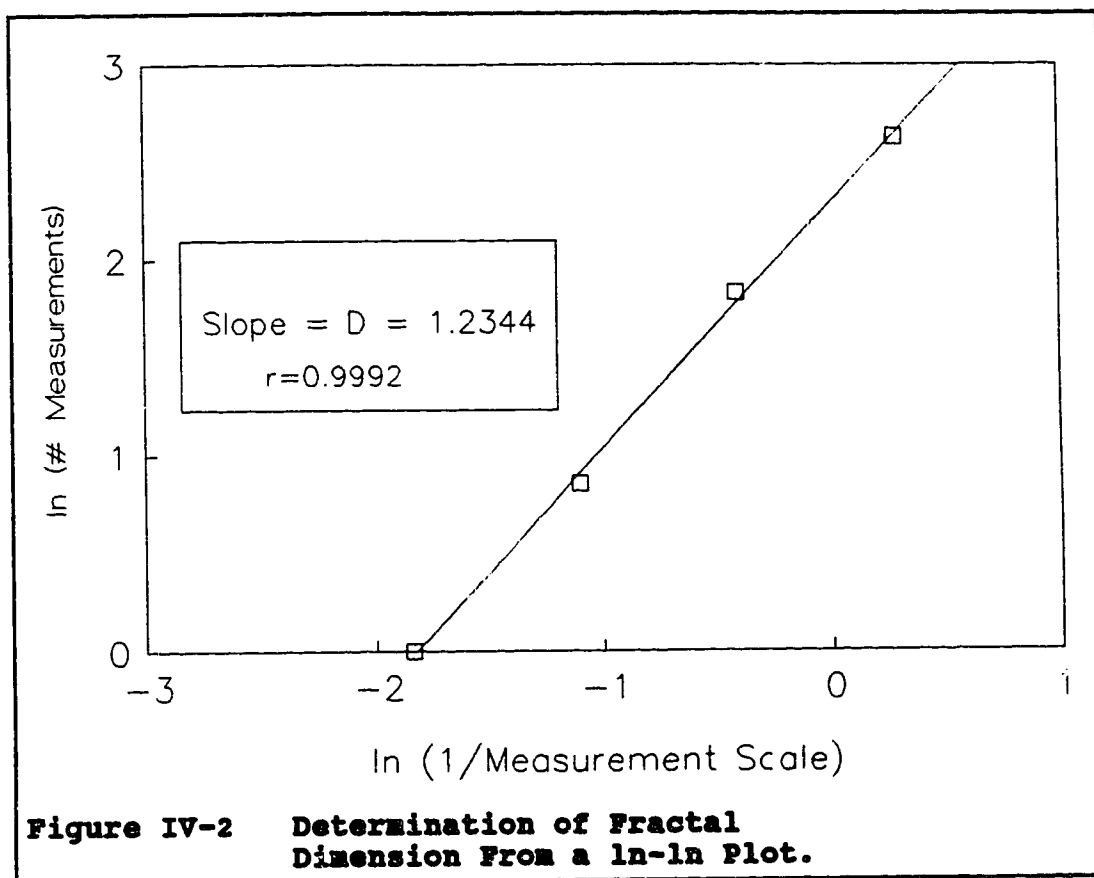
D is the dimension which provides a constant value for F as the scale ξ changes. If Equation IV-3 is re-arranged and solved for D the following equation is obtained:

$$D = \lim_{\xi \rightarrow 0} \left\{ \frac{\ln N}{\ln \frac{1}{\xi}} \right\} \quad \text{For a constant } F. \quad (\text{IV-4})$$

This result is the basis for the box counting theorem which is sometimes used to calculate fractal dimension (Barnsley, 1988). In the box counting technique, the number of boxes (N) of side length (ξ) required to cover an irregular surface is determined for a range of ξ values. The slope of a plot of $\ln N$ vs $\ln \frac{1}{\xi}$ then approximately defines the fractal dimension of the surface. A variation of this technique applicable to irregular, two-dimensional curves is the so called "structured walk" method. Returning to the example of the coastline, we may define two points of reference A and B. Four measurements of the length of this coastline are taken, each time using a measuring stick of shorter length. The only rule in the measurement process is that the measuring stick cannot be bent. Figure IV-1 illustrates this process.

For the first measurement, a measurement scale of 6.3 miles was used. Under these conditions, only a single measurement was required and the length of the shoreline was 6.3 miles. During the second measurement, a scale of 3.0 miles was chosen and 2.36 measurements were required to reach point B. This procedure was repeated for scales of 1.5 and 0.75 miles, respectively. The results of these measurements are summarized in Figure IV-1. Figure IV-2 shows a plot of the natural log of the number of measurements vs the natural log of the reciprocal of the measurement scale employed. From Equation IV-4, the fractal dimension may be represented by the slope of the best-fit line through these points. From Figure IV-2, the fractal dimension describing the irregularity of our imaginary coastline is 1.2344. This means that the degree of irregularity or roughness of the curve may be defined as constant over the scales of measurement used in the analysis. It should be pointed out, however, that this does not necessarily mean that the same fractal dimension applies to measurement scales larger or smaller than those evaluated.





From Equation IV-4, the fractal dimension may be represented by the slope of the best-fit line through these points. From Figure IV-2, the fractal dimension describing the irregularity of our imaginary coastline is 1.2344. This means that the degree of irregularity or roughness of the curve may be defined as constant over the scales of measurement used in the analysis. It should be pointed out, however, that this does not necessarily mean that the same fractal dimension applies to measurement

scales larger or smaller than those evaluated. An indication of the applicability of the fractal dimension calculated for the observed scales of measurement may be obtained from the correlation coefficient (r) associated with Figure IV-2. As can be seen, the correlation of the best-fit line is excellent ($r=0.9992$). This implies that the degree of irregularity is constant over the measurement scales investigated. For two-dimensional objects such as irregular lines on x-y coordinates the fractal dimension D may vary between 1 and 2. For the limiting case where $D=1$ the geometrically simple case exists where the tracing is completely differentiable and is composed of simple line segments or arcs, eg. a simple polynomial function which may be differentiated into an infinite number of straight lines. For the case where $D=2$ the tracing is so rough and irregular that it effectively takes up the whole of two-dimensional space (Burrough, 1981). By way of illustration, a flat plane containing two points A and B has a fractal dimension of 2. In this case D is equivalent to the Euclidean dimension in which the plane lies, that is, the plane completely fills a two-dimensional space. Another object, formed from an irregular, non-differentiable line confined to the two-dimensional plane without crossing itself, may be

irregular enough to nearly fill two-dimensional space. The object is considered to have a fractional dimension since it is neither a line nor a plane in the standard geometrical sense (Barnsley, 1988). The co-dimension (H) of this object is a measure of the void space on the plane and is defined by $H = \eta - D$ where $\eta = 2$ (Goggin, 1988). The fractal co-dimension in Equation IV-3 is related to the semi-variogram in the following manner (Journel and Huijbregts, 1978):

$$\gamma(h) = \frac{1}{2} E \{ (Z(x+h) - Z(x))^2 \} = \frac{1}{2} \sigma^2 h^{2H} \quad (\text{IV-5})$$

Where: σ^2 is the total variance.

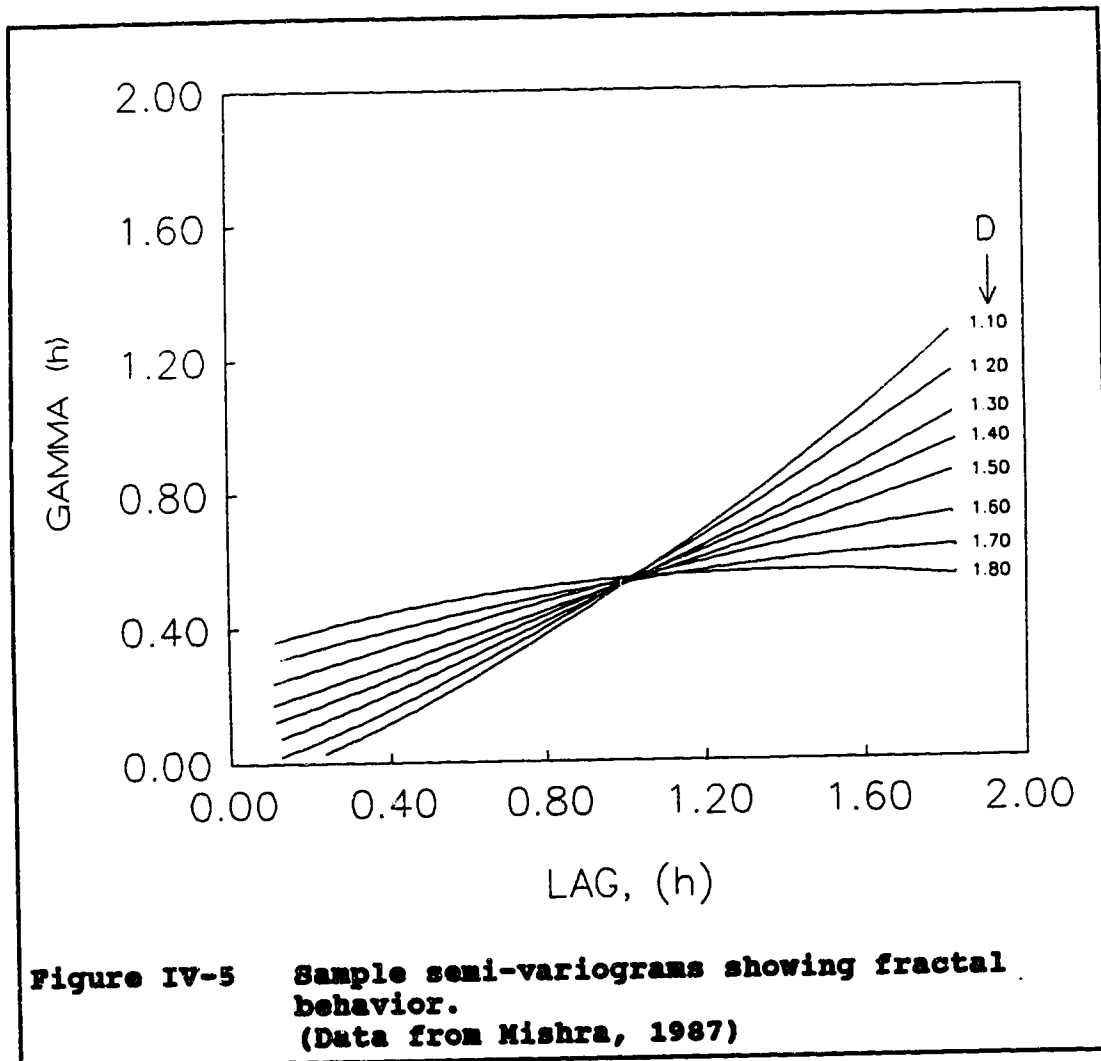
$$0 < H < 1$$

Equation IV-5 implies statistical self-similarity, because variance at any scale may be computed from the variance at any other measurement scale by the following relationship (Mishra, 1987):

$$\gamma(bh) = b^{2H} \gamma(h) \quad (\text{IV-6})$$

A visual realization of the effect of D on the shape of the semi-variogram curve is shown in Figure IV-5. The group of curves where $1.5 > D > 1.0$ ($0.5 < H < 1.0$) represent data which are more regular than ordinary white noise. Ordinary white noise is represented by $D = 1.5$ ($H = 0.5$) and traces where $1.5 < D < 2.0$ ($0.0 < H < 0.5$) are noisier and more erratic

than white noise (Mishra, 1987).



Stated another way, if $D < 1.5$, the data series may be considered to be heterogeneous in terms of long range effects eg. the data shows correlation at smaller scales of measurement. If $D > 1.5$, a process is described which tends to fluctuate between high and low values more

commonly than would be expected for a purely random variable.

The data series of interest in the current study consist of permeability, porosity and mean pore throat size values which are equally spaced in the spatial domain. These values could be plotted on Cartesian coordinates and the resulting curve analyzed for its irregularity using the structured walk technique previously illustrated. The disadvantage of such an approach is that this method is very time consuming and tedious to implement. Geostatistical methods provide a more convenient approach to the measurement of fractal dimension. The following section will describe two such methods which were employed in this study.

B. Geostatistical Methods

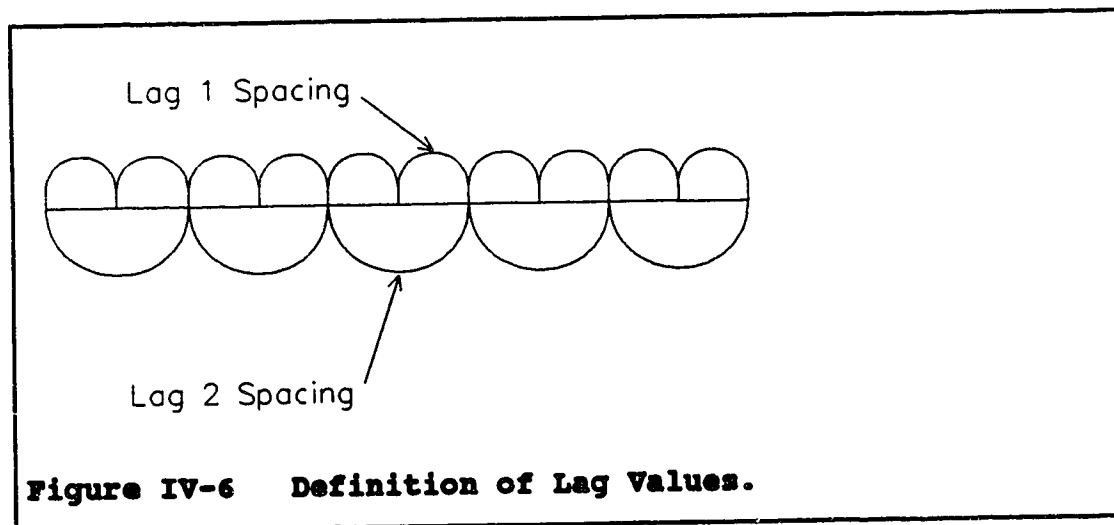
A regionalized variable may be defined as a variable distributed in space (Journel and Huijbregts, 1978). Several methods for determining a spatial correlation structure for regionalized variables are available. After a review of the literature, the following methods were chosen as the basis for a fractal analysis of the available data:

1. Autocorrelation functions.
2. Semi-Variogram analysis.

Before providing a detailed description of these methods and their relationship to the fractal dimension D , some statistical terminology will be briefly defined. The remainder of this chapter will then deal with fractal theory and provide a mathematical definition of the fractal dimension D .

Lag Distance (h)

In the discussion to follow, reference will be made to the lag distance h as it applies to a data series. By way of example, consider a core of a fixed length.



At regular intervals along the length of the core, a permeability value is obtained by removing a small sample and analyzing it by mercury porosimetry methods. In our discussion the length of the constant length interval between samples is the value of the lag distance h . For

example, lag 1 refers to one spacing interval between samples, lag 2 to two spacing intervals between samples, etc. For our example lag 1 spacing will provide 10 data values in the data series while lag 2 spacing will provide only 5 data points (Figure IV-6).

Mean, Variance and Autocovariance

A common measure of central tendency is given by the mean value defined in Equation IV-7.

$$\bar{\mu}_x = E = \frac{1}{n} \sum_{i=1}^n Z(i) \quad (\text{IV-7})$$

Where: $\bar{\mu}_x$ = mean value

$Z(i)$ = value at location i in the x direction

n = number of observations

The operator E is known as the expectation operator and is equivalent to the mean value. The mathematical expectation E may be applied to measurements of a particular property but is not limited to measurements. The variance for a series of measurements may be defined by Equation IV-8 where the expectation operator is applied to the squared difference between the value at a given location and the mean value for all locations.

$$\sigma_x^2 = E(Z(x) - \bar{\mu}_x)^2 = \frac{1}{n} \sum_{i=1}^n (Z(x) - \bar{\mu}_x)^2 \quad (\text{IV-8})$$

Where: σ_x^2 = variance

Variables separated by lag distance h may be related to one another through the use of the covariance function. In the case of measurements of the same property conducted at a regular lag spacing h , the term autocovariance is often employed. Equation IV-9 defines the autocovariance function:

$$C_v(x, x+h) = E((Z(x) - \bar{\mu}_x)(Z(x+h) - \bar{\mu}_x)) \quad (\text{IV-9})$$

Where: $C_v(x, x+h)$ = autocovariance function.

E = expectation operator.

$\bar{\mu}_x = E(Z(x))$

h = lag distance.

The preceding discussion will provide the reader with a basis for the following discussion of two methods of determining the correlation structure of a property in space. The discussion of each method will conclude with the procedure required to use each method in the determination of the fractal dimension D .

1. Autocorrelation Functions

If two random variables separated in space by lag h are of the same type, eg. permeability, then a measure of their spatial correlation may be obtained through the use of the autocorrelation function. The autocorrelation function is defined by:

$$C(x, x+h) = \frac{C_v(x, x+h)}{\sigma_x^2} = \frac{E\{(Z(x) - \bar{\mu}_x)(Z(x+h) - \bar{\mu}_x)\}}{\sigma_x^2} \quad (\text{IV-10})$$

Where:

$C(x, x+h)$ = autocorrelation function.

$C_v(x, x+h)$ = autocovariance function.

$$E = \frac{1}{n} \sum_{i=1}^n Z(i)$$

$$\bar{\mu}_x = E(Z(x))$$

$$\sigma_x^2 = E(Z(x) - \bar{\mu}_x)^2$$

h = lag distance

The autocorrelation function as defined in Equation IV-10 is the quotient of the autocovariance of the data series and the variance for the same series of data. If $Z(x)$ is stationary in a statistical sense, eg. $E(Z(x+h))$ and the autocovariance both exist and only depend on h , then $C(x, x+h)$ may be interpreted as the population correlation coefficient for the pair of variables $(Z(x), Z(x+h))$ (Chung, 1984). A direct relationship between the autocorrelation function and the semi-variogram discussed in the next section exists under these conditions.

$$\text{Semi-variance} = \text{Variance} - \text{Autocorrelation Function}$$

The fractal dimension (D) may be estimated from the autocorrelation function from the following relationship (Mandelbrot, 1971).

$$D_{acf} = 2 - \frac{\log(2C(x, x+h) + 2)}{2 \log 2} \quad (IV-11)$$

$C(x, x+h)$ is the autocorrelation value at lag 1, eg. the smallest h of the data series. The autocorrelation method has the advantage of being computationally simple, but is essentially a blind method as it only looks at the autocorrelation at lag 1 without incorporating information on longer range correlation. This may be important if the length of lag 1 happens to coincide with a natural periodicity in the property under study. In this case the property may be spatially correlated at lag 1, but not at any other scale of measurement and the autocorrelation function may provide a misleading indicator of the degree of autocorrelation.

Several assumptions are implicit in the use of the autocorrelation function to calculate fractal dimension.

1. $E(Z(x+h))$ exists and is only dependent upon h .
2. The autocovariance exists and only depends upon h .
3. The data series is well represented by a standard Gaussian distribution (D is approximately 1.5).

2. Semi-Variogram Analysis

The semi-variogram is a cornerstone of geostatistical study and has found broad application in the mining industry. Consider two random variables $Z(x)$ and $Z(x+h)$

separated by a lag vector h . The degree to which point measurements show correlation over some distance in space or time may be characterized by the variogram function (Journel and Huijbregts, 1978).

$$2\gamma(x, h) = E\{(Z(x) - Z(x+h))^2\} \quad (IV-12)$$

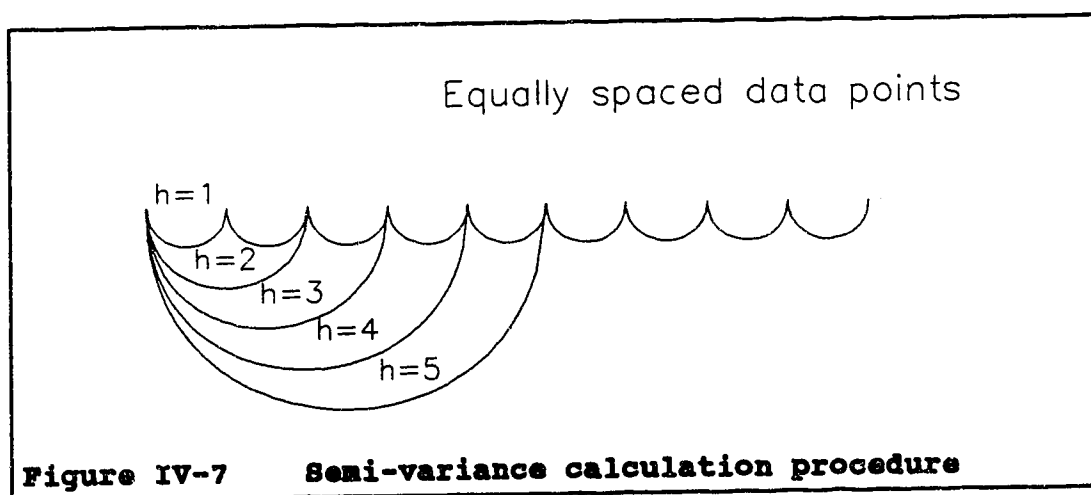
Substituting for the expectation operator E and re-arranging provides an expression for the semi-variance estimator.

$$\gamma(x, h) = \frac{1}{2N(h)} \sum_{i=1}^{N(h)} \{Z(x_i) - Z(x_i+h)\}^2 \quad (IV-13)$$

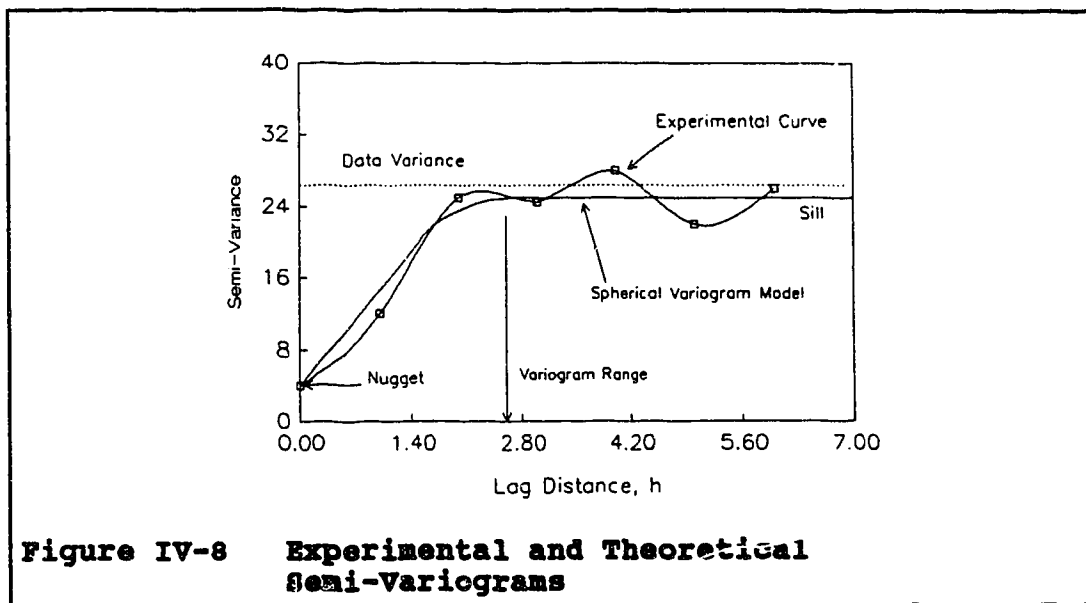
In this case, $Z(x_i)$ is a variable at location x_i in one dimensional space, $N(h)$ is the number of pairs of data points separated by lag value h and $\gamma(x, h)$ is the experimental semi-variance. In general, the semi-variance is a function of the location x as well as the lag value h . In practice, $\gamma(x, h)$ is often assumed to be invariant with x . This assumption is verified by testing the value of the mean within a given core for statistical homogeneity using a standard one-way analysis of variance test (ANOVA). The results of these tests are noted in Appendix B and confirm the applicability of using the variogram approach for the data sets generated by subroutine AREA. The intrinsic hypothesis that $\gamma(h)$ depends only on h allows for the estimation of the

semi-variogram from a series of equally spaced data.

Figure IV-7 illustrates the calculation procedure for a one-dimensional semi-variance.



For data showing spatial correlation, $\gamma(h)$ increases from near zero as $h \rightarrow 0$ to a roughly constant value at some finite distance h . The value of this constant variance is known as the sill and is numerically close to the total variance of the data. The value of h at which the sill is reached is known as the range and represents the point at which spatial correlation ceases (Goggin, 1988) (Figure IV-8).



In some cases $\gamma(h)$ does not approach zero as $h \rightarrow 0$ and a finite discontinuity occurs at the origin. This discontinuity is known as the "nugget effect" and is caused by a combination of sampling errors and (or) small variations at spacings less than the lowest available h . Journel and Huijbregts, (1978) state that local variability on this scale may be likened to the random phenomena of white noise which cannot be resolved at lag h .

Also of interest is the limiting case where $\gamma(h)$ appears only as a discontinuity at the origin and may be modelled by a horizontal line. This case is known as a pure nugget effect and represents a total absence of

autocorrelation at all available scales of measurement. For the purposes of this study the pure nugget effect represents the highest possible level of heterogeneity discernable at a given lag value h .

Structural analysis of a regionalized phenomena involves fitting a mathematical model to the experimental semi-variogram (Figure IV-8). Typical functional forms for semi-variograms with finite sill values are shown in Table IV-1. Fitting a variogram model which characterizes the main features of the regionalization requires a good physical knowledge of the property being studied. The form chosen to model the data will have a significant influence upon the range of the semi-variogram and may significantly influence the variogram interpretation in some cases. Spherical and linear variogram models provided the best fit to the observed data in this study (Appendix B).

The determination of the fractal dimension (D) from semi-variogram analysis in this study will utilize the method of Burrough (1981). This approach uses a log-log plot of the variance of the data separated by lag h vs h . The limiting slope of the plot as $h \rightarrow 0$ is then equated to $4-2D$. Alternatively, the fractal dimension D may be estimated by the equivalent formula for the case of the

Table IV-1
Semi-Variogram Functional Forms

Equation	Model	Comment
Linear	$\gamma(h) = \sigma^2 \left[\frac{h}{a} \right]$ $= \sigma^2$	$0 < h < a$ $h \geq a$
Spherical	$\gamma(h) = \sigma^2 \left\{ \frac{3h}{2a} - \frac{1}{2} \left[\frac{h}{a} \right]^3 \right\}$ $= \sigma^2$	$0 < h < a$ $h \geq a$
Exponential	$\gamma(h) = \sigma^2 \left\{ 1 - \exp \left[-\frac{h}{a} \right] \right\}$	
Note: h = lag distance, a = range		

semi-variogram.

$$\lim_{h \rightarrow 0} \left\{ \frac{\ln \gamma(h)}{\ln h} \right\} = 2 - D_{var} \quad (IV-14)$$

Previous studies indicate that the fractal dimension D is a useful indicator of the complexity of autocorrelation of

natural phenomena over many scales of measurement (Burrough, 1981; Hewett, 1986). The use of Burrough's method of calculating D also greatly reduces the role of interpretation in structural analysis of variograms. For small distances $h \rightarrow 0$ a linear model of the form $\gamma(h) = \omega h$ with ω equal to the slope of the log-log plot at the y-axis may be fitted to any model with linear behavior near the y-axis (Table IV-1). This greatly reduces the importance of model selection, particularly in cases for which the semi-variance is unstable resulting in a large degree of variability in the plotted data. The insensitivity of the value of D to the variogram model has been confirmed in studies by various authors (Shaw, 1988; Crickmore, 1990).

The following assumptions are implicit in the use of the Burrough method.

1. $E(Z(x+h))$ exists and is only dependent upon h .
2. The covariance exists and depends only on h .

Both the autocorrelation method and the semi-variogram method are computationally simple. The semi-variogram method has the advantage of providing a visualization of the spatial correlation behavior of the variable over all lag values and provides a validation of the fractal dimension obtained from the autocorrelation method. This

is not to say that the absolute values of D from both methods will be the same. Indeed, the fact that the methods make differing assumptions as to the probability distribution function that fits the data suggests that they should not be the same. It has been found, however, that in the absence of an *a priori* indication of the probability distribution function of a given set of data a combination of both methods will give a more robust estimator of D than any single method (Crickmore, 1990). As a result, both methods of evaluating D will be used in this study. As Hewett (1986) points out, when the lag distance of the semi-variogram approaches half the total length of the domain being modelled, the reliability of the variogram in estimating correlation structure decreases markedly. Thus, the semi-variogram and, by association, the autocorrelation function will only be useful for determining correlation structure over distances small compared with the total domain. This is not seen as a serious limitation in this study. The Fortran source code used to generate the semi-variogram data as well as the fractal dimension using the autocorrelation method is listed in Appendix E.

V. Experimental Apparatus and Procedure

The experimental work undertaken in this study may be grouped into two broad categories. The initial coreflood studies were conducted to determine recovery factors and effective dispersion coefficients (K_d) for ten different cores. Capillary pressure measurements were conducted subsequent to the corefloods in an attempt to quantify the spatial correlation structure of three different properties for each of the ten cores. The following discussion will deal with the experimental design, apparatus and procedures used in these studies.

A. Coreflood Studies

1. Coreflood Apparatus

The apparatus used in the miscible corefloods (Figure V-1) is composed of the following components:

- A. A solvent injection system permitting displacement at a constant rate.
- B. A sealed coreholder containing the consolidated porous media.
- C. A constant temperature cabinet containing a core rotation unit as well as upatream and downstream pressure gauges.
- D. A backpressure control unit.
- E. A refractometer.

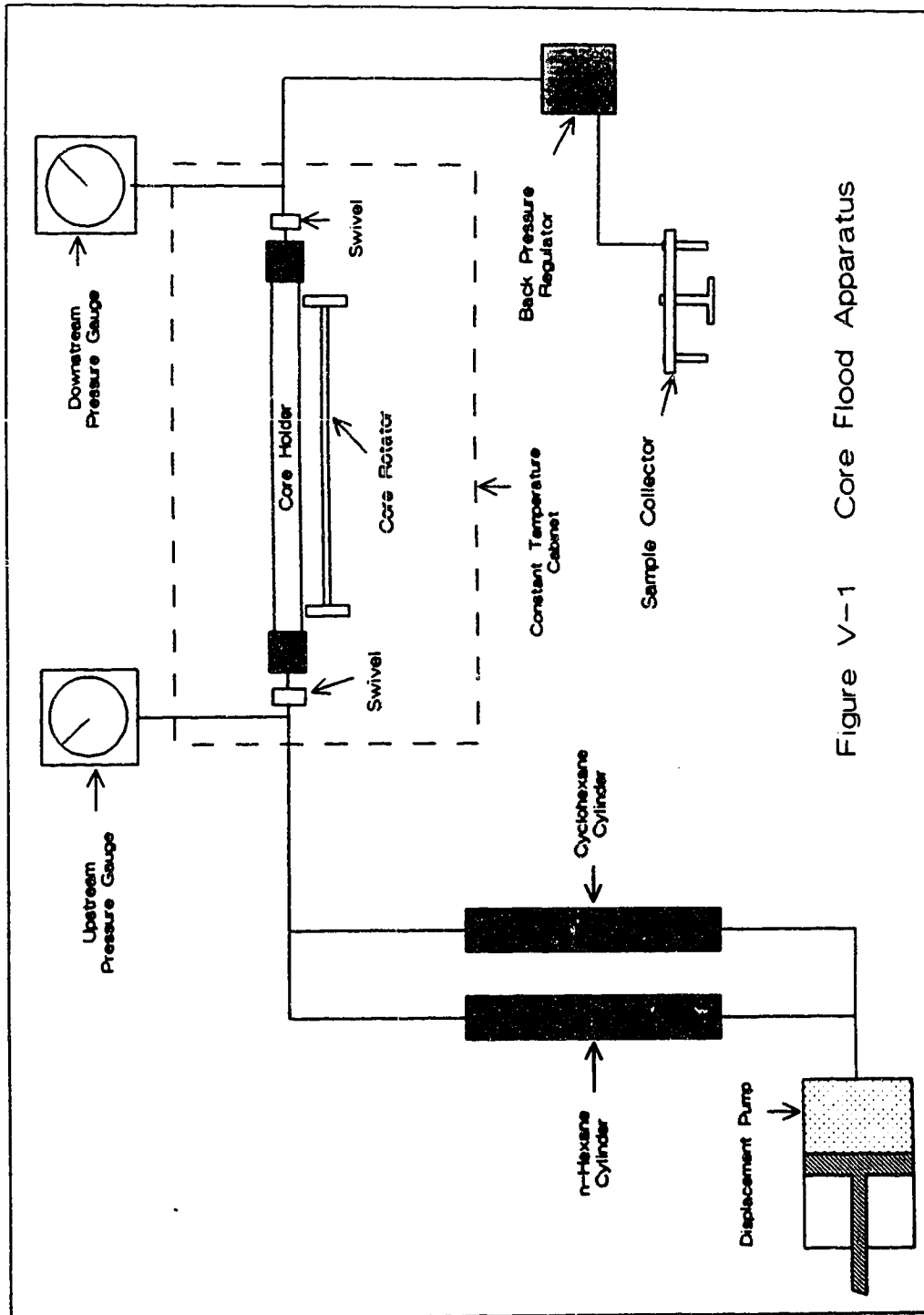


Figure V-1 Core Flood Apparatus

A Ruska positive displacement pump was used as the solvent injection system. The pump was a double cylinder type capable of discharge rates of between 10 and 330 cm^3 per hour per cylinder. Injection rates were varied by changing gears in the transmission of the pump. This pump was connected to cylinders containing *n*-hexane and cyclohexane by a four-way valve. This allowed for the injection of either solvent or resident oil as required.

The coreholder used was constructed of stainless steel and was 48 inches long with an internal diameter of 2.5 inches. Endcaps with o-ring type seals were then bolted to each end of the coreholder. The endcaps used a sintered metal screen to evenly distribute the injected and produced fluids across the inlet and outlet faces of each core. The core rotator shown in Figure V-1 allowed for the rotation of the core at a rate of four revolutions per hour. This was necessary to minimize the effect of gravity segregation of the miscible fluids within the porous medium. A Tescom 2500 backpressure regulator was used to regulate the pressure of the system. This unit was linked to a rotating sample collection tray containing a series of 50 cm^3 graduated centrifuge tubes. The resulting coreflood effluent was analyzed for refractive index using an ABBE model A303 refractometer.

2. Coreflood Design

One of the primary objectives of this study was to quantify the effect of the porespace upon mixing efficiency at the floodfront. As a result, it was deemed important to design the corefloods in such a manner that the effect of the pore structure upon mixing could be isolated. It is important to note that in this study the absolute values obtained for the recovery factor and K , for the corefloods are less important than their relative values. The objective; therefore, was to hold constant or minimize all factors affecting convective mixing with the exception of the pore structure itself. By doing this, the effect of the pore structure on convective mixing is emphasized. (Brigham et al (1961), Perkins and Johnston (1963) and Stalkup (1983) found that the following criteria are important in the design of a laboratory coreflood:

1. Gravity segregation.
2. Viscous fingering.
3. Minimum miscibility pressure.
4. Solvent injection rate.
5. Residual water saturation.
6. Geometric effects.
7. Pore structure effects.

A two-component first-contact miscible system was used in the current study. The components chosen had to satisfy the following requirements:

1. First-contact miscibility at standard temperature and pressure conditions.
2. A large difference in refractive index between the components.
3. A small difference in density between the components.

The choice of *n*-hexane and cyclohexane as the two components was found to satisfy the first two requirements. Table V-1 illustrates the properties of these two chemicals (Reid et al, 1987).

Table V-1
Properties of Miscible Components

Component	μ @ 25° C (cp)	Density (kg/m ³)	Refractive Index
<i>n</i> -hexane (C ₆ H ₁₄)	0.30	662.7	1.3770
cyclohexane (C ₆ H ₁₂)	0.88	782.0	1.4235

Under conditions of miscibility, the mobility ratio of the flood may be obtained from Equation V-1.

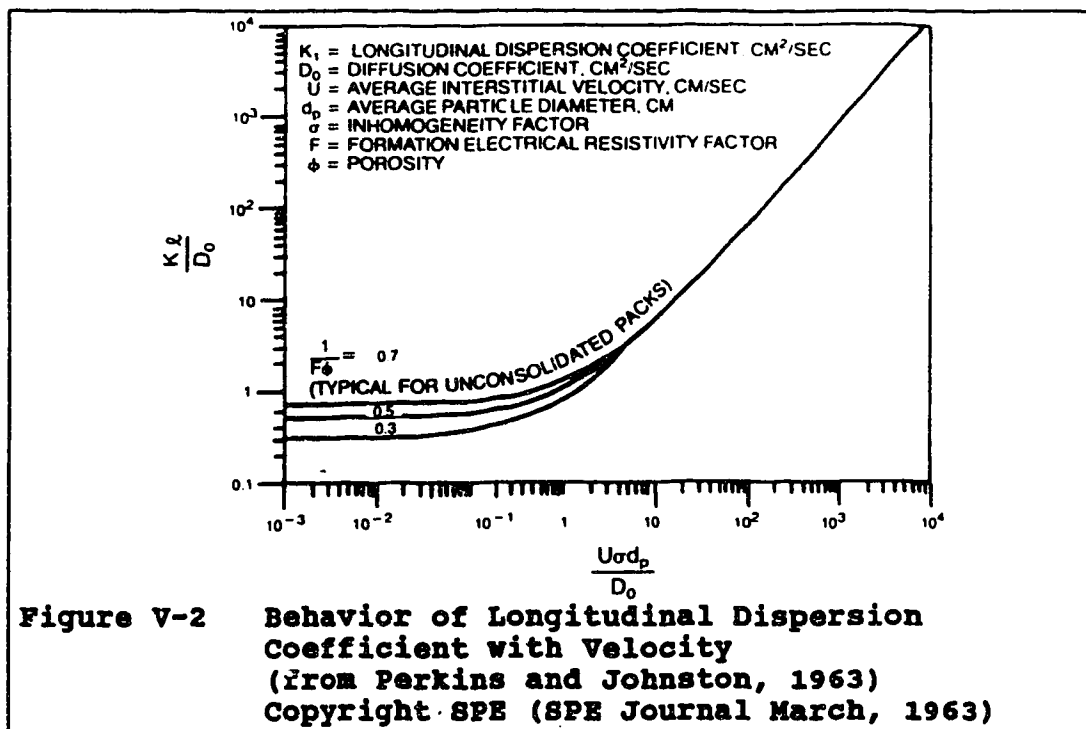
$$M = \frac{\mu_o}{\mu_s} \quad (V-1)$$

Where: μ_s = viscosity of the solvent.

μ_o = viscosity of the resident oil.

By selecting *n*-hexane as the resident oil the effective mobility ratio for each coreflood is held constant at approximately 0.341. By maintaining a favorable mobility ratio, the effect of viscous fingering can be minimized. The density difference between the two components is significant and may result in gravity segregation and a resulting reduction in recovery efficiency. This possibility was addressed by rotating the core using the core rotation unit shown in Figure V-1. Comparison of floods conducted on rotated and unrotated cores shows that the effect of gravity segregation may be greatly reduced using this method. An recovery factor increase of 3.3% was noted for core A using a flood rate of 0.0222 cm/s when the core was rotated.

The floodrate criteria have been examined in detail by Perkins and Johnston (1963). Figure V-2 shows a plot of $\frac{K_L}{D_o}$ vs $\frac{v_{adp}}{D_o}$. For values of $\frac{v_{adp}}{D_o} > 4$ convective dispersion dominates the mixing process.



This plot is based upon Equation II-2 which describes the growth of the longitudinal dispersion coefficient with velocity. In the absence of channeling of the solvent, K_L is equivalent to the effective dispersion coefficient K_e . The objective in setting injection rates is to minimize the effect of molecular diffusion on the process. Three injection rates were used in this study. Darcian velocities of 35.0 cm/hr, 55.0 cm/hr and 80.0 cm/hr were used for each of the corefloods. The following rough

calculation was done to examine the validity of using these injection rates. Values for D_o and d_p are average values for a homogeneous sandstone (Stalkup, 1983).

$$d_p = 0.01 \text{ cm.}$$

$$D_o \cong 1.0 \times 10^{-5} \text{ cm}^2/\text{s}$$

$$\sigma_{\min} = 2.0$$

$$v_{\min} = \frac{35.0 \text{ cm/hr}}{3600 \text{ s/hr}} = 9.722 \times 10^{-3} \text{ cm/s}$$

$$\frac{v_{\min} \sigma_{\min} d_p}{D_o} = 19.44$$

This result would seem to indicate that the effect of the molecular diffusion coefficient D_o is minimal, particularly at the highest velocity tested. In the region where D_o dominates the mixing process, K_i increases very slowly with the injection rate (Figure V-2). Three injection rates were used to ensure that the flood was conducted to the right of this region. By maintaining a constant Darcian velocity for each flood, the value of K_i will be dependent upon the heterogeneity coefficient σ , which; in turn, is a function of the structure of the porous medium.

The residual water saturation has also been found to affect the efficiency of the miscible displacement process (Stalkup, 1970). This factor was minimized by evacuating each of the cores for an extended period of time. This

resulted in the vaporization and removal of most of the residual water from each core. In general, residual water saturation was not seen as a significant factor in these experiments as eight of the ten cores tested were outcrop samples with low residual water saturations.

Geometric effects were first investigated by Brigham *et al*, (1961) who found that boundary effects increased convective dispersion (K_c) when core diameters were less than 3.2 cm. Core diameters in the current study varied between 4.445 cm and 5.556 cm. As a result, the diameter of the core was not seen as a controlling factor. The effect of core length can also have an influence upon the efficiency of the process. Brigham *et al* (1961) found that the amount of mixing was proportional to the square root of the distance travelled. This would imply that recovery is improved when the displacement path length is increased. For eight of the ten cores tested, the core length was held constant at 121.92 cm. The exceptions to this were two oilfield carbonate cores (core F and core G) which were 136.53 and 96.52 cm long, respectively (Table V-2).

**Table V-2
Core Properties**

Core	Lithology	Diameter (cm)	Length (cm)	Porosity %	k (md)
A	Indiana limestone	4.445	121.92	21.04	54.75
B	Brown sandstone	5.080	121.92	21.42	2035.48
C	Brown sandstone	5.080	121.92	21.90	1967.20
D	Indiana limestone	4.445	121.92	21.25	42.92
E	Berea sandstone	4.445	121.92	24.56	2231.72
F	Swan Hills limestone	5.080	136.53	12.26	138.36
G	Golden Spike limestone	4.445	96.52	11.58	51.21
H	Berea sandstone	4.445	121.92	27.05	2155.91
I	Tyndle limestone	5.556	121.92	9.54	2.25
J	Tyndle limestone	5.556	121.92	8.99	5.76

If the assumption is made that the amount of mixing in a given porous medium is proportional to K , then K , for the shorter core should be slightly lower than would be the case for a core 121.9 cm long. Conversely, the longer core should have a slightly higher effective dispersion coefficient than would be expected for a 121.9 cm core.

3. Coreflood Procedure

Eight of the ten cores shown in Table V-2 were obtained from outcrop samples. Cores A, B, C, D, E and H were purchased from Cleveland Quarries and were already cut to the appropriate length. Cores I and J were cored from a solid limestone block while cores F and G were oilfield cores. As can be seen from their characteristics, these cores represent a variety of pore structure styles with varying degrees of heterogeneity. The first step in the coreflood procedure involved installing the cores in the coreholder. A molten metal technique was used whereby each core was initially sealed with an epoxy paint to prevent any absorption of the molten metal into the porespace. The core was then centered in the core barrel using a three pin endcap which sealed one end of the coreholder. The core and coreholder were then placed vertically in an oven and heated to 150° F. A quantity of Cerrobend alloy was then melted and poured into the

annular space between the coreholder and the core and allowed to cool overnight. Cerrobend is an alloy of lead, tin, and silver with several unique properties. It has the advantage of a low melting point (157° F) and expands slightly upon cooling. These characteristics make it ideal for providing a seal around the core. After cooling, the ends of the core were machined to be flush with the end flanges and the endcaps were installed.

Each core was saturated with *n*-hexane by first evacuating the core overnight using a portable vacuum pump. The quality of the vacuum was tested through the use of a vacuum gauge connected to the opposite end of the coreholder. This procedure allowed for the removal of the residual water which remained in the core. After evacuation, the coreholder was attached to the Ruska pump and *n*-hexane was injected into the core until the vacuum as measured by the gauge had dropped to zero and liquid was produced at the gauge end of the core. The amount of *n*-hexane injected was then used to calculate the porosity of the core using a bulk volume obtained from measurements of the core.

After saturation, the coreholder was mounted in the constant temperature cabinet shown in Figure V-1. Permeability was determined by injecting *n*-hexane at four

different rates and measuring the differential pressure across the core at each rate. From this data the liquid permeability was calculated from Darcy's law for linear fluid flow. From the pore volume measured during the core saturation, floodrates corresponding to the desired Darcian velocities were calculated. Because the pump transmission offered a finite choice of gear ratios it was not always possible to obtain the exact velocity required, however, it was usually possible to select an injection rate within 5% of the desired rate. The backpressure was arbitrarily set to 300 psi (2.068 MPA). Although not required for miscibility, this backpressure allowed for better control of the injection process as the Ruska pump would occasionally inject at too high a rate in the absence of backpressure. Once the pump speed was set, the four-way valve was switched over to cyclohexane and the core rotation unit was activated in preparation for the start of the flood. A volume of effluent corresponding to 0.05 pore volumes was calculated and this amount of fluid was collected in each centrifuge tube as the flood progressed. As the tubes were filled the refractive index of the effluent was measured using the refractometer. The flood was allowed to continue until 2.0 pore volumes of cyclohexane had been injected into the core. The data

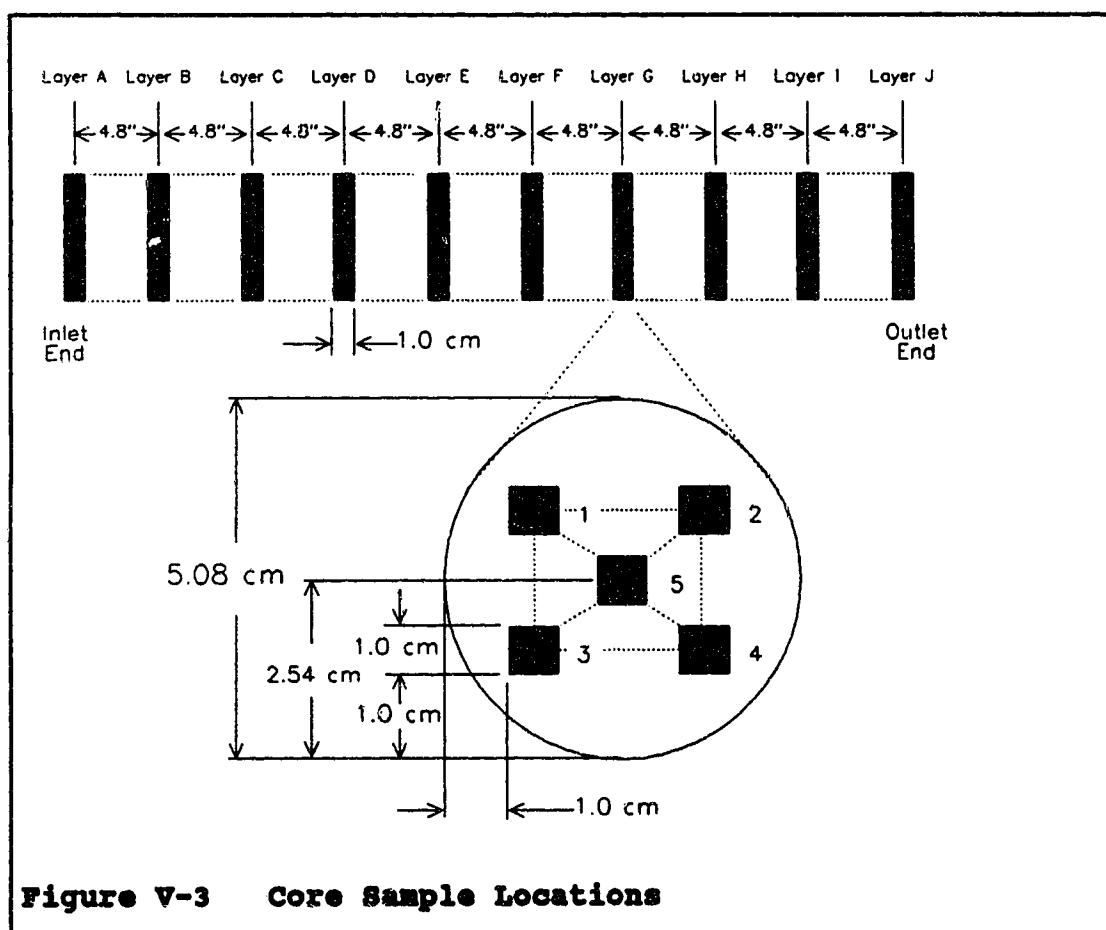
collected consisted of a refractive index value for each 0.05 PV of cyclohexane injected. The computer analysis of this data will be described later in this chapter.

After each cyclohexane flood, the core was re-flooded with *n*-hexane until a refractometer test showed the effluent to be pure *n*-hexane. Due to the adverse mobility ratio of the re-flood, up to 4.0 pore volumes of *n*-hexane were required to achieve complete removal of the cyclohexane. Duplicate cyclohexane floods on core A separated by a *n*-hexane re-flood produced identical effluent concentration profiles. This indicated that the re-flooding procedure could be used to restore the core to its initial state immediately after the initial saturation with *n*-hexane. Each core was flooded at the three rates described earlier, each cyclohexane flood being followed by a re-flood with *n*-hexane.

B. Mercury Porosimetry

The use of mercury porosimetry provides a means of evaluating the pore structure of discrete samples taken from each core. After the corefloods were complete, each core was dried by passing compressed air through it for several days. The core was then removed from the coreholder by melting the surrounding Cerrobend. Figure V-3 illustrates the sample locations chosen for this study. A

requirement for variogram or autocorrelation function calculation is that the data points be evenly spaced. As can be seen, a total of 50 samples per core were analyzed. This number was, by necessity, a compromise between the data requirements of the statistical calculations and the time required to analyze each sample. Each sample had a volume of approximately 1 cm^3 and was obtained by cutting the core into pieces using a diamond saw.



Once the samples were obtained they were first dried in an oven at 150°F for several days and then coded as to their exact location within the core. The analysis of the samples was then undertaken.

The use of mercury porosimetry in the study of pore structure has been undertaken by several investigators. Wardlaw (1976) provides an excellent description of its use in an attempt to quantify pore structure behavior in two-phase flow. In the current study mercury injection was used to determine values for the permeability, porosity and mean pore throat diameter for each of the 500 samples analyzed.

Purcell (1949) was the first to apply the capillary pressure curve determined from mercury porosimetry to the calculation of permeability. Equation V-2 illustrates Purcell's equation for permeability calculation. The integral in Equation V-2 is simply the area under a plot of $\frac{1}{P_c^2}$ vs the corresponding mercury saturation. Porosity is calculated by dividing the total volume of mercury injected into the sample at an arbitrarily high pressure by the bulk volume of the sample.

$$k = 10.24(\sigma_i \cos \theta)^2 \phi \lambda_L \int_{S=0}^{S=1} \frac{dS}{(P_c)^2} \quad (V-2)$$

Where: k = permeability (md).

ϕ = porosity.

S = fraction of perespace invaded
by mercury.

P_c = capillary pressure (psi).

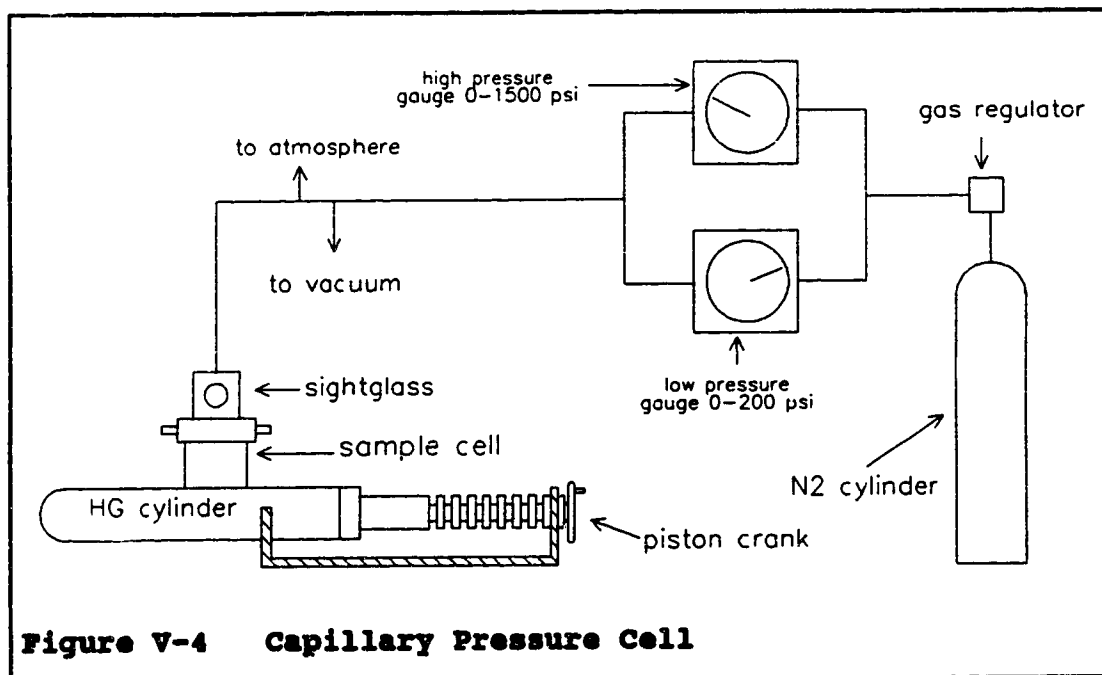
σ_i = interfacial tension (dynes/cm).

θ = contact angle.

λ_L = lithology factor.

The determination of the capillary pressure curve is relatively straightforward. The sample is placed in the sample cell containing mercury shown in Figure V-4.

The first step in the procedure involves the determination of a calibration curve for the apparatus used. The sample cell is first evacuated for several minutes using the vacuum pump. The cell is then flooded with mercury until the mercury reaches a mark in the top sightglass. Pressure is applied to the empty cylinder in increments from 0 to 1000 psi using the nitrogen source. At each pressure increment the piston crank is turned so as to bring the mercury level back up to the sightglass mark. After each movement of the piston crank a volume reading is taken and recorded from the scale on the piston crank.



In this way, a calibration curve of pressure vs volume of mercury injected is obtained. After the calibration curve is obtained the sample is placed in the cell and the cell is flooded with mercury. The bulk volume of the sample is then obtained from the difference between the measured volume of mercury and the known volume of the cell. After determination of the bulk volume a vacuum is then applied to the cell for several minutes. The same procedure of gradually increasing the pressure on the sample by increments while recording the volume of mercury forced into the porespace at each pressure was then followed. The same pressure increments were used as in the case of the

calibration curve and care was taken to allow enough time between pressure increases for mercury intrusion within the sample to occur. Once the data was collected, the calibration curve was subtracted from the sample data leaving the capillary pressure curve. The volumes of mercury injected were converted into mercury saturations at each incremental pressure and the values for permeability, porosity and mean pore throat size were calculated by means of the computer program ANALYZE contained in Appendix E.

C. Data Analysis

Appendix E contains the source code for the Fortran programs EFFPLOT and ANALYZE which were used to analyze the raw data obtained from the coreflood and mercury porosimetry experiments, respectively. The datafile used by the EFFPLOT program consists of a set of calibration data as well as a refractive index value for each 0.05 P.V. of solvent injected. The calibration data was obtained by preparing a series of eleven mixtures of *n*-hexane and cyclohexane and measuring their refractive indices. The mixtures varied in composition from 100% *n*-hexane to 100% cyclohexane by volume and were prepared in increments of 10%. The first part of the EFFPLOT program uses a linear interpolation method to convert each of the refractive index values measured in the coreflood into a cyclohexane

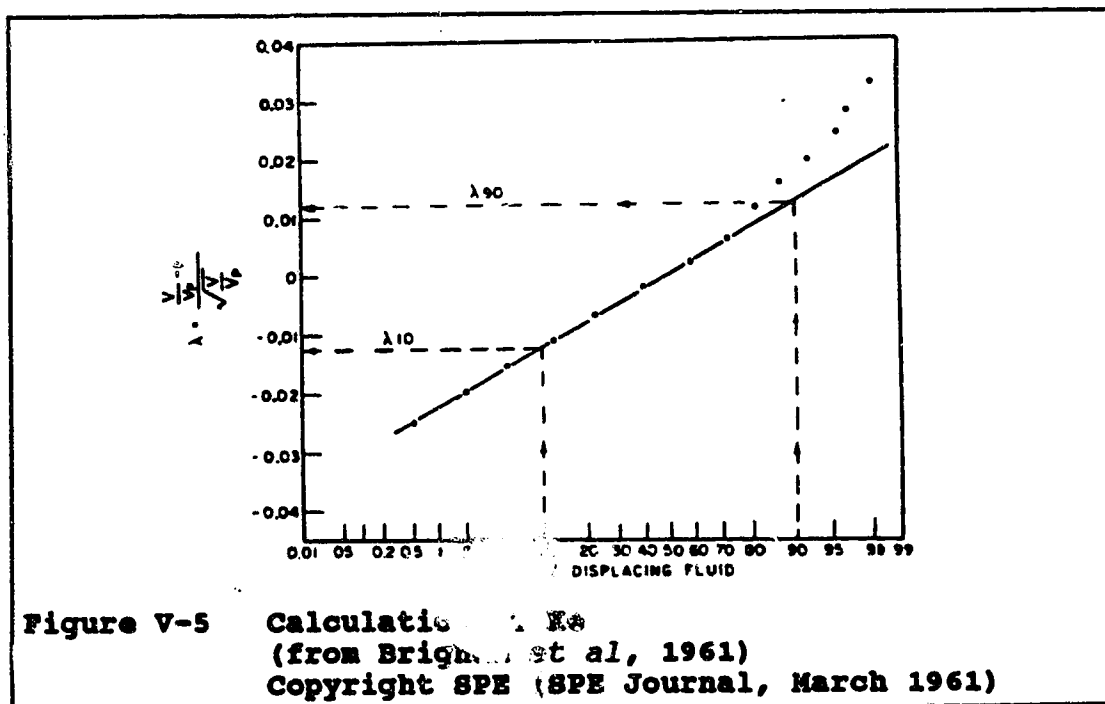
concentration. The values for pore volumes injected are then converted to a lambda function by the following equation:

$$\lambda = \frac{\frac{V}{V_p} - 1}{\sqrt{\frac{V}{V_p}}}$$

Where: V = pore volumes injected.

V_p = total pore volume.

The lambda values along with the corresponding cyclohexane concentrations are then output by the program and are listed in Appendix D. These values are then plotted on an arithmetic probability scale as shown in Figure V-5.



The straight line portion of the plot is used to calculate the effective dispersion coefficient (K_e) using the following equation:

$$K_e = vL \left\{ \frac{\lambda_{90} - \lambda_{10}}{3.625} \right\}^2$$

Where: K_e = effective dispersion coefficient cm^2/s .

v = darcian velocity (cm/s).

L = length of the core (cm).

$\lambda_{90}, \lambda_{10} = \lambda$ values at cyclohexane

concentrations of 90% and 10%.

This procedure was followed for each of the corefloods run. As a final step, the EFFPLOT program calculates the area underneath the cyclohexane concentration curve from 0 to 1.0 P.V. injected and uses this value to obtain a recovery factor for the flood. Since we are interested in the recovery factor for the n -hexane which is the resident oil, the recovery factor may be calculated from the following formula:

$$R.F. = 100 - \int_{0.0P.V.}^{1.0P.V.} C_s dC_s \quad (V-3)$$

Where: $R.F.$ = recovery factor for the resident oil.

C_s = concentration of the solvent (%).

The integral in Equation V-3 was evaluated numerically using Simpson's 1/3 rule (Gerald and Wheatley, 1985). Due to errors in the calculation of the area beneath the curve

it was found that the recovery factor sometimes exceeded 100% after injection of 1.5 and 2.0 pore volumes of solvent. A maximum value of 105.5% recovery efficiency was noted for Core E after the injection of 2.0 pore volumes of solvent. The program automatically reduces any value over 100% back to 100% recovery before printout. This over prediction of recovery was not seen at the 1.0 pore volume injection level which was used for the comparisons in this study (Tables VII-1 - VII-3).

Program ANALYZE was used to process the data from the capillary pressure measurements into values for permeability, porosity and mean pore throat size for each sample. The main portion of the program reads in the data and subtracts the calibration curve values from the sample data. The resulting capillary pressure curve is then passed on to subroutine AREA where the porosity is calculated. The pressure at which 50% mercury saturation occurs is then calculated by linear interpolation. It has been noted that this pressure may be related to the mean pore throat size in the sample by Equation V-4 (Wardlaw, 1976). For the purposes of this calculation and the calculation of permeability, it was assumed that the interfacial tension was 480.0 dynes/cm and the contact angle between mercury and the non-wetting surface was 140° .

$$d = \frac{4\sigma_i \cos \theta}{P_c} \quad (V-4)$$

Where: d = mean pore throat diameter (10^{-9} m.)

σ_i = interfacial tension (dynes/cm).

θ = contact angle.

P_c = capillary pressure (mpa).

These are average values obtained from the original work by Purcell (1949). After the calculation of the mean pore throat diameter the program calculates permeability using Purcell's equation (Equation V-2). For this calculation, an average lithology factor (λ_i) of 0.216 was used (Amyx et al, 1960). The integral portion of Equation V-2 was calculated by fitting a natural spline curve to the calculated data points and numerically evaluating the area beneath the curve using the spline coefficients. This approach does not require equally spaced data points as is the case with Simpson's rule and is somewhat more accurate (Gerald and Wheatley, 1985). Once the permeability has been calculated a table is printed giving the sample location as well as the permeability, porosity and mean pore throat diameter for each sample. These tables are listed in Appendix A.

Subroutine VARIO uses the permeability data to calculate the semi-variogram and autocorrelation function

at lag 1 for the data series using the equations described in chapter IV. The data obtained was joined into one continuous series by taking each location series of ten data points (eg. location 2, levels A to J, Figure V-3) and adding the location series to the end of the previous location series (eg. location 1, levels A to J, Figure V-2). The values for the mean and variance were then calculated for the series and printed out. This method of calculation is similar to the calculation of the semi-variogram in two dimensions (Journel and Huijbregts, 1978 p 220.). The major difference is that the assumption is made that each of the location vectors (Figure V-3) may be represented by a column in a rectangular two-dimensional matrix. Each layer represents a row in the matrix and the semi-variance is calculated in the direction parallel to the axis of the core only. Due to the fact that the semi-variogram calculation is sensitive to the occurrence of extreme values it is common to calculate the log semi-variance of the property under study to minimize this effect (Chung, 1984; Mishra, 1987). This approach was followed in subroutine VARIO which calculates lag values and the natural log of the associated semi-variances. As a final step, the calculated autocorrelation function at lag 1 was transformed into a fractal dimension using Equation IV-11.

VI. Heterogeneity Description

Traditionally, heterogeneity within a porous medium has been defined in a variety of ways. In the case of immiscible displacement, by far the most commonly used estimator of heterogeneity is the Dykstra-Parsons permeability variation coefficient, V_{DP} . For the case of miscible displacement, the Koval heterogeneity factor (H) is commonly used. In this chapter the calculation of these heterogeneity indicators from the data obtained in the current study will be discussed. These calculations will form the basis for a comparison with a fractal heterogeneity estimator which will be discussed in the following chapters.

A. Dykstra - Parson's V_{DP}

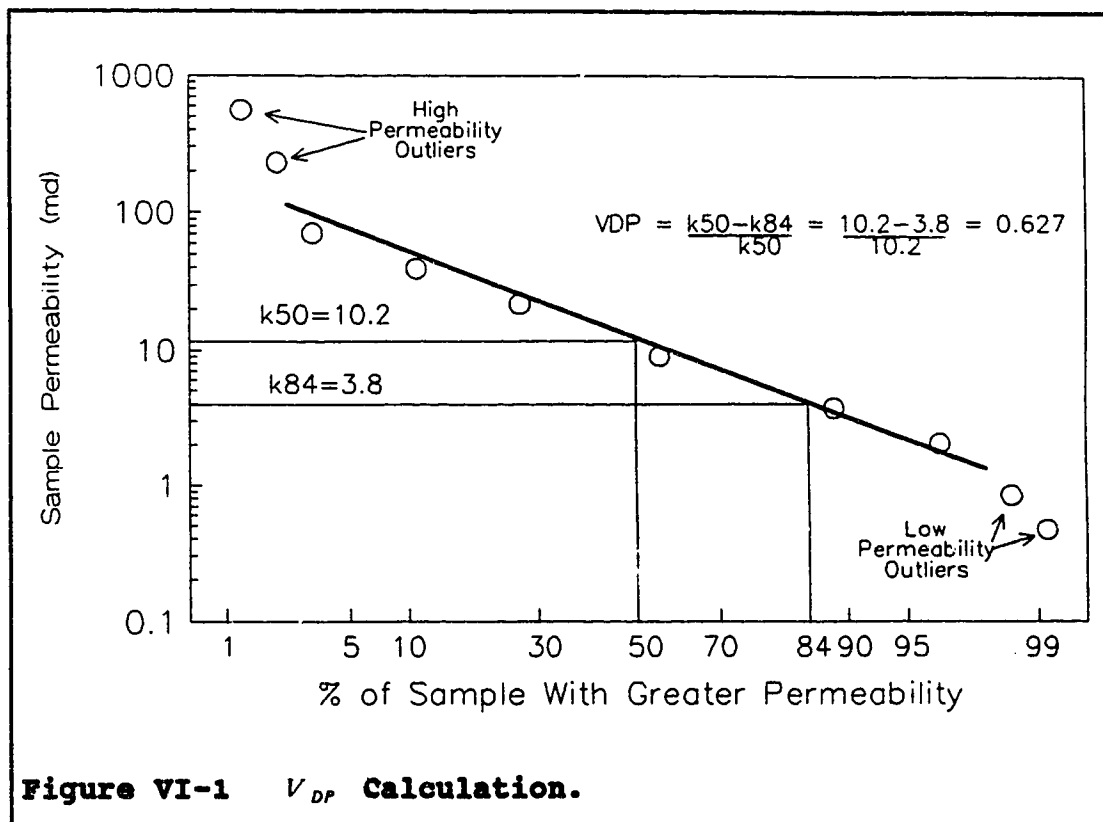
Original work conducted by Dykstra-Parsons (1950) resulted in a method of calculating oil recovery from a field subject to immiscible displacement. It was found that recovery was a function of the mobility ratio (M), the initial oil and water saturations and the variation in absolute permeabilities within the porous medium. For our purposes, only the method of quantifying the permeability variation will be discussed in detail.

The calculation of the permeability variation

coefficient V_{DP} assumes a log-normal distribution of permeability within the porous medium. The calculation procedure is as follows (Dykstra-Parsons, 1950):

1. All permeabilities in a distribution are listed in descending order.
2. The percentage of the permeabilities exceeding each listed permeability are computed and tabulated as the portion of the total sample having a higher permeability.
3. The permeability values in step 1 are plotted on a log scale while the percentage of permeabilities greater than the permeability value are plotted on the probability axis of a log-probability scale.
4. A best-fit straight line is drawn through the points. If the points do not lie on a straight line, the terminal points are weighted less.
5. The permeability at 84.1 cumulative percent is subtracted from the median permeability. The result is then divided by the median permeability yielding the permeability variation V_{DP} .

Figure VI-1 illustrates the calculation procedure for a sample data set:



The graphical method of calculating V_{DP} implicitly ignores the effects of any extreme permeability values. These outliers are typically few in number. High values for permeability may occur due to localized fractures and will occur as points to the upper left on Figure VI-1. Conversely, low permeability outliers caused by impermeable streaks in the rock will occur to the lower right of Figure VI-1. The exclusion of these values is equivalent to a truncation of one or both tails of a frequency distribution curve for the data set in question.

V_{DP} may also be calculated without the use of graphical techniques provided that the standard deviation of the natural log of the permeability distribution is known (Jensen and Lake, 1988). Equation VI-1 provides a means of calculating V_{DP} under these circumstances:

$$V_{DP} = 1 - e^{(-\sigma_{\ln(k)})^2} \quad (\text{VI-1})$$

Where: V_{DP} = Dykstra-Parsons permeability variation.

$\sigma_{\ln(k)}$ = standard deviation of the permeability distribution.

The use of Equation VI-1 will require the removal of any outliers in the data which may tend to cause bias in the results. The criteria for the removal of outliers is discussed further in Chapter VII. Appendix C contains a listing of the outliers removed as well as the calculated variance of the natural log of the permeability distribution for each core. After removal of the extreme values, $\sigma_{\ln(k)}$ was calculated through a slight modification of the source code of program ANALYZE in Appendix E. Table VI-1 lists the results of these calculations.

Table VI-1
 V_{DP} Results

Core	$\sigma_{ln(k)}$	V_{DP}
A	2.05	0.87
B	0.56	0.43
C	0.99	0.63
D	1.83	0.84
E	1.09	0.66
F	2.44	0.91
G	2.42	0.91
H	0.43	0.35
I	0.94	0.61
J	1.18	0.69

B. Koval's H Parameter

Koval (1963) adapted the Buckley-Leverett fractional flow equation for use in miscible displacement. In Koval's analysis, the flowing fraction of the displacing phase, F , is assumed to be dependent upon solvent saturation, heterogeneity effects and viscosity differences. Equation VI-2 was developed by Koval for use in miscible displacement and is analogous to the familiar Buckley-Leverett fractional flow equation.

$$F_s = \frac{1}{1 + \left(\frac{1-S}{S}\right)\left(\frac{1}{H}\right)\left(\frac{1}{E}\right)} \quad (\text{VI-2})$$

Where: F_s = flowing fraction of solvent.

S = solvent saturation.

H = heterogeneity factor.

E = effective viscosity ratio.

The effective viscosity ratio E is further defined by Equation VI-3 which is an empirical correlation based upon the fourth root mixing rule used in refinery calculations.

$$E = \left(0.78 + 0.22 \left(\frac{\mu_o}{\mu_s} \right)^{\frac{1}{4}} \right)^4 \quad (\text{VI-3})$$

Where: E = effective viscosity ratio.

μ_o = viscosity of the resident oil.

μ_s = viscosity of the solvent.

Substituting $K=HE$ into Equation VI-2 and re-arranging the terms yields:

$$V_{pi} = \frac{K}{(K - F_s(K - 1))^2} \quad (\text{VI-4})$$

Where: V_{pi} = pore volumes of solvent injected.

Equation VI-4 suggests a simple means of calculating K and hence, the heterogeneity coefficient, H . At a point in time just prior to solvent breakthrough, $F_s = 0.0$. If we substitute $F_s = 0$ into Equation VI-4 we obtain the

following expression for K based upon the volume of solvent injected at the time that breakthrough occurs (Koval, 1963):

$$K = \frac{1}{(V_{pi})_{b.t.}} \quad (VI-5)$$

Where: $(V_{pi})_{b.t.}$ = volume of solvent injected at breakthrough (P.V.)

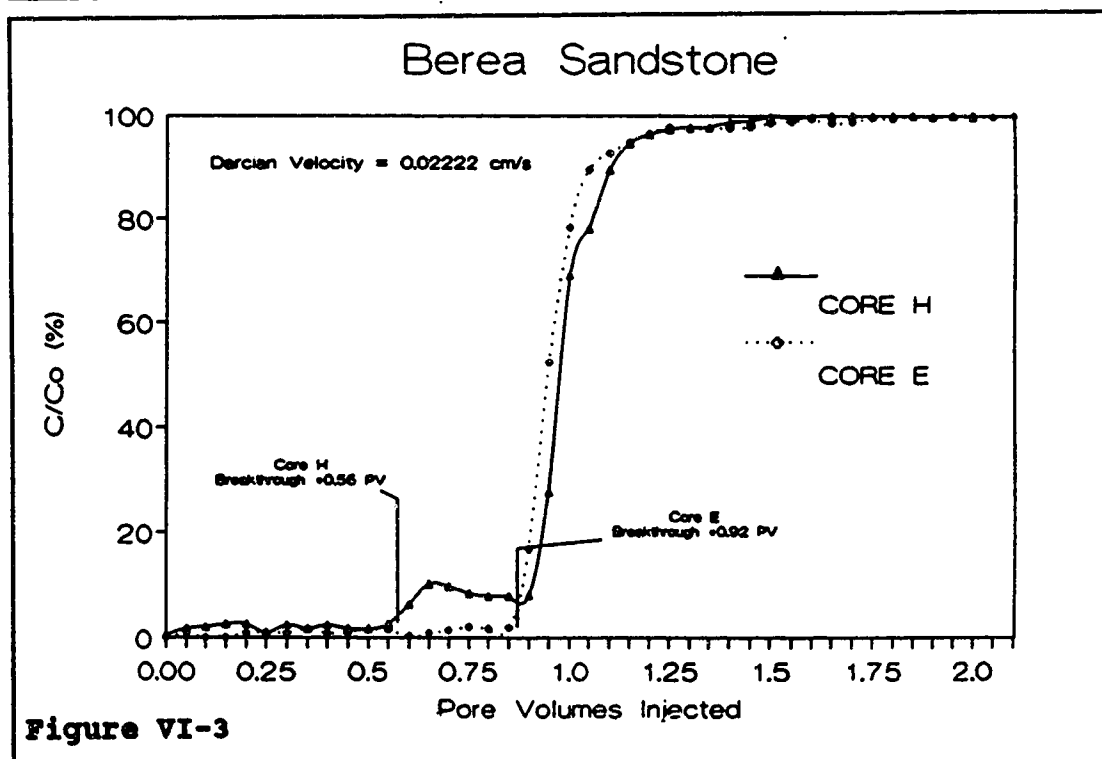
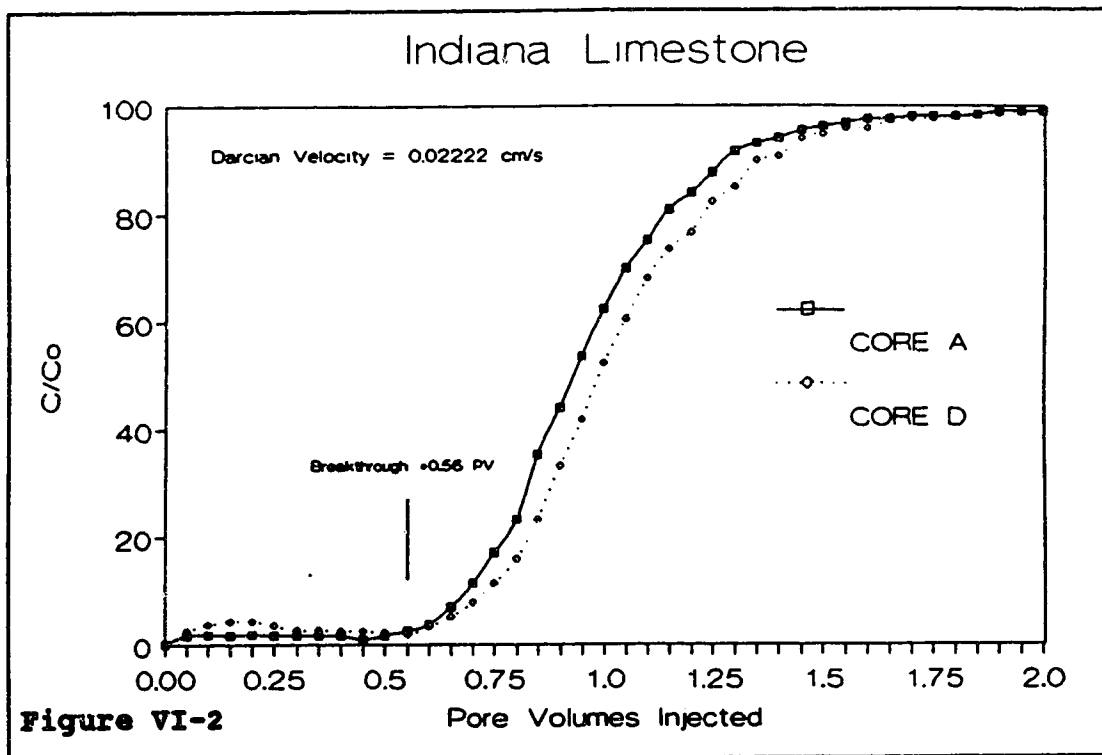
$$K = HE$$

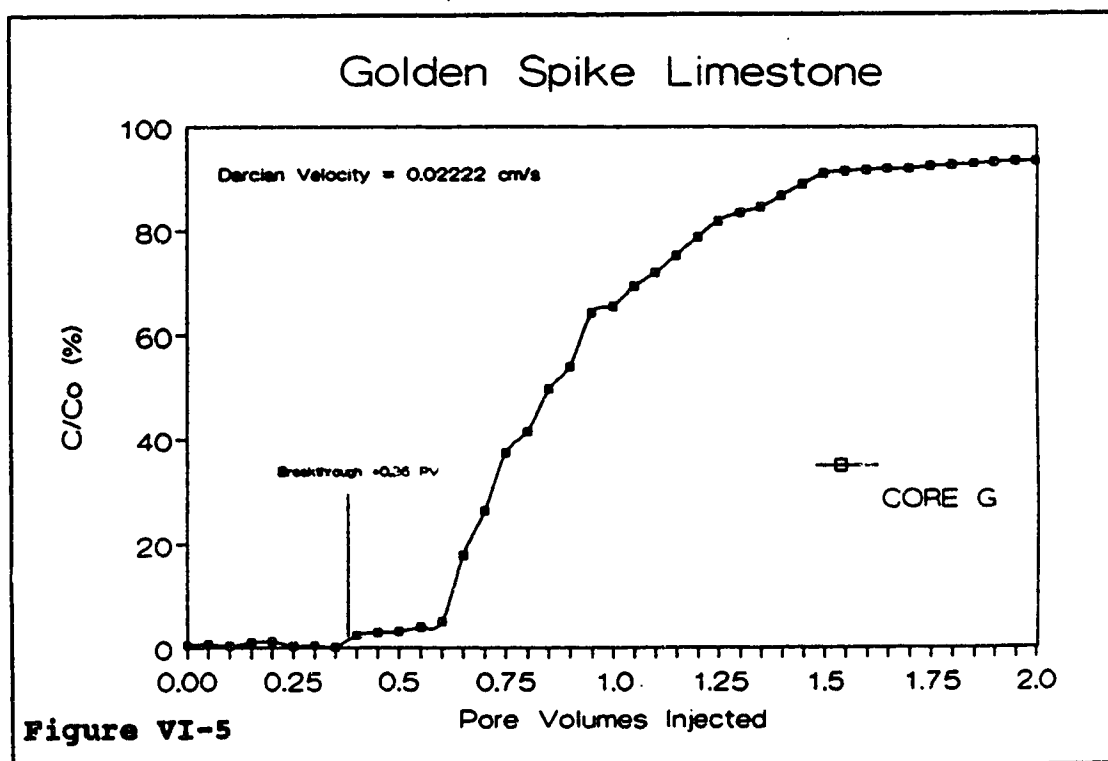
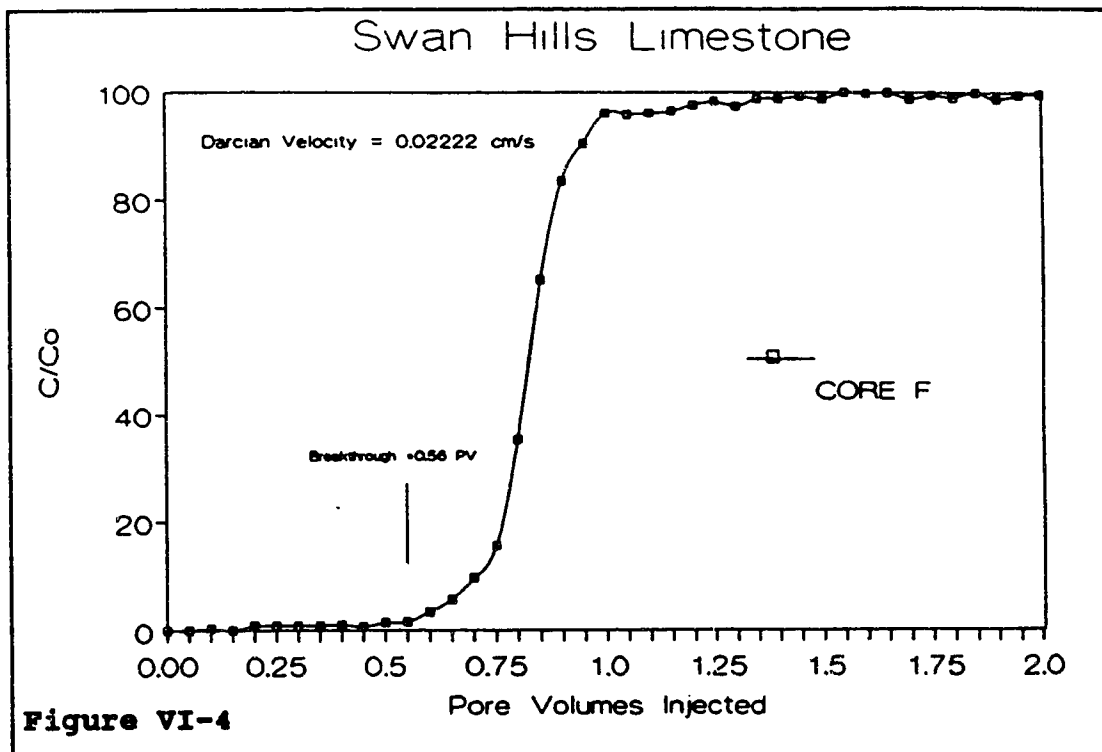
Equation VI-5 is the basis for the calculation of the Koval heterogeneity factor H in the current study and is valid under the following conditions:

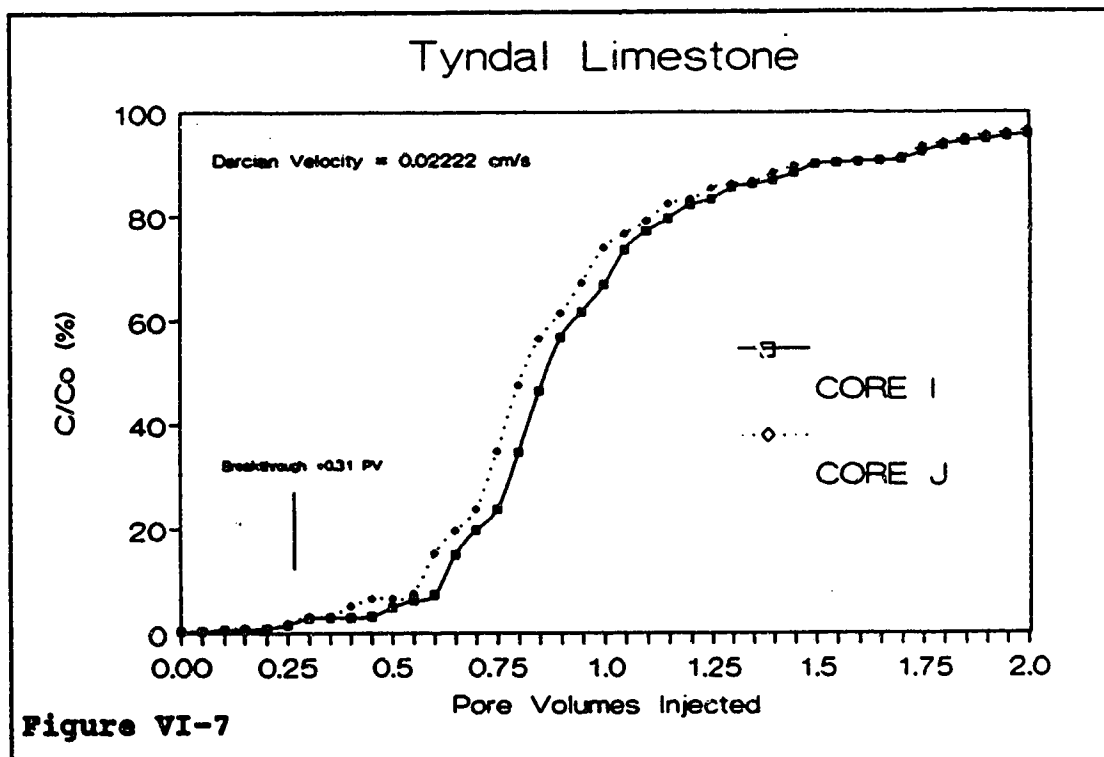
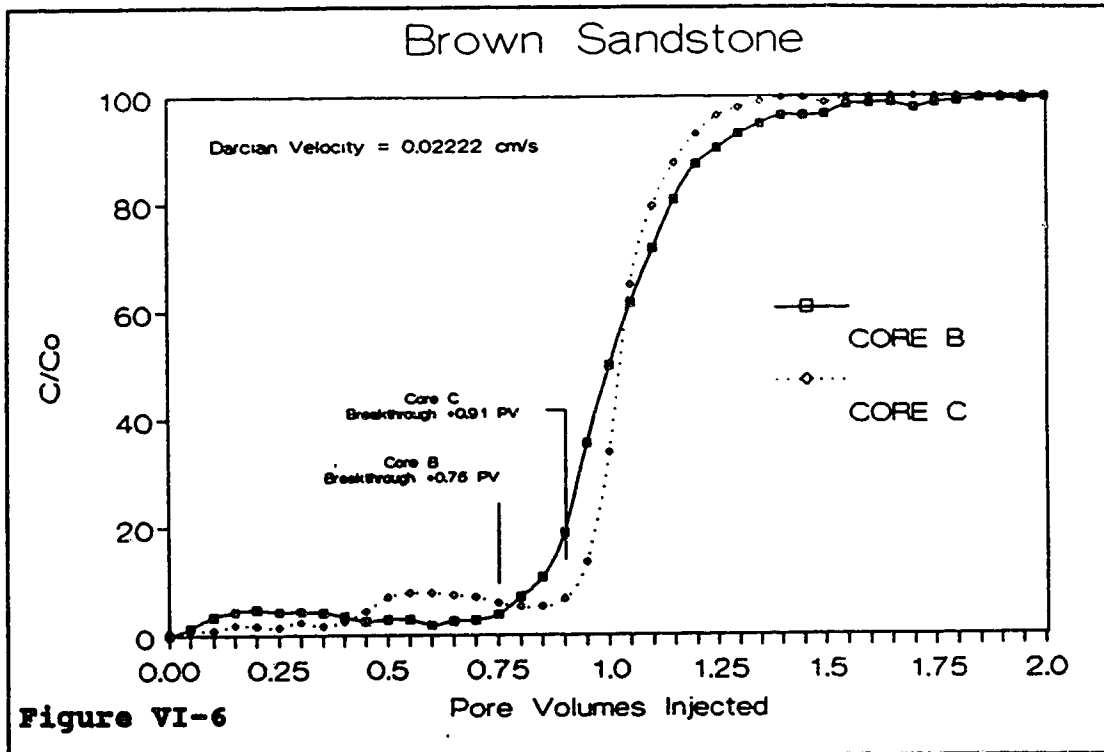
1. A linear, first-contact miscible system is used.
2. Solvent is injected continuously.
3. Gravity effects are eliminated.
4. Flood rates are high in order to minimize diffusion effects.
5. Permeability depends only upon the saturation of the oil or solvent.

The design of the coreflood experiments in this study satisfies conditions 1-4 while the 5th condition was assumed to be valid in the absence of interfacial tension.

Figures VI-2 to VI-7 show the effluent concentration profiles for the ten cores evaluated in this study. In each figure, the point at which solvent breakthrough occurred is indicated.







Based upon Equation VI-3 and the viscosity data contained in Table V-1, the effective viscosity ratio E for the floods shown in Figures VI-2 to VI-7 is 0.80803. For a completely homogeneous system, $H=1$ and breakthrough would occur at 1.237 P.V.. This calculation shows that Equation VI-3 cannot be applied to systems with favorable viscosity ratios without modification as material balance considerations limit the breakthrough pore volume to 1.0 P.V.. In light of this, we will simply assume that a completely homogeneous system will have an H value of 1.237. We can then normalize all of the H values by dividing them by 1.237 to be consistent with the scaling used by Koval. By doing this we can arrive at a relative scale where a completely homogeneous system is represented by a normalized H value of 1.0. This normalization is required to account for the fact that the mobility ratio of the displacements was less than 1.

Table VI-2 shows the results of these calculations.

Table VI-2
Koval's H Parameter

Core	P.V. @ Breakthrough	K	H	Normalized H
A	0.56	1.785	2.209	1.785
B	0.75	1.333	1.650	1.333
C	0.91	1.098	1.359	1.098
D	0.56	1.785	2.209	1.785
E	0.92	1.086	1.345	1.086
F	0.56	1.785	2.209	1.785
G	0.62	1.612	1.996	1.612
H	0.83	1.204	1.491	1.204
I	0.27	3.703	4.583	3.703
J	0.27	3.703	4.583	3.703

VII. Results and Discussion

A. Line of Investigation

A review of the literature reveals that the effect of spatial correlation of hydraulic properties (eg. permeability, porosity and pore throat characteristics) upon miscible recovery efficiency has received relatively little attention. In the current study an investigation of the following topics related to convective dispersion (K_e) and the efficiency of a first-contact miscible process was carried out:

1. Relationship between floodrate, convective dispersion (K_e) and recovery factor.
2. Effect of lithology on convective dispersion (K_e) and recovery efficiency.
3. Effect of permeability, porosity and mean pore throat size variances on convective dispersion and recovery efficiency.
4. Relationship between fractal dimension of permeability, porosity and mean pore throat size and dispersion and recovery efficiency behavior.

Unlike many coreflood experiments described in the literature, the current study was designed to isolate the effect of the pore structure on convective dispersion and

recovery factor. As a result, the effect of the lithology type upon K , and recovery efficiency may be qualitatively assessed. To the best of the author's knowledge, the current study is also unique in its evaluation of the relationship between fractal dimension and convective dispersion on the laboratory scale.

In the remainder of this chapter the four topics noted above will be discussed. In addition, a comparison of a fractal heterogeneity estimator with the well-known Dykstra-Parsons and Koval heterogeneity coefficients will be presented. As a final step, a possible method of predicting field scale dispersivities from laboratory measured dispersivities using fractal dimensions will be examined.

B. Discussion of Results

1. Effect of Floodrate and Convective Dispersion on Recovery Efficiency

Tables VII-1 through VII-3 summarize the results obtained for each of the corefloods undertaken in this study.

Table VII-1
Coreflood Results (Target rate=0.0222 cm/s)

Core	Lithology	v (cm/s)	K_r cm ² /s	R.F. @ 1.0 P.V.	R.F. @ 1.5 P.V.	R.F. @ 2.0 P.V.
A	Indiana Lst.	0.0224	0.0948	87.6	95.1	96.1
B	Brown Sst.	0.0215	0.0270	92.6	98.3	100.0
C	Brown Sst.	0.0220	0.0105	94.6	100.0	100.0
D	Indiana Lst.	0.0223	0.0108	89.9	98.7	99.3
E	Berea Sst.	0.0216	0.0037	92.9	96.3	96.3
F	S.Hills Lst.	0.0229	0.3050	81.8	83.0	83.2
G	G.Spike Lst.	0.0213	0.1930	82.5	92.5	96.3
H	Berea Sst.	0.0222	0.0053	84.9	86.2	86.4
I	Tyndle Lst.	0.0229	0.2913	84.4	93.3	97.0
J	Tyndle Lst.	0.0230	0.5149	80.4	88.3	91.8

Table VII-2
Coreflood Results (Target rate=0.0153 cm/s)

Core	Lithology	v (cm/s)	K_r cm ² /s	R.F. @ 1.0 P.V.	R.F. @ 1.5 P.V.	R.F. @ 2.0 P.V.
A	Indiana Lst.	0.0145	0.0437	88.0	94.0	94.7
B	Brown Sst.	0.0152	0.0165	94.2	100.0	100.0
C	Brown Sst.	0.0155	0.0062	96.9	100.0	100.0
D	Indiana Lst.	0.0167	0.0455	89.9	96.7	97.2
E	Berea Sst.	0.0161	0.0020	97.4	100.0	100.0
F	S.Hills Lst.	0.0185	0.0122	92.8	95.4	96.0
G	G.Spike Lst.	0.0164	0.1220	89.0	100.0	100.0
H	Berea Sst.	0.0142	0.0040	91.0	93.7	93.8
I	Tyndle Lst.	0.0146	0.1462	85.5	96.0	99.8
J	Tyndle Lst.	0.0148	0.2535	81.0	90.1	93.6

Table VII-3
Coreflood Results (Target rate=0.0097 cm/s)

Core	Lithology	v (cm/s)	K_o cm ² /s	R.F. @ 1.0 P.V.	R.F. @ 1.5 P.V.	R.F. @ 2.0 P.V.
A	Indiana Lst.	0.0110	0.0210	90.6	97.9	98.3
B	Brown Sst.	0.0088	0.0099	95.5	100.0	100.0
C	Brown Sst.	0.0086	0.0030	96.9	100.0	100.0
D	Indiana Lst.	0.0090	0.0246	90.4	98.8	99.3
E	Berea Sst.	0.0092	0.0011	98.0	100.0	100.0
F	S.Hills Lst.	0.0092	0.0294	93.7	96.7	96.8
G	G.Spike Lst.	0.0095	0.0709	89.5	100.0	100.0
H	Berea Sst.	0.0091	0.0017	94.7	97.0	97.2
I	Tyndle Lst.	0.0091	0.0768	86.2	98.1	100.0
J	Tyndle Lst.	0.0096	0.0924	83.6	93.9	97.4

In general, it may be noted that recovery efficiency for a given rock type increases with a decrease in the flood velocity. Figure VII-1 illustrates the behavior of the ten cores studied. The first point on the left of each polygon represents a floodrate of 0.0222 cm/s (80 cm/hr), the second point, a rate of 0.0153 cm/s (55 cm/hr) and the point on the right a rate of 0.0097 cm/s (35 cm/hr). Note that the recovery factor shows an increase with decreasing rate in all cases.

Flood Velocity vs R.F. @ 1 P.V.

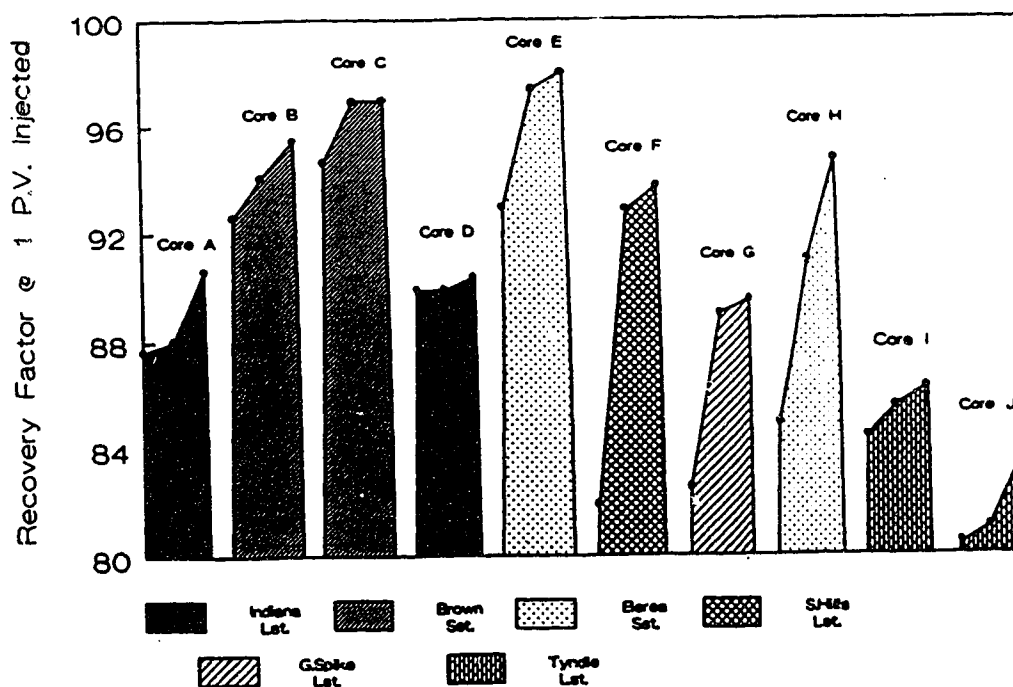
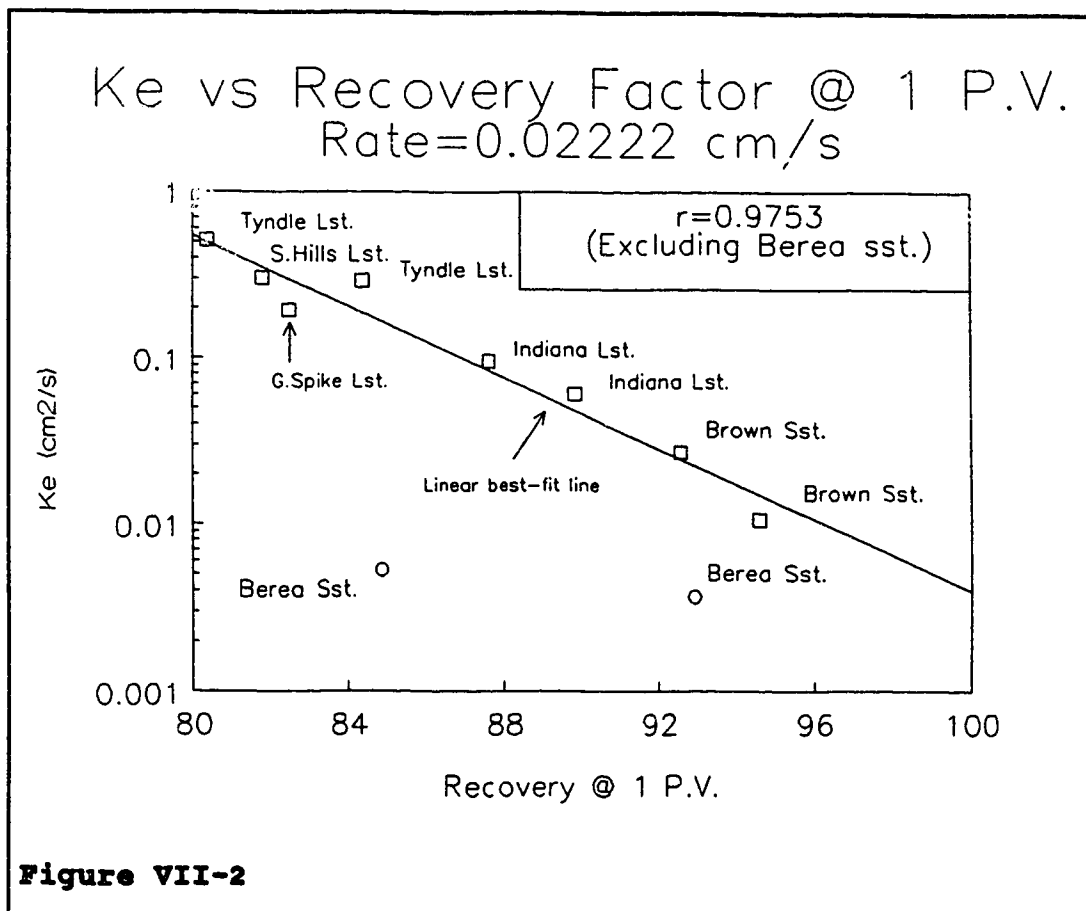


Figure VII-1

This effect occurs in stable displacements as a result of the reduced effect of convective dispersion at lower flow rates (Perkins and Johnston, 1963). Shelton and Schneider (1975) also attributed this result to a more efficient stripping of the resident oil from dead-end porespace by diffusion processes.

Several studies have focused on the effect of convective dispersion upon the recovery efficiency of a first-contact miscible process. Spence and Watkins (1980) showed that recovery efficiency decreased with increasing convective dispersion. Stalkup (1983) observed that recovery efficiency is affected by the degree of dispersion in the miscible transition zone. Increasing amounts of convective dispersion tended to produce wider transition zones and less efficient displacements. Figure VII-2 shows a semi-log correlation of convective dispersion and the recovery factor. It may be observed that the recovery factor at 1 pore volume of solvent injected increases as K_r decreases. Based upon studies conducted on Berea sandstones by other researchers, there is reason to suspect that the recovery factor of 84.87% obtained for Core H is unusually low for this type of sandstone (Shelton and Schneider, 1975). An inspection of the effluent concentration profile reveals that early breakthrough of the solvent occurred during flooding of Core H indicating that channeling of the solvent may have occurred, thus explaining the relatively low recovery factor. In any case, the value obtained for K_r appears to be valid based upon the fact that K_r is only calculated from the portion of the effluent concentration profile



which occurs after breakthrough as well as the fact that these portions of the profile are very similar for both Core E and Core H (Figure VI-3). A further validation of K_e is found in the work of Spence and Watkins (1980) who reported K_e values of approximately $0.005 \text{ cm}^2/\text{s}$ for Berea cores. If the Berea sandstone cores are grouped separately from all of the other rock types then the remaining data are well fit ($r=0.9753$) (Figure VII-2) by a logarithmic

correlation of the following form:

$$K_e = 199774015.9 (10)^{-0.107027(R.F.)} \quad (\text{VII-1})$$

Where: K_e = effective dispersion coefficient (cm^2/s).

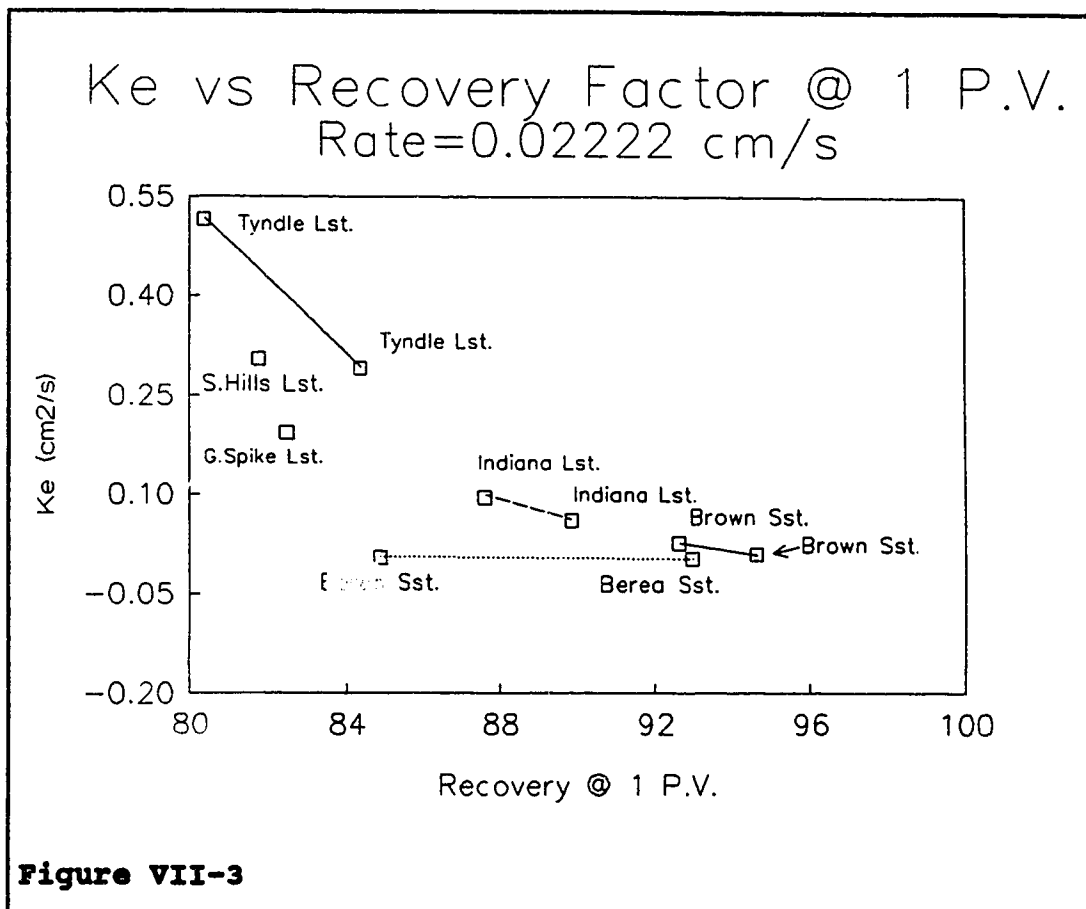
$R.F.$ = recovery factor @ 1 P.V. injected.

This equation is equivalent to plotting $\log K_e$ vs $R.F.$ and obtaining a linear "best-fit" line through the points. The data from the Berea cores also appear to show an inverse correlation between K_e and the recovery factor although this inference is only based upon two data points.

The results obtained agree with earlier findings regarding the inverse relationship between convective dispersion and recovery efficiency (Spence and Watkins, 1980).

2. Effect of Lithology on K_e and Recovery Efficiency

Several observations were noted regarding the effect of lithology upon the value of K_e and the associated recovery factor. Figure VII-3 shows the effect of grouping the core data points by lithology on a standard coordinate axis.



It is interesting to note that for the Berea cores, K , is as much as an order of magnitude less than the K , values for any of the other cores. This may be explained qualitatively by the fact that Berea sandstone is recognized as one of the most homogeneous rock types available. Hence, it would be expected that convective dispersion caused by heterogeneity in the pore structure would be relatively small.

In general, it was also noted that the cores having higher values of K , and lower recovery factors tended to be carbonates while those having higher recoveries tended to be sandstones (Figure VII-1). Also of interest is the fact that the recovery factor appears to be much more sensitive to changes in K , for the sandstones than is the case for the (presumably) more heterogeneous limestones. Figure VII-3 shows this effect. Note that the slope of the straight lines connecting cores of equivalent rock type tend to flatten out as one progresses from limestones to sandstones. The relationship between lithology and K , is a complex one and caution must be exercised in the interpretation of these results. The fact that only ten cores were tested under identical conditions suggests that these findings should be viewed as qualitative results only.

3. Effect of Permeability, Porosity and Mean Pore Throat Size Variance on Dispersion Behavior and Recovery Efficiency

Studies by Bretz et al (1988) related pore size variation to convective dispersion using thin-section techniques. It was found that wide pore size distributions could be correlated with larger amounts of convective dispersion. In the following discussion an examination will be carried out on the effect of variance of the three

properties tested upon the values of K_r , $\log K_r$, and the recovery factor. The use of σ^2 to represent the width of the frequency distribution curve is valid provided that any outliers in the data are removed first. In general, outliers were recognized by comparing the data values obtained for each core and removing data which appeared to be unusually high. This process was fairly straightforward in that the outliers were few in number and were often at least an order of magnitude higher than values in the rest of the data set. Aside from making the estimation of variance more representative for the particular core being studied, the removal of outliers also has a physical basis. In the case of porosity, outlier values between 0.40 and 0.50 occurred occasionally and are probably the result of errors in the measurement of bulk volume. Permeability values greater than 1000 md were also excluded from the analysis on the basis that they appear to represent samples which were fractured. The case may be made that these fractures are an important part of the structure of the porous medium and should not be removed. As a test of this possibility, they were removed in calculating variance estimates but were used in the calculation of fractal dimension. None of the mean pore throat size data sets showed evidence of outliers using

the above criteria (Appendix C).

Table VII-4 illustrates the findings of the study regarding the relationship between variance estimates and K_r and R.F.

Table VII-4
Correlation of Variance
With K_r and R.F.

Property Variance	vs	K_r	$\log K_r$	R.F. @ 1 P.V.
Porosity		$r=0.126$	$r=0.354$	$r=0.312$
Permeability		$r=0.100$	$r=0.284$	$r=0.289$
Mean Pore Throat Diameter		$r=0.349$	$r=0.036$	$r=0.214$

A variety of correlation models were applied to the data. A linear "least-squares" model was found to yield the highest values for the correlation coefficient, r and was used in all cases.

In all cases, the degree of positive or negative correlation between the calculated parameters is quite low. This would indicate that convective dispersion and recovery factor are relatively insensitive to statistical variance estimates of the measured properties. Although this finding appears valid for the current study, it is by no means conclusive. It is quite possible that the number of samples studied and their location were inappropriate

for the proper estimation of variance in each core. If the procedure is accepted as valid, however, then it appears that the use of property variance as a means of describing the heterogeneity of a porous medium and hence predicting its flow characteristics cannot be recommended.

4. Relationship Between Fractal Dimension of Permeability, porosity and Mean Pore Throat Size and Dispersion and Recovery Efficiency

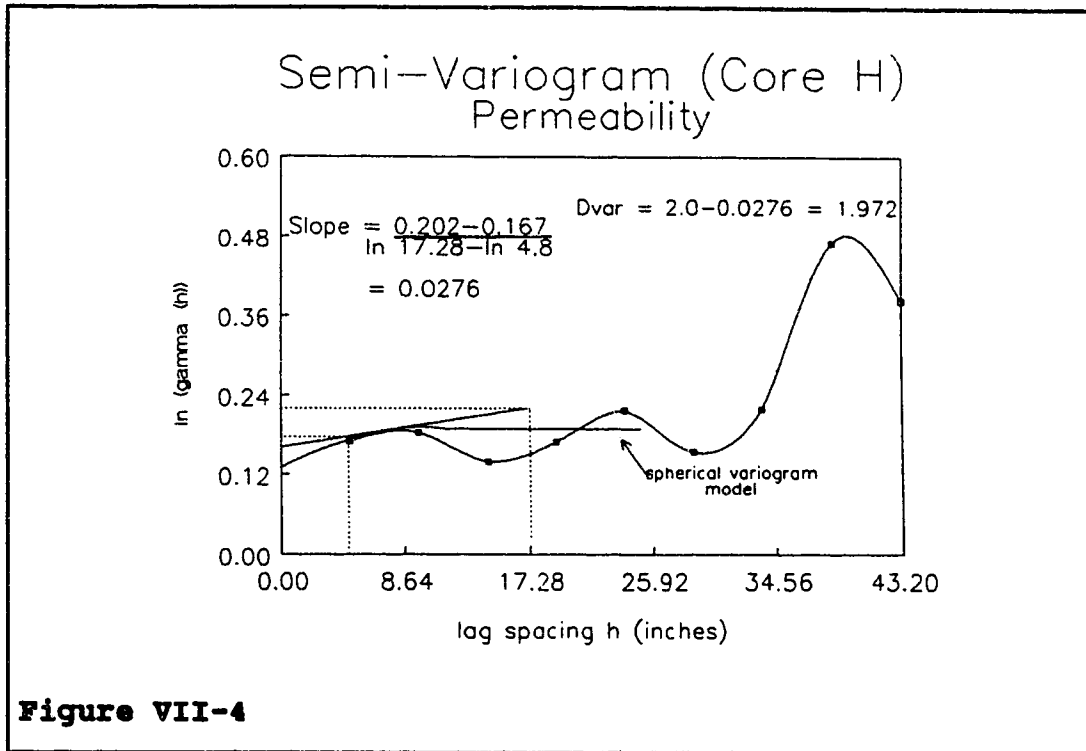
Table VII-5 summarizes the results of the fractal dimensional analysis for each core. It may be noted that the fractal dimensions obtained using semi-variograms are much higher and more erratic than those calculated from autocorrelation functions. This is due, in large part, to the fact that many of the semi-variograms were highly variable in nature thus making the determination of the slope near the origin a somewhat subjective process. Particular difficulty was experienced when the initial slope of the plot was negative. Figure VII-4 shows a sample calculation. Note that the determination of the slope as h approaches zero is subject to a fair amount of uncertainty. In addition, many of the semi-variograms exhibited a fairly low slope near the origin.

Table VII-5
Calculated Fractal Dimensions

Core	Permeability		Porosity		Mean Pore Throat Size	
	D_{acf}	D_{var}	D_{acf}	D_{var}	D_{acf}	D_{var}
A	1.546	1.071	1.437	1.937	1.437	1.821
B	1.521	1.889	1.496	1.998	1.620	1.985
C	1.510	1.621	1.489	1.996	1.357	1.975
D	1.513	1.917	1.577	1.992	1.688	1.948
E	1.467	1.136	1.467	1.993	1.364	1.945
F	1.525	1.541	1.560	1.675	1.438	1.770
G	1.531	1.357	1.565	1.926	1.509	1.973
H	1.479	1.972	1.403	1.996	1.546	1.953
I	1.518	1.862	1.532	1.989	1.636	1.996
J	1.546	1.437	1.391	1.987	1.469	1.968

As a result of these factors, the fractal dimensions obtained from the two processes were treated separately (Appendix B).

The values shown in Table VII-5 were compared with K_r , $\log K_r$, and recovery factor (R.F.) using a linear "least-squares" approach. As was the case in the previous section, the effect of excluding data for the Berea cores was also evaluated. Correlation coefficients (r) were calculated for the case where all cores were included and the correlation was then recalculated excluding the Berea cores.



Tables VII-6 through VII-8 show the results of these calculations.

Table VII-6
Permeability Fractal Correlations

	vs	K_p	$\log K_p$	R.F.
$D_{acf}(\text{w/o B. sst.})$		$r=0.800$	$r=0.634$	$r=0.697$
$D_{acf}(\text{all cores})$		$r=0.740$	$r=0.858$	$r=0.515$
$D_{var}(\text{w/o B. sst.})$		$r=0.208$	$r=0.274$	$r=0.374$
$D_{var}(\text{all cores})$		$r=0.128$	$r=0.084$	$r=0.042$

Table VII-7
Porosity Fractal Correlations

	vs	K_r	$\log K_r$	R.F.
$D_{acf}(\text{w/o B. sst.})$		$r=0.261$	$r=0.011$	$r=0.049$
$D_{acf}(\text{all cores})$		$r=0.017$	$r=0.296$	$r=0.042$
$D_{var}(\text{w/o B. sst.})$		$r=0.271$	$r=0.392$	$r=0.468$
$D_{var}(\text{all cores})$		$r=0.343$	$r=0.431$	$r=0.454$

Table VII-8
Mean Pore Throat Size Fractal Correlations

	vs	K_r	$\log K_r$	R.F.
$D_{acf}(\text{w/o B. sst.})$		$r=0.189$	$r=0.004$	$r=0.060$
$D_{acf}(\text{all cores})$		$r=0.008$	$r=0.251$	$r=0.133$
$D_{var}(\text{w/o B. sst.})$		$r=0.079$	$r=0.243$	$r=0.270$
$D_{var}(\text{all cores})$		$r=0.119$	$r=0.240$	$r=0.255$

Calculations involving the fractal dimension of porosity and mean pore throat size did not show a significant degree of correlation with K_r and R.F. This suggests that K_r and R.F. are independent of the fractal dimension of porosity and mean pore throat size. This finding is not surprising in that flow characteristics in

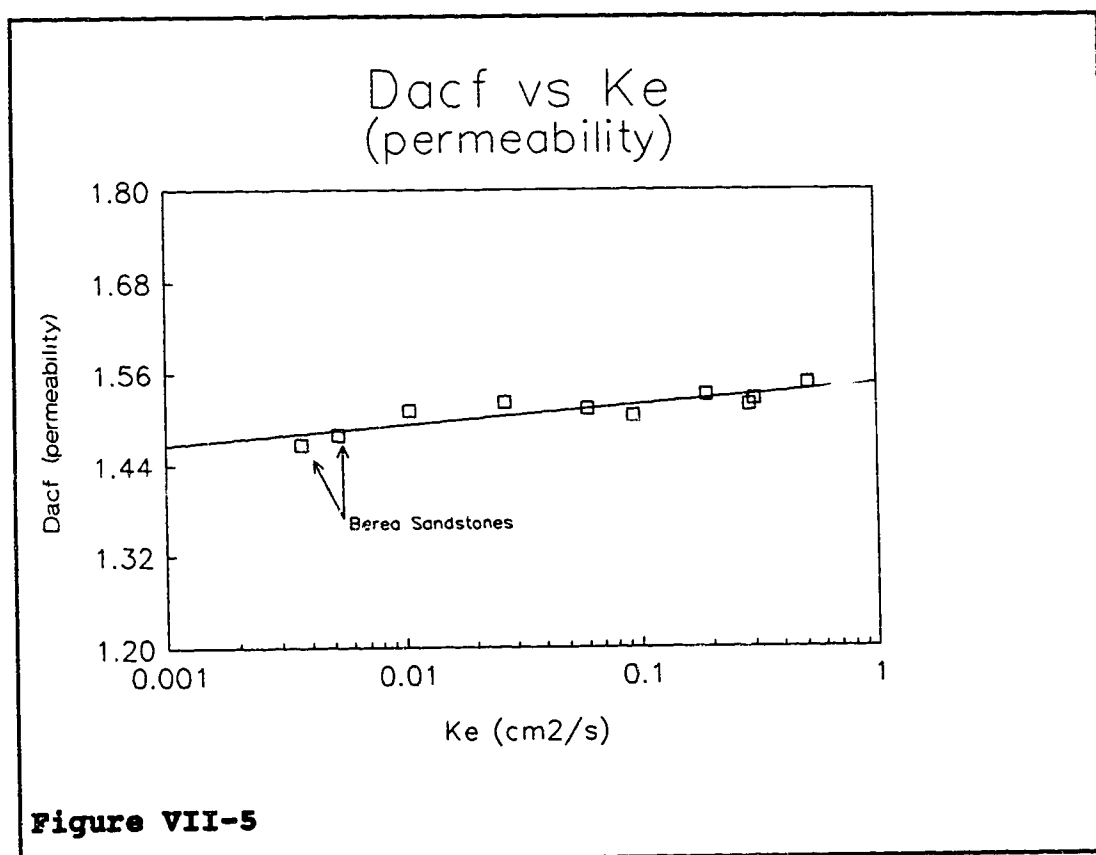
a porous medium have been found to be controlled by permeability variations. Dykstra and Parsons (1950) noted that although total recovery is a function of porosity, the recovery factor is influenced by permeability variations. Under conditions of miscible and immiscible displacements, we may expect the porosity distribution to influence only the total recovery and then only if all of the porosity were contacted with equal efficiency by the displacing fluid. This would require that the permeability be the same at all locations.

The lack of significance of the fractal dimension for mean pore throat size may be attributed to the absence of capillary forces under miscible conditions. Under conditions of immiscible displacement, the size of the pore throats will have a direct influence upon relative permeability and hence will directly affect fluid flow in the porous medium. In the case of miscible displacement, mean pore throat size does not appear to be as important.

The most significant correlations were observed when the fractal dimension of permeability was examined. An examination of Table VII-6 shows that there is a large difference in the degree of correlation when using fractal dimensions calculated by the semi-variogram method (D_{var}) and using the method of autocorrelation functions

(D_{acf}). While the use of semi-variograms in the calculation of fractal dimension is valid on a theoretical basis, in practice it was found to be difficult to apply. In particular, it was difficult to determine the slope of the semi-variogram as $h \rightarrow 0$ due to the erratic behavior of some of the semi-variograms (Appendix B). The fitting of a model to a semi-variogram and the determination of the slope of the model as $h \rightarrow 0$ is a very subjective process for the most part and is subject to errors of interpretation on the part of the user. Because the calculation of the fractal dimension by the method of Burrough (Equation IV-14) is sensitive to these variations the use of D_{var} as a consistent indicator of fractal dimension cannot be recommended. A more promising approach involves the use of autocorrelation functions in the calculation of fractal dimension. This method has the advantage of eliminating subjectivity from the calculation procedure.

Figure VII-5 illustrates the degree of correlation between D_{acf} and $\log K$, for permeability. Note that the degree of correlation is generally very good and improves when the Berea cores are included in the analysis ($r=0.858$). Conversely, Table VII-6 shows that the degree of correlation between D_{acf} and R.F. decreased when



the Berea cores were included. It appears that this result may be attributed to a lower than expected recovery factor for core H. The calculated values for convective dispersion (K_c) are considered to be accurate for all cores as discussed earlier. As a result, including the Berea cores improves the correlation in the case of the D_{acf} vs K_c plot.

A correlation of the following form exists between D_{acf} and K_c in Figure VII-5:

$$K_e = 4.8698442 \times 10^{-60} (10)^{38.41279204(D_{acf})} \quad (\text{VII-3})$$

Where: K_e = effective convective dispersion coefficient (cm^2/s).

D_{acf} = fractal dimension for permeability

calculated from autocorrelation functions.

The fact that a correlation appears to exist between D_{acf} and K_e (Equation VII-3) and also between K_e and R.F. (Equation VII-1) suggests the development of an equation which directly relates D_{acf} to R.F.. Substituting K_e from Equation VII-3 into Equation VII-1, we get:

$$R.F. = 631.73801 - 358.9075(D_{acf}) \quad (\text{VII-4})$$

$$1.4815 < D_{acf} < 1.7602$$

Where: R.F. = recovery factor (%).

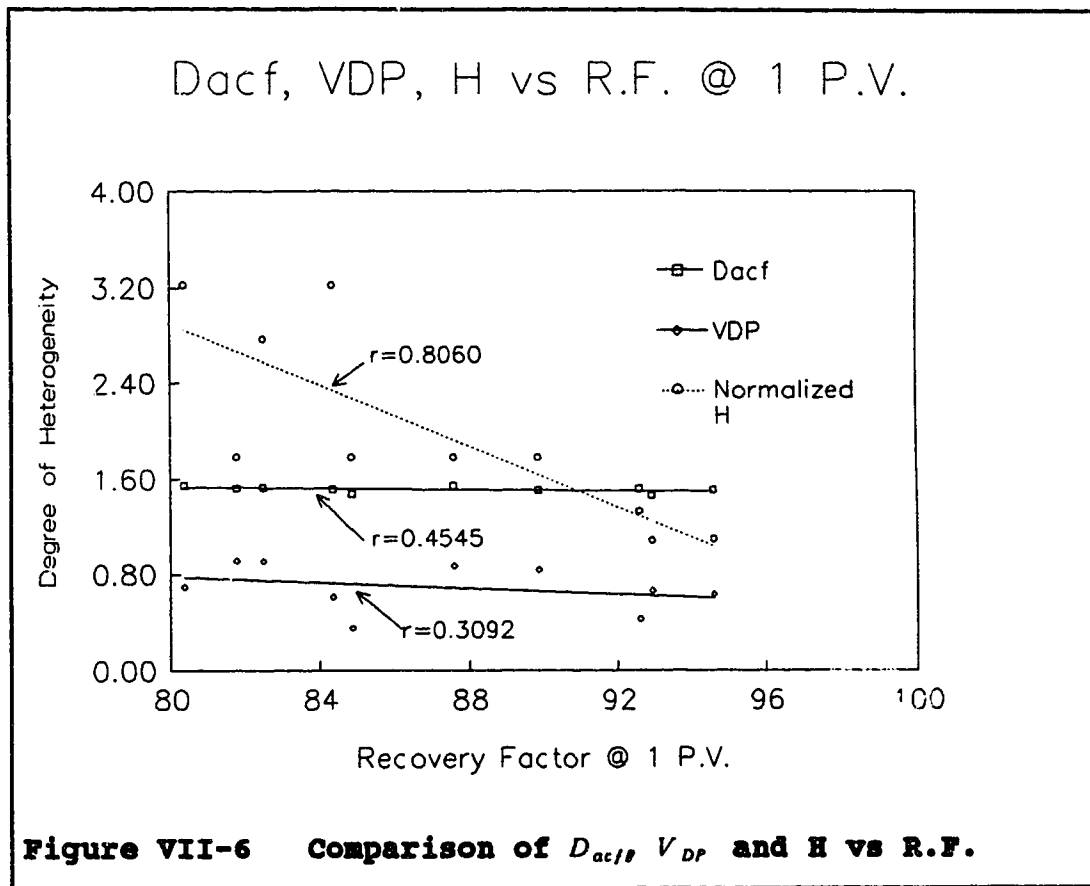
D_{acf} = fractal dimension for permeability

determined from autocorrelation functions.

5. Comparison of D_{acf} with V_{DP} and Koval's H

Figure VII-6 provides a comparison of D_{acf} , the Dykstra-Parsons permeability variation, V_{DP} , and Koval's heterogeneity factor, H. Data from Tables VI-1, VI-2 and VII-5 were plotted vs the recovery factor at 1 P.V. injected.

While the spread of the data points around the best-fit line may seem otherwise, the best correlation with R.F. ($r=0.806$) is obtained for the Koval factor, H. The reason for this is that the calculation of H is very

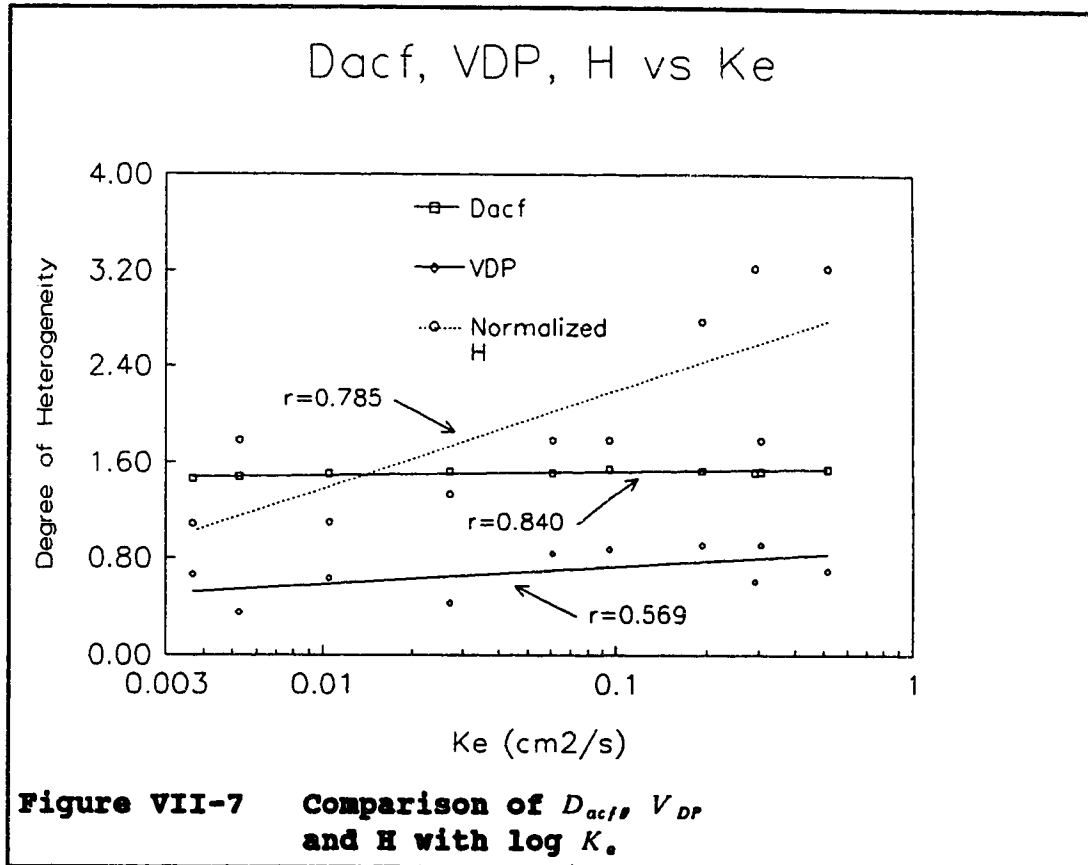


sensitive to the degree of channeling which takes place within the core. This channeling effect is measured directly from effluent concentration profiles and has a direct influence upon the calculated R.F. (eg. early breakthrough implies that some of the oil is being bypassed and recovery will be less efficient). Also of interest is the fact that as the H factor increases, the data points appear to show a greater degree of scatter. This result appears to support the contention of McCaffery

et al. (1978) who questioned the assumption that effective permeability is dependent only upon the saturation of the oil or solvent in more heterogeneous systems.

It seems probable that the defining equation for the effective viscosity ratio (Equation VI-3) used by Koval is inadequate for describing the effective viscosity ratio in more heterogeneous systems. This would not be surprising in that Equation VI-3 was based upon experiments conducted in homogeneous cores only (Koval, 1963). This result invites further study into the applicability of the effective viscosity ratio equation in more heterogeneous systems.

Unlike Koval's H , D_{ac} , and V_{DP} are calculated independently of the effluent concentration profile (eg. are independent variables) and show a lesser degree of correlation with recovery factor. Figure VII-7 shows the degree of correlation between the heterogeneity estimators and $\log K_r$. Note that in this case the best correlation is provided by D_{ac} ($r=0.840$). This result was noted earlier however, Koval's H factor also shows a relatively good fit to $\log K_r$ ($r=0.785$). This suggests that channeling is a strong contributor to the value of the effective dispersion coefficient K_r . The Dykstra-Parson's coefficient showed the lowest degree of correlation when



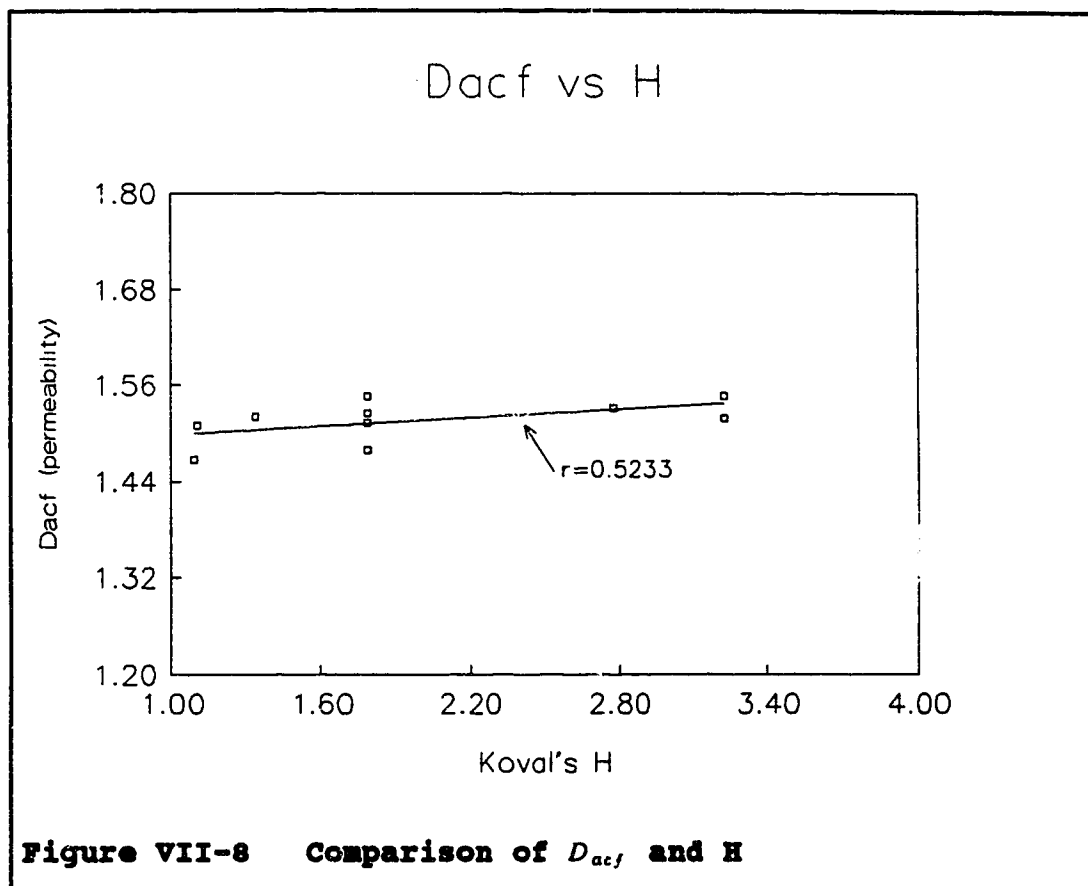
plotted vs R.F. and $\log K_e$. This result was expected in light of the fact that V_{DP} represents an estimate of the width of the permeability frequency distribution and should show similar results to attempts to correlate permeability variance with R.F. and $\log K_e$ (Table VII-4).

Of importance in these comparisons between heterogeneity estimators are the treatment of outliers or extreme values. It is significant that V_{DP} and the permeability variance were calculated by excluding

outliers from the analysis while D_{acf} included all values. It is possible that these extreme permeability values control the behavior of fluid flow within a porous medium by facilitating the channeling of solvent and bypassing of resident oil. Koval's H factor quantifies the effect of these extreme values in causing early breakthrough however, its efficiency in predicting R.F. and K, in more heterogeneous rock types is in doubt considering the spread of the data points about the best-fit line for more heterogeneous cores shown in Figures VII-6 and VII-7. The use of V_{DP} is unsuitable in that it ignores the effect of high permeability values which may predispose the porous medium to channeling of the solvent. Unlike waterflooding, channeling in miscible displacement is more critical to the process in that dilution of a solvent slug and loss of miscibility can occur very rapidly, thus rendering the process ineffective.

Figure VII-8 shows a comparison between D_{acf} and H. Although the correlation is only fair ($r=0.523$), the point of breakthrough on the effluent concentration profile is subject to an error of 0.05 P.V.. This translates into an error in H of ± 0.22 . Qualitatively, however, it appears that D_{acf} can give an indication of the degree of channeling provided that extreme values are included in

the analysis.



6. Scale Dependence and D_{acf}

The question we must now ask is why go to the trouble of determining D_{acf} when Koval's H seems to correlate with $\log K$, and R.F. nearly as well? The answer to this question lies in the fact that K , varies with the scale of the system under consideration. It is this scale dependence which creates difficulties in applying the results of laboratory investigations to field scale

developments. The use of the fractal dimension (D) as an estimator of heterogeneity suggests a means of overcoming this difficulty. The basic advantage of this approach is that *the fractal dimension is invariant over all scales of measurement that it is evaluated from*. Wheatcraft and Tyler (1988) observed that dispersivity does not vary in a linear manner with scale but appears to be dependent upon the degree of "regularity" of the permeability variation at all available scales of measurement within a given system. Equation VII-5 illustrates an equation developed by Wheatcraft and Tyler (1988) describing the relationship between fractal dimension and dispersivity under conditions where the laboratory and field flood rates are the same.

$$Ke_{field} = Ke_{lab} \xi_c^{1-D} L^{D-1} \quad (VII-5)$$

Where: Ke_{field} = field measured dispersivity (m).

Ke_{lab} = lab measured dispersivity (m).

ξ_c = smallest scale of measurement used
in determining D.

L = length of the system under study (m).

D = fractal dimension for permeability.

note that Ke_{field} and $Ke_{lab} = \frac{K_e}{v}$ where K_e = the effective dispersion

coefficient $\left(\frac{cm^2}{s}\right)$ and v = the darcian velocity of the displacement $\left(\frac{cm}{s}\right)$.

This equation has several interesting characteristics. For the limiting case where the porous medium is perfectly homogeneous ($D_{acf}=1.0$) Ke_{field} is equal to Ke_{lab} and is independent of scale. In addition, dispersivity increases proportionately to L^{D-1} . For the limiting case where $D=2$, dispersivity is proportional to the scale of measurement, L . A preliminary test of the applicability of this equation may be undertaken by substituting D_{acf} (permeability) from Table VII-5 for D , setting $\xi_c = 0.1219$ m. and using Ke_{lab} values from Table VII-3 ($v \approx 0.0097$ cm/s). Ke_{field} values for a variety of different scales (L) may then be generated. It was decided to group the ten cores by lithology with the value of D_{acf} (perm.) used being a mean value in cases where more than one core was available. The following is a sample calculation for the Indiana limestones.

mean value of $K_p = 0.0228$ cm²/s

mean darcian velocity = 0.01003 cm/s

$$Ke_{lab} = \frac{0.0228}{0.0100} = 2.2721 \text{ cm.}$$

mean value of $D_{acf} = 1.5295$.

$L = 100$ m, $Ke_{field} = 79.31$ m.

$L = 1000$ m, $Ke_{field} = 268.44$ m.

A set of six curves were generated illustrating the growth of dispersivity with fractal dimension (Figure VII-9). As a test of the applicability of this approach, field data relating dispersivity to the scale of observation is also shown. This data, obtained by Gelhar et al (1985) represents the results of numerous tracer tests from around the world. Gelhar's data is based upon field displacement rates which are lower than the lowest rate evaluated in this study (Table VII-3). As a result each of the curves shown in Figure VII-9 may be treated as being upper boundaries on the expected value of Ke_{field} at a given scale (L) for each lithology type. In addition, the rock types represented in Gelhar's data were primarily sandstones with a small number of limestone aquifers being included.

Figure VII-9 shows that the curves generated for Indiana limestone, Berea and Brown sandstone as well as Swan Hills limestone show a realistic growth in dispersivity with scale as indicated by the clustering of the field data. The Golden Spike and Tyndle limestones tended to lie above the region occupied by the field data. These lithologies had the highest fractal dimension (D_{acf}) and tended to show a greater increase in dispersivity with scale. Although none of the field data obtained falls into

Dispersivity vs Scale

Lab Rate = 0.009722 cm/s

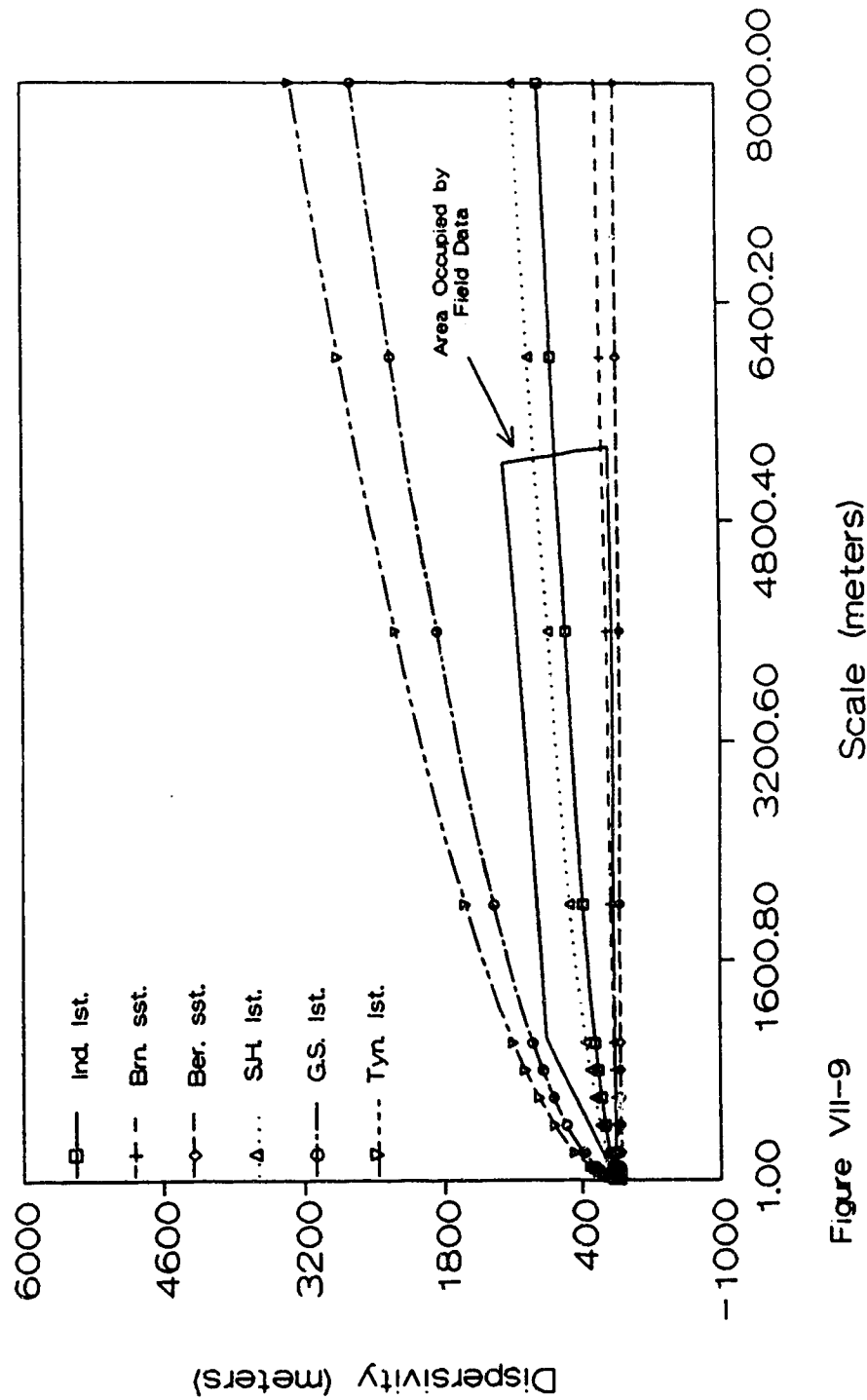


Figure VII-9

the region of these curves it does not necessarily follow that they are unrealistic. The first point to consider is that much of Gelhar *et al*'s data described aquifers in which the source rock was significantly different than the Golden Spike and Tyndle limestones in the current study. It may be the case that all of the field data represents lithologies that are more homogeneous than Golden Spike or Tyndle limestones.

The second point to consider involves the behavior of dispersivity with displacement rate. In general, as the rate decreases, dispersivity also decreases for a given porous medium. For more heterogeneous rock types (eg. higher D_{acf}), it appears that this reduction of dispersivity is much more pronounced as the rate is decreased than is the case for more homogeneous rock types. If this is the case, a reduction to actual field rates may reduce Ke_{lab} for the limestones in question to the point where the upper two curves in Figure VII-9 lie within the upper boundary of the available field data.

Use of the fractal dimension as a means of determining dispersivities on a field scale will require a better validation of the preliminary comparison shown in Figure VII-9. It would be instructive to isolate the field tracer data by lithology and compare it with individual

dispersivity curves shown in Figure VII-9. In addition, it is important that D_{acf} be determined using larger scales of measurement than were practical in the present study. Current research into this possibility is centering around the use of S.P. logs in the calculation of fractal dimension on a field wide basis. By defining the fractal dimension for a field or portion of a field it may be possible to develop a set of correlation curves relating dispersivity to scale using fractal dimension as a cross-plotting parameter.

VIII. Conclusions and Recommendations

The relationship between several heterogeneity indicators and the mixing behaviour of a first-contact miscible process was investigated in the current study. Based upon the experiments conducted in this study, it may be concluded that:

1. The fractal dimension for permeability (D_{acf}) may be used to scale up dispersivity values $\left(\frac{\alpha_s}{\alpha}$) from laboratory scale to field scale.
2. The Dykstra-Parson's permeability variation V_{DP} does not correlate well with either $\log K_r$ or R.F.. It appears that the calculation of V_{DP} ignores the effect of extreme permeability values which appear to influence channeling and convective dispersion.
3. A positive logarithmic correlation exists between K_r and the calculated fractal dimension for permeability (D_{acf}).
4. The recovery factor shows a linear correlation with D_{acf} .
5. The Koval heterogeneity factor (H) shows the best correlation with recovery factor but appears to be less reliable for more heterogeneous rock types.
6. D_{acf} and Koval's H provide the best correlation with

$\log K_*$.

7. Recovery efficiency increases with decreased flood velocity for a given rock type.
8. Recovery efficiency (R.F.) shows an inverse logarithmic correlation with convective dispersion (K_*) for all rock types.
9. Carbonates showed the highest values of K_* and the lowest recovery factors while sandstones; in general, showed lower K_* values and a higher recovery factor.
10. The more homogeneous the rock type, the greater the sensitivity of the recovery factor to changes in the degree of convective dispersion.
11. Permeability, porosity and mean pore throat size variances showed little correlation with K_* or R.F. and cannot be recommended as a means of describing heterogeneity in porous media.
12. Calculation of fractal dimensions is best accomplished through the use of autocorrelation functions (D_{acf}). The erratic behavior of some of the semi-variograms near the origin makes their use unreliable.

Several additional areas of experimentation are suggested from the results of this study:

1. The effect of length upon convective dispersion for different rock types needs to be quantified in greater detail.
2. A revised equation for the effective viscosity ratio (E) used in the calculation of Koval's H will need to be developed. The current equation does not appear to adequately describe the effective viscosity in more heterogeneous rock types.
3. Methods of calculating fractal dimensions for permeability on a field wide basis will need to be developed. This work is ongoing.

In general, the use of the fractal dimension for permeability (D_{ac}) to describe heterogeneity shows promise. The chief advantage of this approach is that it opens up the possibility of scaling up laboratory measured dispersion to field levels in a theoretically valid manner. This study, although preliminary in nature, points out several avenues of additional research which may allow for the practical implementation of such a method in the future.

References

- Amyx, J. W., Bass, D. M. and Whiting, R. L. (1960): *Petroleum Reservoir Engineering*, McGraw-Hill Book Company, New York.
- Aronofsky, J. W. and Heller, J. P. (1957): "Diffusion Model to Explain Mixing of Flowing Miscible Fluids in Porous Media", *Trans., AIME* Vol. 210, 345.
- Baker, L. E. (1977): "Effects of Dispersion and Dead-End Pore Volume in Miscible Flooding", *SPE. J.* 6,219.
- Barnsley, M. F. (1988): *Fractals Everywhere*, Academic Press, Boston.
- Blackwell, R. J. (1962): "Laboratory Studies of Microscopic Dispersion Phenomena", *SPE. J.* 3,1.
- Blatt, N., Middleton, G. and Murray, R. (1980): *Origin of Sedimentary Rocks*, Prentice-Hall Inc., Englewood Cliffs, New Jersey.
- Bretz, R. E., Spector, R. M. and Orr, F. M. (1988): "Effect of Pore Structure on Miscible Displacement in Laboratory Cores", *SPE. J.* 3,857.
- Brigham, W. E., Reed, P. W., and Dew, J. N. (1961): "Experiments on Mixing During Miscible Displacements in Porous Media", *SPE. J.* 3,1.
- Brigham, W. E. (1974): "Mixing Equations in Short Laboratory Cores", *SPE. J.* 2,91.
- Burrough, P. A. (1981): "Fractal Dimensions of Landscapes and Other Environmental Data", *Nature*, 294,240.
- Cant, D. J. and Walker, R. G. (1976): "Development of a Braided Fluvial Facies Model for the Devonian Battery Point Sandstone, Quebec", *Canadian Jour. Earth Sci.*, V. 13, 102.
- Chilinger, G. V., Mannon, R. W. and Rieke, H. H. (eds.) (1972): *Oil and Gas Production From Carbonate Rocks*, American Elsevier Publishing Company, Inc., New York.

Chung, C. F. (1984): "Use of the Jackknife Method to Estimate Autocorrelation Functions (or Variograms)", in *Geostatistics for Natural Resource Characterization*, Verly, M. D., Journel, A. G. and Marechal, A. (eds.) NATO ASI Series, D. Reidel Publishing Company, Dordrecht.

Coats, K. H. and Smith, B. D. (1964): "Dead-End Pore Volume and Dispersion in Porous Media", *SPE. J.* 6,73.

Correa, A. C., Pande, K. K., Ramey Jr., H. J. and Brigham, W. E. (1987): "Prediction and Interpretation of Miscible Displacement Performance Using a Transverse Matrix Dispersion Model", paper 16704 presented at the SPE 62nd Annual Technical Conference and Exhibition, Dallas, Sept. 27-30.

Crickmore, P. J. (1990): personal communication.

Dykstra, H. and Parsons, R. L. (1950): "The Prediction of Oil Recovery by Waterflood", *Secondary Recovery of Oil in the United States*, American Petroleum Institute, Washington, D.C.

Gelhar, R. W., Mantoglou, C. W. and Rehfeldt, K. R. (1985): "A Review of Field Scale Physical Solute Transport Processes in Saturated and Unsaturated Porous Media", Rep. EA-4190, Electr. Power Res. Inst., Palo Alto, Calif.

Gerald, C. F. and Wheatley, P. O. (1985): *Applied Numerical Analysis*, 3rd ed., Addison-Wesley Publishing Company, Don Mills, Ontario.

Gleick, J. (1987): *Chaos, Making a New Science*, Viking Penguin Inc., New York.

Goggin, D. J. (1988): "Geologically-Sensible Modelling of the Spatial Distribution of Permeability in Eolian Deposits: Page Sandstone (Jurassic), Northern", Ph.D. Dissertation, University of Texas at Austin.

Griffin, W. H. (1990): personal communication.

Hewett, T. A. (1986): "Fractal Distribution of Reservoir Heterogeneity", paper SPE 16170 presented at the SPE 61st Annual Technical Conference and Exhibition, New Orleans, Oct. 5-8.

Jasti, J. K., Vaidya, R. N. and Fogler, H. S. (1987): "Capacitance Effects in Porous Media", paper 16707 presented at the SPE 62nd Annual Technical Conference and Exhibition, Dallas, Sept. 27-30.

Jensen, J. L. and Lake, L. W. (1988): "The Influence of Sample Size and Permeability Distribution on Heterogeneity Measures", *SPE*, 2,629.

Jodry, R. L. (1972): "Pore Geometry of Carbonate Rocks", in *Oil and Gas Production From Carbonate Rocks*, Chilingar, G. V., Mannon, R. W. and Rieke, H. H. (eds.), American Elsevier Publishing Company, Inc., New York.

Journel, A. G. and Huijbregts, C. J. (1978): *Mining Geostatistics*, Academic Press, London.

Koval, E. J. (1963): "A Method for Predicting the Performance of Unstable Miscible Displacement in Heterogeneous Media", *SPE. J.* 6,145

Langton, R. J. and Chin, G. E. (1968): "Rainbow Member Facies and Related Reservoir Properties, Rainbow Lake, Alberta", *Bull. Canadian Pet. Geology*, 16, 104.

Mandlebrot, B. B. (1971): "A Fast Fractional Gaussian Noise Generator", *Water Resources. Res.* 7, 543.

McCaffery, F. G., Sigmund, P. M., and Fosti, J. E. (1977): "Pore Space Characterization and Displacement Studies of Alberta Carbonate Reservoir Rocks", Research Report RR-33, Petroleum Recovery Institute, Alberta, Canada.

McCulloch, R. C., Langton, J. R. and Spival, A. (1969): "Simulation of High Relief Reservoirs, Rainbow Field, Alberta, Canada. *J. Pet. Tech.*, 11,1399.

Mishra, S. (1987): "On the Use of Pressure and Tracer Test Data for Reservoir Description", Ph.D Dissertation, Stanford University.

Perkins, T. K. and Johnston, O. C. (1963): "A Review of Diffusion and Dispersion in Porous Media", *SPE.J.* 3,70.

Purcell, W. R. (1949): "Capillary Pressures-Their Measurement Using Mercury and the Calculation of Permeability Therefrom", *Trans. AIME*.

- Reid, R. C., Prausnitz, J. M. and Poling, B. E. (1987): *The Properties of Gases and Liquids* 4th ed., McGraw-Hill Book Company, New York.
- Schwartz, F. W. (1977): "Macroscopic Dispersion in Porous Media: The Controlling Factors", *Water Resources Res.*, 13, 743.
- Shaw, R. C. (1988): "Near IR Diffuse Reflectance Analysis of Oilsand", M.Sc. Thesis, University of Alberta.
- Shelton, J. L. and Schneider, F. N. (1975): "The Effects of Water Injection on Miscible Flooding Methods Using Hydrocarbons and Carbon Dioxide", *SPE. J.* 6,217.
- Spence, A. P. and Watkins, R. W. (1980): "The Effect of Microscopic Core Heterogeneity on Miscible Flood Residual Oil Saturation", paper 9229 presented at the SPE 55th Annual Technical Conference and Exhibition, Dallas, Sept. 21-24.
- Stalkup, F. I. (1970): "Displacement of Oil by Solvent at High Water Saturation", *SPE. J.* 12,337.
- Stalkup, F. I. (1983): *Miscible Displacement*, Monograph Series, SPE, Dallas, 8.
- Till, R. (1974): *Statistical Methods for the Earth Scientist*, The MacMillan Press Ltd., London.
- Vossoughi, s., Smith, J. E., Green, D. W. and Willhite, G. P. (1984): "A New Method to Simulate the Effects of Viscous Fingering on Miscible Displacement Processes in Porous Media", *SPE. J.* 2,56.
- Wardlaw, N. C. (1976): "Pore Geometry of Carbonate Rocks as Revealed by Pore Casts and Capillary Pressure", *AAPG Bull.*, 60-2,245.
- Wardlaw N. C. and Cassem, J. P. (1979): "Oil Recovery Efficiency and the Rock-Pore Properties of Some Sandstone Reservoirs", *Bull. Cdn. Pet. Geol.*, 27-2, 117.
- Warren, J. E. and Price, H. S. (1961): "Flow in Heterogeneous Porous Media", *SPE. J.* 1,153.
- Warren, J. E. and Skiba, F. F. (1964): "Macroscopic Dispersion", *SPE. J.* 4,215.

Wheatcraft, S. W. and Tyler, S. W. (1988): "An Explanation of Scale-Dependent Dispersivity in Heterogeneous Aquifers Using Concepts of Fractal Geometry", *Water Resources Res.*, 24, 566.

Wyllie, M. R. J. (1962): "Reservoir Mechanics-Stylized Myth or Potential Science?", *JPT*, 6, 583.

Appendix A

The following is a listing of the raw data calculated for each core by the computer program ANALYZE which is listed in Appendix C. The layer and location headings refer to the location of the sample in the core (Figure V-3).

Table A-1
Data Summary - Core A

Layer	Location	Porosity	Permeability (md.)	Mean Pore Throat Size (nM)
A	1	0.45	170.19	6012.19
B	1	0.18	62.27	5650.28
C	1	0.11	30.93	1987.08
D	1	0.13	0.10	1631.11
E	1	0.12	38.04	2884.06
F	1	0.11	3.69	1119.32
G	1	0.13	28.08	273.13
H	1	0.13	396.65	5257.15
I	1	0.15	57.59	2546.02
J	1	0.16	74.48	6175.54
A	2	0.25	59.19	3173.74
B	2	0.41	187.34	6824.40
C	2	0.13	41.34	1503.45
D	2	0.13	47.99	1221.62
E	2	0.14	46.24	1494.82
F	2	0.14	38.88	2319.48
G	2	0.10	209.31	1141.39
H	2	0.15	53.52	3325.58
I	2	0.14	72.53	6219.95
J	2	0.15	0.1	2378.74
A	3	0.44	243.18	7342.27
B	3	0.15	0.1	1105.09
C	3	0.15	37.37	2809.45
D	3	0.18	70.91	4140.57
E	3	0.15	0.1	5619.84

Table A-1
Data Summary - Core A
(cont'd)

Layer	Location	Porosity	Permeability (md.)	Mean Pore Throat Size (nM)
F	3	0.14	44.41	2438.83
G	3	0.12	6885.13	4316.91
H	3	0.15	207.48	1635.50
I	3	0.14	68.33	2278.93
J	3	0.14	170.41	1325.11
A	4	0.16	41.72	1514.36
B	4	0.42	234.77	7397.46
C	4	0.15	63.6	6208.80
D	4	0.14	41.99	2278.93
E	4	0.13	39.42	1699.48
F	4	0.14	0.1	1999.27
G	4	0.15	59.51	3089.14
H	4	0.16	55.27	3504.41
I	4	0.13	47.20	2546.03
J	4	0.13	38.11	1605.29
A	5	0.18	51.46	1234.01
B	5	0.23	54.38	2649.54
C	5	0.48	117.10	4232.77
D	5	0.13	53.06	2306.21
E	5	0.12	3.19	1141.38
F	5	0.14	26.73	1246.65
G	5	0.14	46.37	2201.92
H	5	0.12	55.18	2062.55
I	5	0.16	54.74	2509.26
J	5	0.14	36.70	1620.26

Table A-2
Data Summary - Core B

Layer	Location	Porosity	Permeability (md.)	Mean Pore Throat Size (nM)
A	1	0.19	51.09	4383.91
B	1	0.18	65.32	5731.44
C	1	0.18	72.59	6301.16
D	1	0.15	203.56	7718.46
E	1	0.18	49.26	4474.66
F	1	0.13	27.34	3852.12
G	1	0.17	61.36	5591.47
H	1	0.28	35.98	2334.58
I	1	0.22	53.09	4268.42
J	1	0.20	79.33	6178.19
A	2	0.27	121.99	6701.32
B	2	0.13	155.38	7892.10
C	2	0.15	44.9	4897.74
D	2	0.19	50.41	4163.66
E	2	0.22	269.89	7962.33
F	2	0.19	61.12	4195.31
G	2	0.17	62.03	5554.52
H	2	0.21	94.12	6633.69
I	2	0.21	32.66	3437.19
J	2	0.18	49.07	4369.52
A	3	0.18	77.52	6664.83
B	3	0.14	34.69	3899.61
C	3	0.16	28.20	3615.50
D	3	0.18	47.24	4134.31
E	3	0.17	57.59	5237.65

Table A-2
Data Summary - Core B
(cont'd)

Layer	Location	Porosity	Permeability (md.)	Mean Pore Throat Size (nM)
F	3	0.12	33.13	4166.36
G	3	0.18	1610.78	7948.57
H	3	0.21	109.83	7106.77
I	3	0.21	55.97	4342.27
J	3	0.18	59.77	5155.08
A	4	0.20	67.28	5144.51
B	4	0.19	197.67	7975.11
C	4	0.28	54.60	2818.96
D	4	0.16	123.57	7911.63
E	4	0.19	91.69	6728.25
F	4	0.17	63.94	5549.46
G	4	0.17	48.38	4357.48
H	4	0.21	59.56	4584.87
I	4	0.22	127.28	7264.23
J	4	0.19	77.21	7678.57
A	5	0.28	61.35	3022.98
B	5	0.11	231.01	7746.54
C	5	0.17	31.45	3683.43
D	5	0.16	44.12	4401.94
E	5	0.20	70.04	5265.11
F	5	0.17	138.03	7273.44
G	5	0.18	164.76	7835.41
H	5	0.22	56.48	4429.75
I	5	0.22	52.24	4112.57
J	5	0.22	159.84	7610.64

Table A-3
Data Summary - Core C

Layer	Location	Porosity	Permeability (md.)	Mean Pore Throat Size (nM)
A	1	0.19	84.59	6563.13
B	1	0.21	68.08	5219.72
C	1	0.22	75.11	5219.72
D	1	0.22	118.44	7104.54
E	1	0.22	72.75	5063.46
F	1	0.21	60.78	4629.70
G	1	0.21	45.04	3986.78
H	1	0.21	72.51	5387.54
I	1	0.21	74.08	5330.06
J	1	0.18	125.71	5878.48
A	2	0.19	58.55	4970.03
B	2	0.20	72.78	5576.12
C	2	0.21	79.96	5957.44
D	2	0.21	62.36	4821.91
E	2	0.22	65.94	4732.90
F	2	0.22	61.52	4492.25
G	2	0.18	36.25	3835.50
H	2	0.23	39.85	3573.02
I	2	0.23	53792.41	8107.00
J	2	0.24	82.05	5285.14
A	3	0.22	93.05	6817.42
B	3	0.22	107.88	7041.46
C	3	0.19	75.47	6213.79
D	3	0.20	70.52	5421.15
E	3	0.23	231.42	4793.16

Table A-3
Data Summary - Core C
(cont'd)

Layer	Location	Porosity	Permeability (md.)	Mean Pore Throat Size (nM)
F	3	0.22	85.97	6078.5
G	3	0.20	38.84	3601.23
H	3	0.22	49.05	3803.93
I	3	0.24	58.30	4048.70
J	3	0.17	0.1	6256.92
A	4	0.2	100.13	6918.34
B	4	0.20	91.99	6698.60
C	4	0.20	127.94	6406.27
D	4	0.19	58.94	4877.23
E	4	0.20	56.87	4602.73
F	4	0.21	89.27	6519.36
G	4	0.23	88.18	5939.98
H	4	0.23	82.69	5650.28
I	4	0.27	44.22	3688.59
J	4	0.19	117.51	7670.36
A	5	0.23	81.77	5585.43
B	5	0.21	161.86	7823.84
C	5	0.18	84.08	4793.15
D	5	0.21	56.39	4260.44
E	5	0.16	55.55	5479.36
F	5	0.21	63.31	4772.90
G	5	0.19	85.68	6694.06
H	5	0.23	42.04	3749.22
I	5	0.24	46.54	3733.88
J	5	0.20	36.78	3587.71

Table A-4
Data Summary - Core D

Layer	Location	Porosity	Permeability (md.)	Mean Pore Throat Size (nM)
A	1	0.16	42.90	2278.93
B	1	0.13	29.51	1266.12
C	1	0.18	123.14	6591.68
D	1	0.20	100.01	4212.26
E	1	0.14	42.24	3242.84
F	1	0.19	85.71	5940.00
G	1	0.17	68.27	2791.40
H	1	0.18	74.58	6282.96
I	1	0.11	51.79	4112.57
J	1	0.21	107.12	6476.17
A	2	0.22	49.05	2922.86
B	2	0.17	62.62	5484.70
C	2	0.23	135.89	6278.32
D	2	0.20	7910.38	2278.92
E	2	0.19	39.43	3926.72
F	2	0.16	48.20	2622.88
G	2	0.18	52.53	4949.16
H	2	0.19	45.24	4007.20
I	2	0.16	67.82	6401.14
J	2	0.19	90.83	6288.49
A	3	0.14	38.48	1461.30
B	3	0.25	88.47	6384.11
C	3	0.18	34.41	2112.69
D	3	0.16	80.91	3926.72
E	3	0.15	48.12	3601.23

Table A-4
Data Summary - Core D
(cont'd)

Layer	Location	Porosity	Permeability (md.)	Mean Pore Throat Size (nM)
F	3	0.16	78.27	4426.86
G	3	0.16	54.09	3390.46
H	3	0.16	0.1	6514.54
I	3	0.16	52.47	5020.39
J	3	0.21	149.66	6883.24
A	4	0.18	33.33	2062.54
B	4	0.14	53.35	2450.30
C	4	0.17	74.35	6245.27
D	4	0.15	48.29	2509.26
E	4	0.16	31.27	1180.13
F	4	0.16	120.07	4793.15
G	4	0.16	0.1	5873.07
H	4	0.14	34.71	2062.55
I	4	0.15	0.1	2165.34
J	4	0.19	84.07	5387.56
A	5	0.19	32.87	1969.06
B	5	0.16	40.77	657.20
C	5	0.18	90.32	6311.02
D	5	0.20	74.64	3756.94
E	5	0.18	34.09	2546.03
F	5	0.16	55.91	3325.58
G	5	0.13	691.36	2044.89
H	5	0.19	91.46	4495.57
I	5	0.10	0.1	845.29
J	5	0.21	69.44	5000.02

Table A-5
Data Summary - Core E

Layer	Location	Porosity	Permeability (md.)	Mean Pore Throat Size (nM)
A	1	0.24	112.76	6767.60
B	1	0.21	90.77	6506.76
C	1	0.25	100.06	6233.25
D	1	0.27	58.08	3777.35
E	1	0.26	161.50	7462.50
F	1	0.24	92.31	5854.23
G	1	0.23	122.10	5310.07
H	1	0.26	44.22	3383.12
I	1	0.24	89.82	6043.27
J	1	0.3	53.34	3417.12
A	2	0.22	87.18	5873.07
B	2	0.21	79.03	5763.72
C	2	0.28	56.25	4061.98
D	2	0.32	88.42	4518.14
E	2	0.21	119.13	7678.10
F	2	0.22	86.38	6187.75
G	2	0.24	85.83	5278.44
H	2	0.27	41.76	3371.66
I	2	0.27	47.12	3340.62
J	2	0.29	46.06	3189.92
A	3	0.24	170.43	7042.74
B	3	0.22	89.10	6275.62
C	3	0.24	84.83	5495.13
D	3	0.24	92.31	6068.39
E	3	0.22	146.38	7597.20

Table A-5
Data Summary - Core E
(cont'd)

Layer	Location	Porosity	Permeability (md.)	Mean Pore Throat Size (nM)
F	3	0.20	95.38	6571.96
G	3	0.27	127.55	6747.16
H	3	0.25	188.21	7819.02
I	3	0.26	102.75	6298.82
J	3	0.28	58.48	3523.35
A	4	0.22	83.87	6059.90
B	4	0.27	58.13	3677.44
C	4	0.25	80.38	4916.43
D	4	0.212	0.1	4639.59
E	4	0.21	85.99	6335.77
F	4	0.23	162.52	7799.96
G	4	0.24	558.16	7837.04
H	4	0.23	111.45	6808.85
I	4	0.28	47.89	3450.69
J	4	0.24	44.84	3601.23
A	5	0.22	62.39	4586.16
B	5	0.24	42.02	3504.41
C	5	0.22	65.92	4694.50
D	5	0.21	76.97	5608.84
E	5	0.26	190.76	7793.72
F	5	0.22	84.64	6202.23
G	5	0.24	85.10	5496.60
H	5	0.23	66.22	4351.48
I	5	0.25	423.64	7595.27
J	5	0.26	45.68	3601.23

Table A-6
Data Summary - Core F

Layer	Location	Porosity	Permeability (md.)	Mean Pore Throat Size (nM)
A	1	0.02	17.50	1266.12
B	1	0.10	42.34	6268.52
C	1	0.07	27.77	6607.49
D	1	0.09	50.93	6864.75
E	1	0.16	1310.61	7767.68
F	1	0.19	0.1	7931.10
G	1	0.06	27.19	6659.81
H	1	0.07	30.50	7086.50
I	1	0.07	53.86	7191.98
J	1	0.11	78125.68	7432.90
A	2	0.03	15.38	7025.37
B	2	0.09	44.99	8149.99
C	2	0.06	0.82	1294.41
D	2	0.23	151.68	7741.50
E	2	0.05	43.09	7724.92
F	2	0.21	79.88	5932.47
G	2	0.04	13.02	3089.11
H	2	0.05	0.1	6773.46
I	2	0.09	19095.19	7164.41
J	2	0.15	69.32	7515.56
A	3	0.12	97.18	7651.40
B	3	0.16	38.99	7207.62
C	3	0.14	86.55	7177.13
D	3	0.06	0.1	2649.54
E	3	0.05	19.25	3089.11

Table A-6
Data Summary - Core F
(cont'd)

Layer	Location	Porosity	Permeability (md.)	Mean Pore Throat Size (nM)
F	3	0.20	0.1	7832.48
G	3	0.06	24.53	6349.95
H	3	0.06	33.26	6409.44
I	3	0.03	33.06	2546.02
J	3	0.09	694.71	7467.20
A	4	0.04	1087.09	7692.99
B	4	0.05	0.1	2704.52
C	4	0.16	59.15	6104.72
D	4	0.16	86.53	7408.75
E	4	0.15	66.04	7413.04
F	4	0.16	64.58	6570.25
G	4	0.03	513.92	7067.29
H	4	0.11	0.1	6604.31
I	4	0.13	110.84	7515.14
J	4	0.10	61.32	6638.91
A	5	0.06	0.1	7513.88
B	5	0.09	48.33	7493.95
C	5	0.09	81.70	7363.09
D	5	0.08	36.62	6898.95
E	5	0.10	47.14	6404.04
F	5	0.05	296.91	6991.46
G	5	0.10	47.14	6404.04
H	5	0.08	2.10	523.04
I	5	0.10	25.06	3457.92
J	5	0.08	408.17	6283.63

Table A-7
Data Summary - Core G

Layer	Location	Porosity	Permeability (md.)	Mean Pore Throat Size (nM)
A	1	0.10	61.03	7428.62
B	1	0.05	33.11	6750.91
C	1	0.04	82913.06	6397.18
D	1	0.11	79196.68	7515.14
E	1	0.09	57.86	7686.32
F	1	0.04	287.60	7337.25
G	1	0.06	0.1	2546.02
H	1	0.09	25.01	3986.77
I	1	0.08	22093.80	6970.35
J	1	0.09	35.53	6185.23
A	2	0.15	66.61	7581.13
B	2	0.02	53.40	4316.89
C	2	0.09	148.68	7537.29
D	2	0.11	44.72	6791.11
E	2	0.14	67.04	7275.73
F	2	0.06	0.1	6568.65
G	2	0.05	0.1	6206.89
H	2	0.07	33.88	7216.14
I	2	0.07	22.84	4464.77
J	2	0.07	400.67	7035.49
A	3	0.13	63.22	7058.58
B	3	0.03	31724.70	3926.72
C	3	0.08	0.1	7276.91
D	3	0.12	100.38	7802.32
E	3	0.19	0.1	7911.17

Table A-7
Data Summary - Core G
(cont'd)

Layer	Location	Porosity	Permeability (md.)	Mean Pore Throat Size (nM)
F	3	0.09	57.29	7408.75
G	3	0.06	24.90	6563.12
H	3	0.07	581.13	7700.57
I	3	0.08	44.09	6862.62
J	3	0.08	0.1	7244.05
A	4	0.13	388.88	7232.95
B	4	0.03	14.29	5387.54
C	4	0.07	313.14	6669.48
D	4	0.05	14.99	7353.02
E	4	0.14	79.54	7252.53
F	4	0.07	55.70	7329.22
G	4	0.04	10.37	2405.08
H	4	0.05	283643.6	7193.34
I	4	0.09	50.9	6961.81
J	4	0.06	2.81	6818.44
A	5	0.15	70.05	6710.14
B	5	0.06	27.85	7363.09
C	5	0.08	57.96	6740.03
D	5	0.12	93.09	6807.81
E	5	0.09	0.1	7267.12
F	5	0.06	388891.3	7358.56
G	5	0.04	242.51	7105.81
H	5	0.09	5.24	6935.66
I	5	0.08	71.12	7408.75
J	5	0.1	45.65	6442.02

Table A-8
Data Summary - Core H

Layer	Location	Porosity	Permeability (md.)	Mean Pore Throat Size (nM)
A	1	0.27	90.52	4882.94
B	1	0.26	99.01	5849.11
C	1	0.25	52.02	3765.51
D	1	0.23	44.76	3697.00
E	1	0.23	101.58	6451.03
F	1	0.25	46.39	3629.89
G	1	0.25	45.91	3479.78
H	1	0.23	85.65	5786.16
I	1	0.36	69.15	3512.62
J	1	0.33	33.40	2365.23
A	2	0.21	71.55	5296.94
B	2	0.22	63.53	4516.34
C	2	0.25	46.41	3508.18
D	2	0.23	35.30	3427.12
E	2	0.24	90.18	5492.32
F	2	0.21	79.34	5854.23
G	2	0.25	66.47	4221.56
H	2	0.25	46.56	3661.94
I	2	0.24	40.88	3463.91
J	2	0.23	38.66	3534.64
A	3	0.26	105.98	6298.82
B	3	0.25	76.58	4988.44
C	3	0.26	54.12	3697.00
D	3	0.26	43.23	3447.36
E	3	0.29	53.71	3519.99

Table A-8
Data Summary - Core H
(cont'd)

Layer	Location	Porosity	Permeability (md.)	Mean Pore Throat Size (nM)
F	3	0.25	72.03	4404.42
G	3	0.25	46.68	3436.33
H	3	0.22	143.92	7654.46
I	3	0.24	41.67	3476.36
J	3	0.22	67.26	4522.87
A	4	0.26	133.59	7033.29
B	4	0.24	37.84	3336.68
C	4	0.26	48.20	3542.50
D	4	0.21	56.54	4365.08
E	4	0.24	70.68	4499.80
F	4	0.24	39.12	3476.36
G	4	0.22	92.57	6454.78
H	4	0.23	46.59	3613.21
I	4	0.24	40.06	3636.70
J	4	0.34	230.49	6161.84
A	5	0.23	142.96	7717.34
B	5	0.23	56.01	4053.04
C	5	0.25	43.79	3504.41
D	5	0.25	45.48	3483.12
E	5	0.21	66.05	4755.68
F	5	0.24	40.50	3483.59
G	5	0.26	39.05	3238.80
H	5	0.24	40.98	3536.09
I	5	0.23	37.49	3512.62
J	5	0.23	35.46	3420.79

Table A-9
Data Summary - Core I

Layer	Location	Porosity	Permeability (md.)	Mean Pore Throat Size (nM)
A	1	0.18	21.09	2066.90
B	1	0.13	26.59	3145.02
C	1	0.24	50.60	2916.32
D	1	0.16	17.92	1661.97
E	1	0.14	28.58	3300.31
F	1	0.16	24.19	2315.73
G	1	0.17	22.64	2187.84
H	1	0.12	36.73	4048.70
I	1	0.12	6.60	1978.34
J	1	0.18	29.64	2720.91
A	2	0.15	30.98	2834.53
B	2	0.13	19.77	2484.08
C	2	0.12	21.02	3259.05
D	2	0.13	25.08	3311.49
E	2	0.15	28.91	2903.32
F	2	0.14	2.79	1536.18
G	2	0.16	28.96	2975.76
H	2	0.13	14.06	1931.54
I	2	0.15	25.09	2896.87
J	2	0.19	66.56	5581.84
A	3	0.18	24.16	2846.26
B	3	0.19	38.59	2630.09
C	3	0.18	31.95	2473.54
D	3	0.16	39.56	3045.80
E	3	0.12	24.51	2833.88

Table A-9
Data Summary - Core I
(cont'd)

Layer	Location	Porosity	Permeability (md.)	Mean Pore Throat Size (nM)
F	3	0.14	21.11	2622.88
G	3	0.12	16.81	2062.54
H	3	0.15	44.81	2008.07
I	3	0.14	73.45	7713.36
J	3	0.16	26.74	2325.84
A	4	0.14	17.11	3255.79
B	4	0.15	29.52	1999.26
C	4	0.20	35.11	1742.07
D	4	0.17	16.64	2062.54
E	4	0.15	21.37	2056.24
F	4	0.19	0.1	1925.43
G	4	0.13	29.52	3844.00
H	4	0.16	36.62	2129.95
I	4	0.08	6.72	1947.00
J	4	0.17	26.34	2835.78
A	5	0.18	22.81	2566.42
B	5	0.16	29.45	2062.54
C	5	0.15	29.10	2751.22
D	5	0.19	10.58	2132.13
E	5	0.14	28.36	2728.78
F	5	0.16	28.01	2556.01
G	5	0.12	23.08	3648.99
H	5	0.18	22.42	1864.74
I	5	0.14	35.99	4197.72
J	5	0.14	25.86	3003.69

Table A-10
Data Summary - Core J

Layer	Location	Porosity	Permeability (md.)	Mean Pore Throat Size (nM)
A	1	0.11	31.94	3863.24
B	1	0.16	21.76	2323.24
C	1	0.14	30.60	2936.02
D	1	0.15	27.00	2922.86
E	1	0.17	20.45	2284.49
F	1	0.20	44.36	2495.16
G	1	0.18	24.35	2195.98
H	1	0.18	0.1	2419.96
I	1	0.17	25.16	2598.01
J	1	0.12	27.66	3968.92
A	2	0.14	22.21	2410.42
B	2	0.16	17.60	1999.27
C	2	0.16	15.24	1934.00
D	2	0.15	31.95	2691.62
E	2	0.17	22.48	1918.34
F	2	0.16	36.49	2564.81
G	2	0.18	32.72	2995.92
H	2	0.16	18.55	2479.96
I	2	0.15	28.54	3050.83
J	2	0.14	29.58	3417.12
A	3	0.15	0.1	1893.95
B	3	0.19	16.88	2546.02
C	3	0.19	22.29	2139.94
D	3	0.15	32.15	2955.39
E	3	0.12	24.93	3852.11

Table A-10
Data Summary - Core J
(cont'd)

Layer	Location	Porosity	Permeability (md.)	Mean Pore Throat Size (nM)
F	3	0.22	55.18	3399.93
G	3	0.15	27.30	2717.53
H	3	0.21	15.16	1426.12
I	3	0.16	30.01	2445.70
J	3	0.16	30.19	3048.47
A	4	0.14	22.69	2682.73
B	4	0.15	19.81	3167.95
C	4	0.15	297.83	2573.44
D	4	0.11	18.83	2051.72
E	4	0.14	21.64	1987.07
F	4	0.12	20.45	3109.21
G	4	0.17	21.51	2159.01
H	4	0.19	36.08	2775.66
I	4	0.14	37.45	4056.11
J	4	0.13	19.29	2713.40
A	5	0.17	15.56	2475.98
B	5	0.14	15.76	2515.52
C	5	0.11	31.42	4371.18
D	5	0.18	31.05	2546.02
E	5	0.18	39.63	3202.98
F	5	0.21	33.41	2454.91
G	5	0.18	19.24	2319.48
H	5	0.18	21.49	2627.05
I	5	0.14	44.12	4178.50
J	5	0.14	22.68	3060.73

Appendix B

1. ANOVA Calculations

An important requirement for the use of semi-variograms and autocorrelation functions in the calculation of fractal dimension is that the mean be stationary in a statistical sense. Recall from Chapter IV the assumption that $E(Z(x+h))$ exists and is only dependent upon h . In practical terms, this assumption may be tested by a comparison of the variance of properties within each layer of the core to the variance between each layer of core (Figure V-3). If the variance within the layers and between the layers are similar then the mean is stationary and the application of semi-variograms and autocorrelation functions to the data set is valid (W. H. Griffin, personal communication).

The comparison of variances between the two groups is readily achieved through the use of a standard one-way analysis of variance (ANOVA) test. Till (1974) provides a good description of this test which calculates the ratio of the variance between layers in the core and variance within layers of the core. This variance ratio is expressed as an F statistic which may be tested by comparing it to the value of F at the 1% confidence level. If $F_{calc} < F_{0.01}$ then the assumption that the mean is stationary is valid. The

following calculation is an example of the ANOVA procedure as applied to Core A permeability data contained in Appendix A.

Data Groups	Group A	Group B	Group C	Group D	Group E
(md)	170.2	62.3	30.9	0.1	38.0
	59.2	187.3	41.3	48.0	46.2
	243.2	0.1	37.4	71.0	0.1
	41.7	234.8	63.6	42.0	39.4
	51.5	54.4	118.0	53.1	3.2
Mean	113.1	107.8	58.2	42.8	25.4
	Group F	Group G	Group H	Group I	Group J
	3.7	28.1	396.6	57.5	74.5
	38.9	209.3	53.5	72.5	0.1
	44.4	6885.1	207.5	68.3	170.4
	0.1	59.5	55.3	47.2	38.1
	26.7	46.3	55.2	54.7	36.7
Mean	22.8	1807.1	85.8	60.1	63.9

$$\bar{x} = \frac{1}{10} \sum_{i=1}^J \bar{x}_i = 238.7$$

$$BSS = n \sum_{i=1}^J (\bar{x}_i - \bar{x})^2 = 5(1342011.12) = 6710055.6$$

$$WSS = \sum_{i=1}^J \sum_{j=1}^5 (x_{ij} - \bar{x}_i)^2 = 12063086.0$$

ANOVA Analysis

Variation	Sum of Squares	Degrees of Freedom	Mean Sum of Squares	Ratio (F)
Between Groups	6710055.6	9	745561.73	
Within Groups	12063086.0	40	301577.15	2.472
Total	18773141.6	49		

$$F_{(0.01;9,40)} = 2.89$$

Since $2.472 < 2.89$ we accept the hypothesis that the mean is stationary.

This test was repeated for each property in each of the ten cores. In each case the test of the stationary mean was satisfied.

2. Semi-Variogram Plots

The following pages contain the semi-variogram plots used to calculate the D_{var} values shown in Table VII-5. The procedure for the calculation of the slope as h approached zero followed several rules:

1. The model fit to the semi-variogram weighted the first two points of the semi-variogram more highly than the rest of the points because the first two lag spacings are based upon the greatest number of data pairs.
2. The slope was arbitrarily defined as the slope of the tangent line to the semi-variogram model between $h=9.6$ inches and $h=4.8$ inches.
3. The slope was determined between $h=17.28$ and $h=4.8$ in the following manner:

$$slope = \frac{\Delta y}{\ln 17.28 - \ln 4.8} = \frac{\Delta y}{\ln 3.6}$$

4. The slope was always positive.

Semi-Variogram (Core A)
Permeability

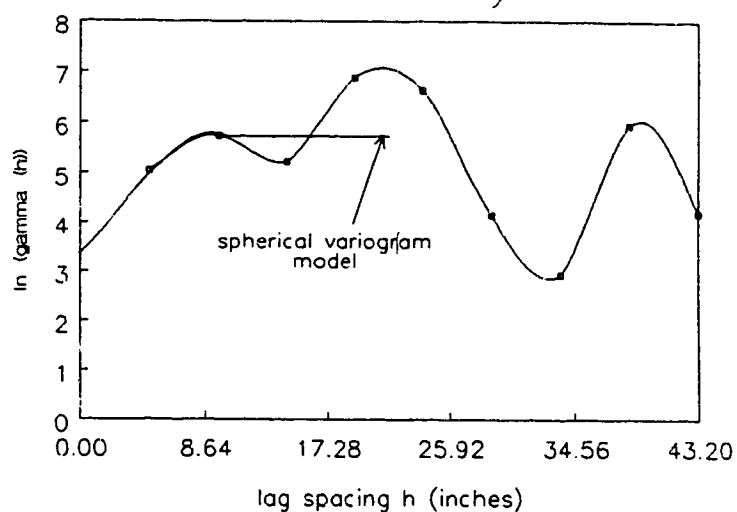


Figure B-1

Semi-Variogram (Core B)
Permeability

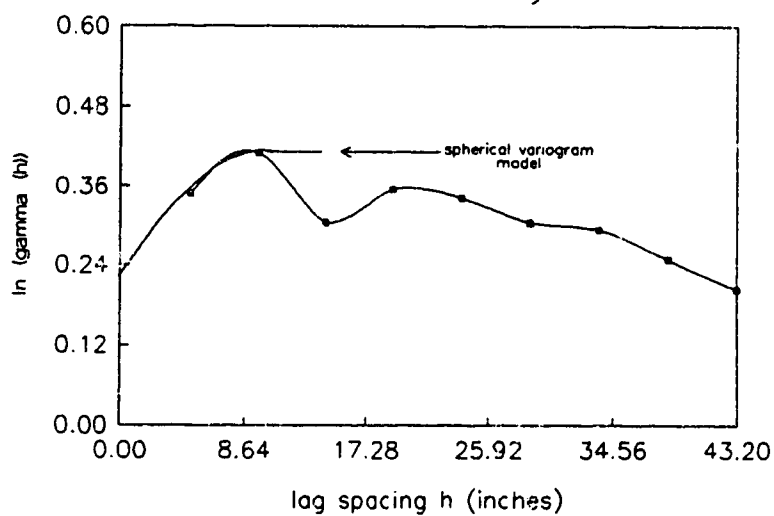
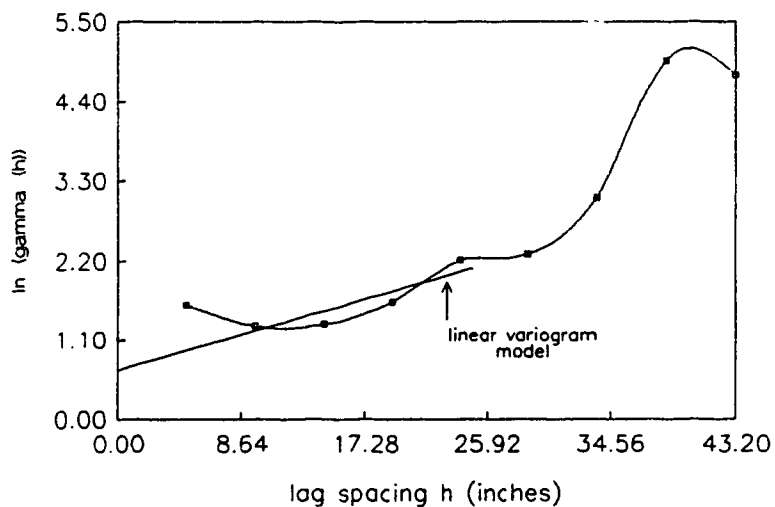
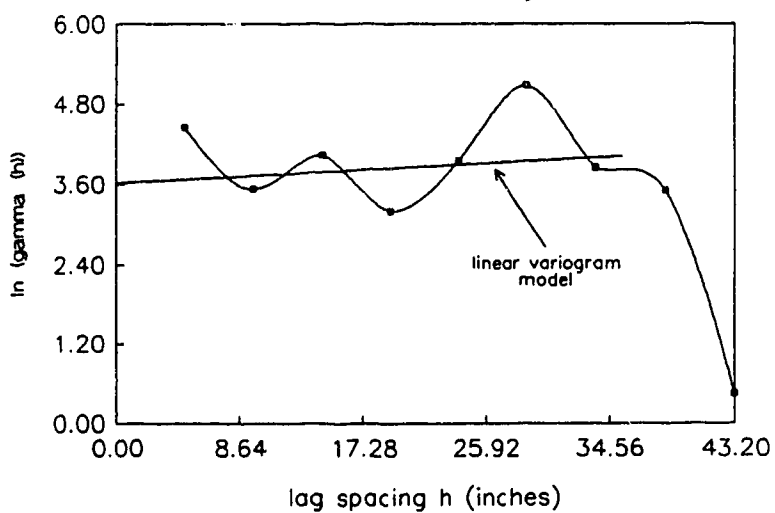


Figure B-2

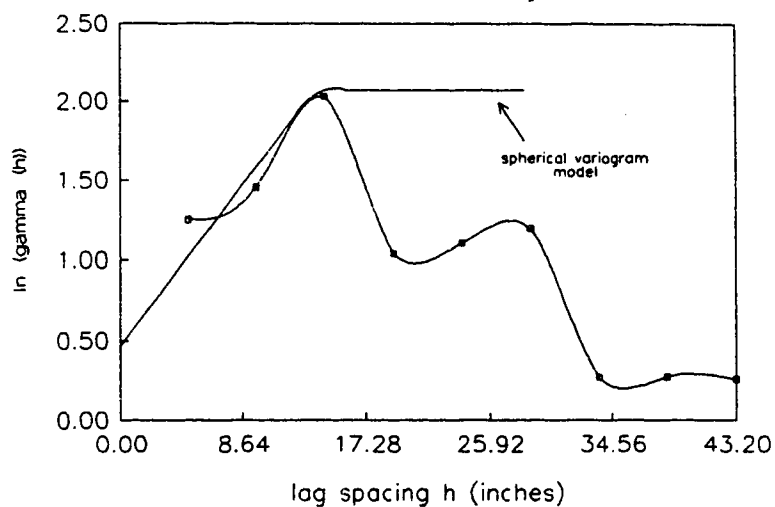
Semi-Variogram (Core C) Permeability

**Figure B-3**

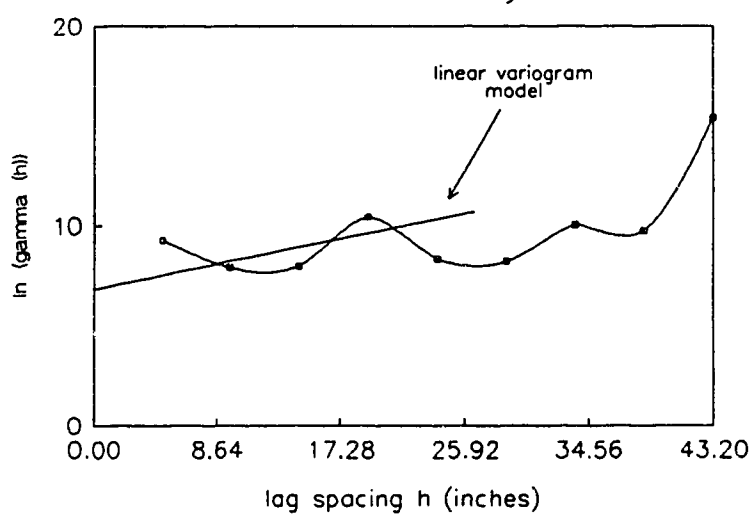
Semi-Variogram (Core D) Permeability

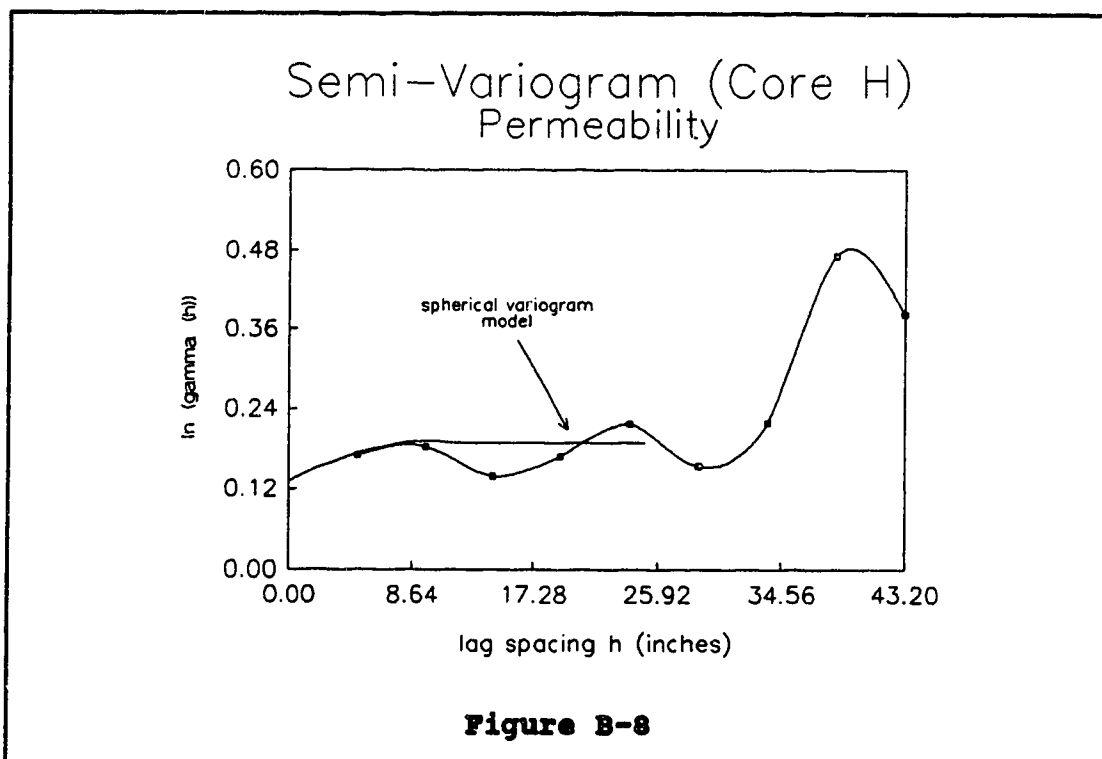
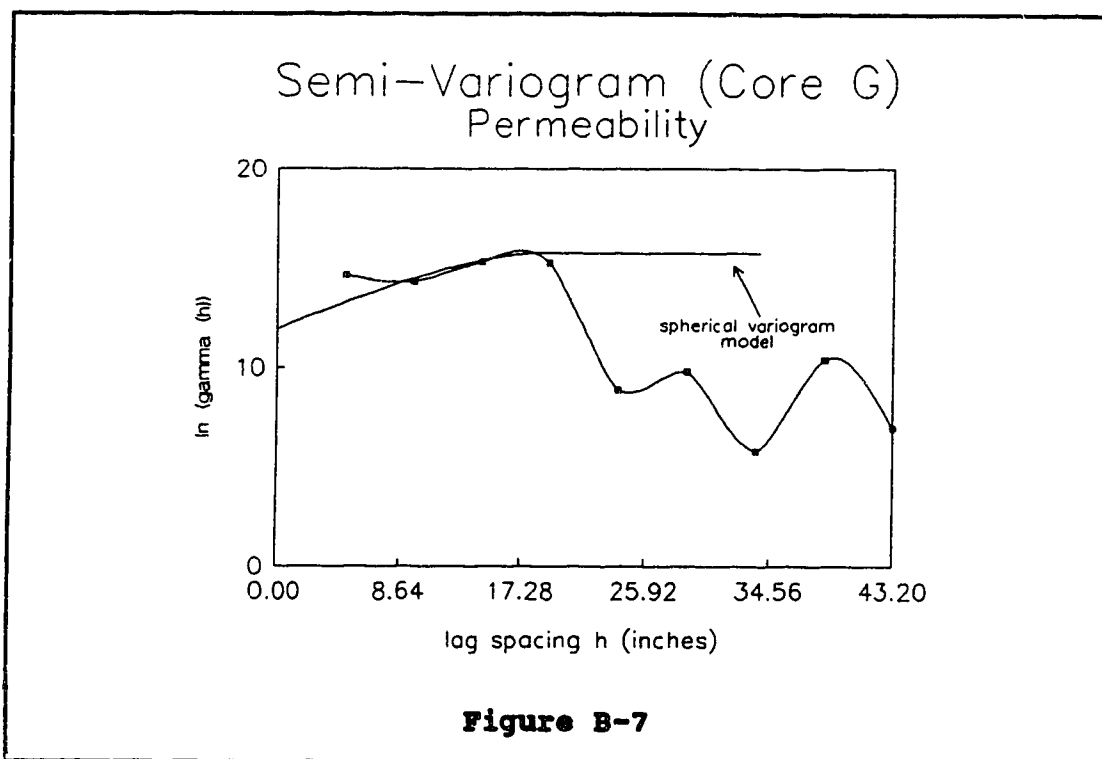
**Figure B-4**

Semi-Variogram (Core E) Permeability

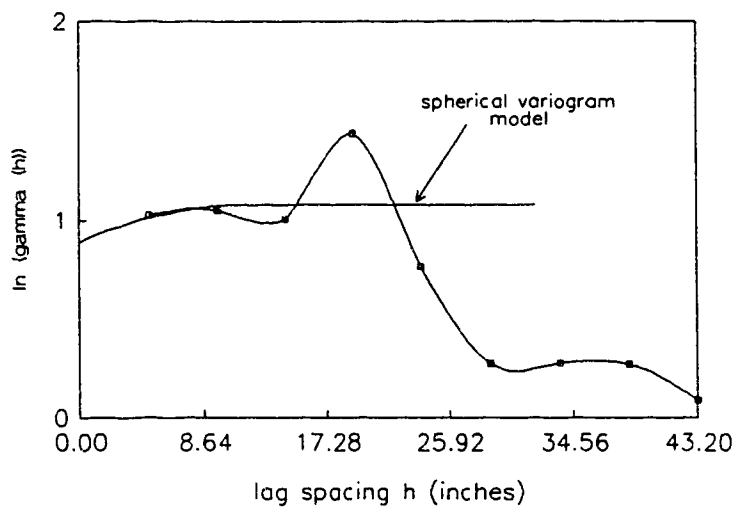
**Figure B-5**

Semi-Variogram (Core F) Permeability

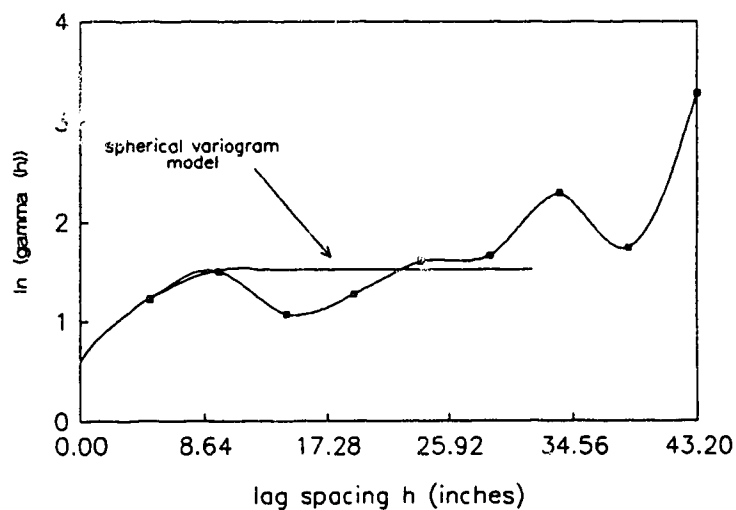
**Figure B-6**



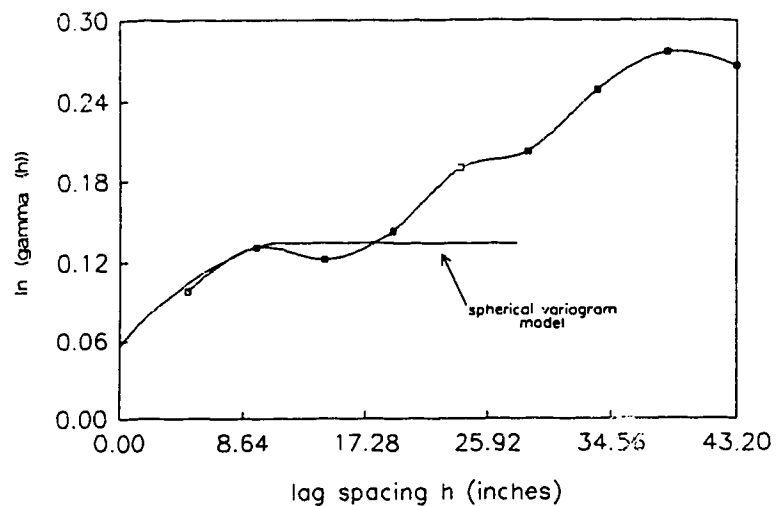
Semi-Variogram (Core I) Permeability

**Figure B-9**

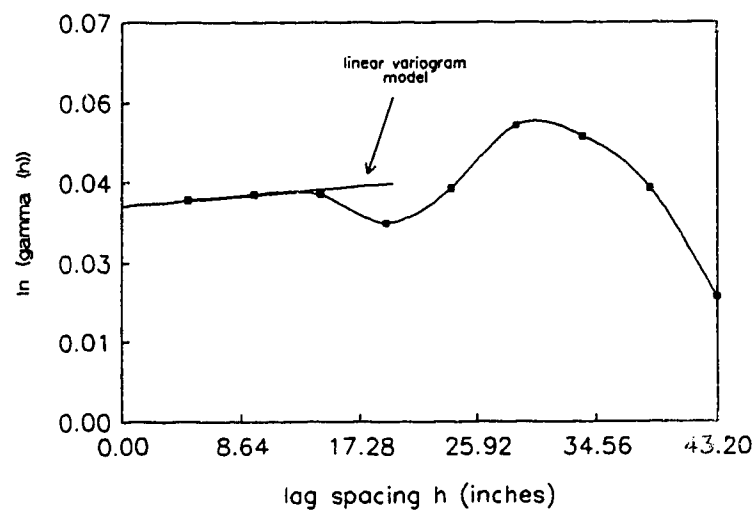
Semi-Variogram (Core J) Permeability

**Figure B-10**

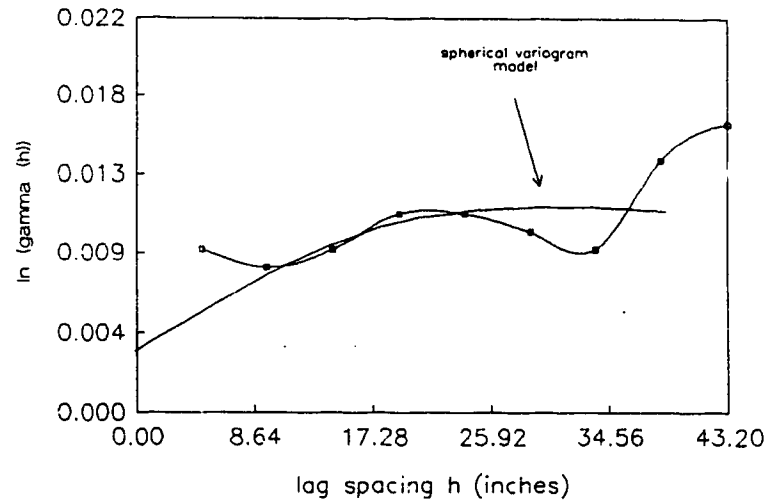
Semi-Variogram (Core A) Porosity

**Figure B-11**

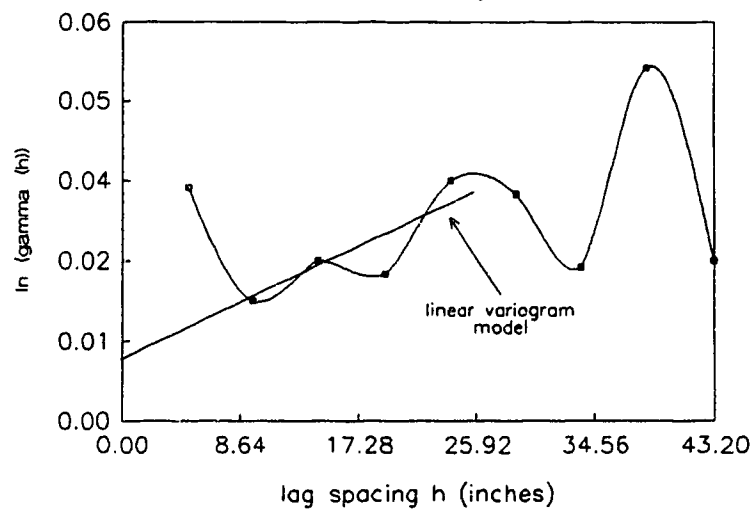
Semi-Variogram (Core B) Porosity

**Figure B-12**

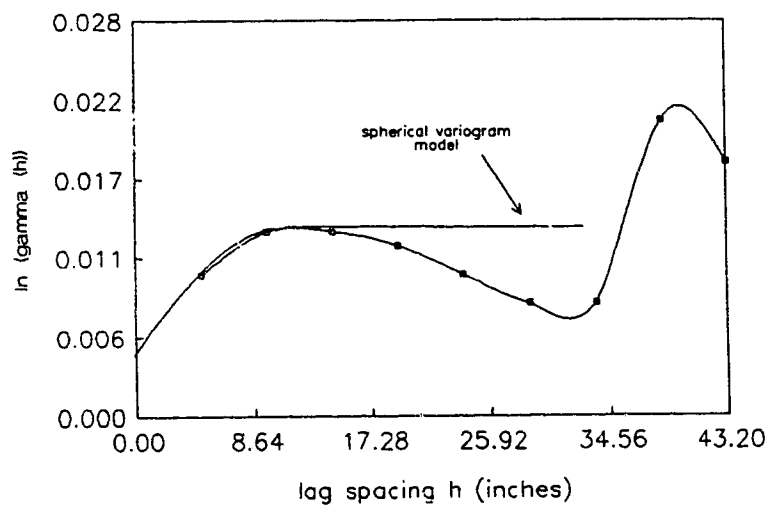
Semi-Variogram (Core C) Porosity

**Figure B-13**

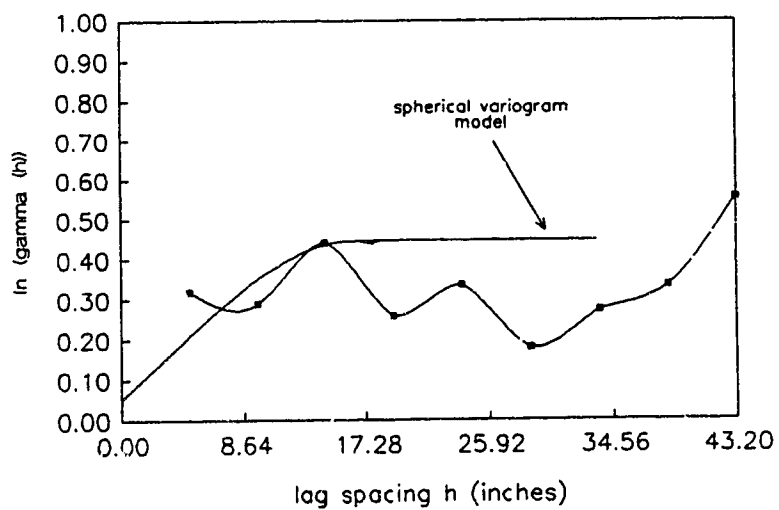
Semi-Variogram (Core D) Porosity

**Figure B-14**

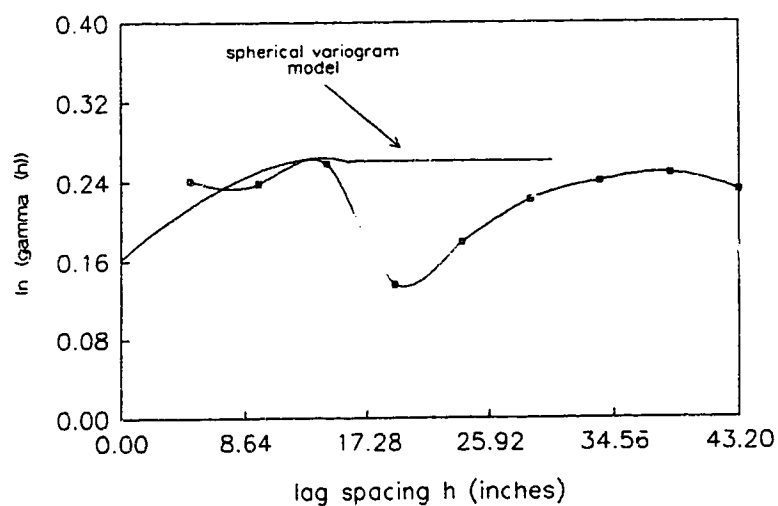
Semi-Variogram (Core E) Porosity

**Figure B-15**

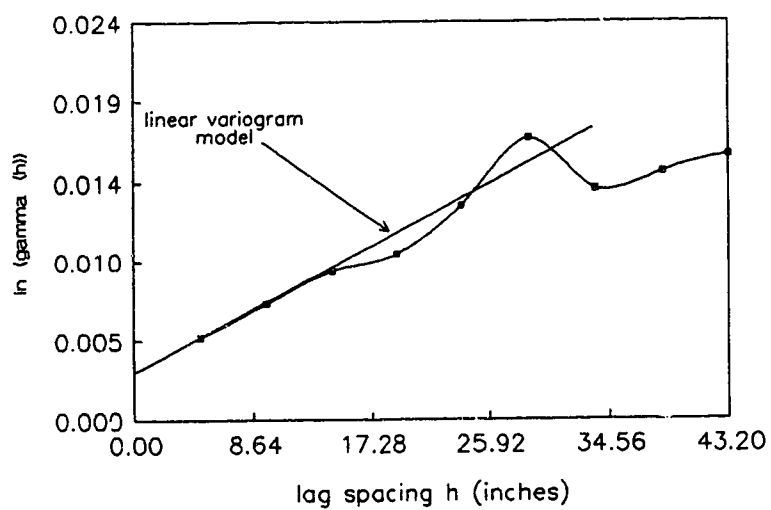
Semi-Variogram (Core F) Porosity

**Figure B-16**

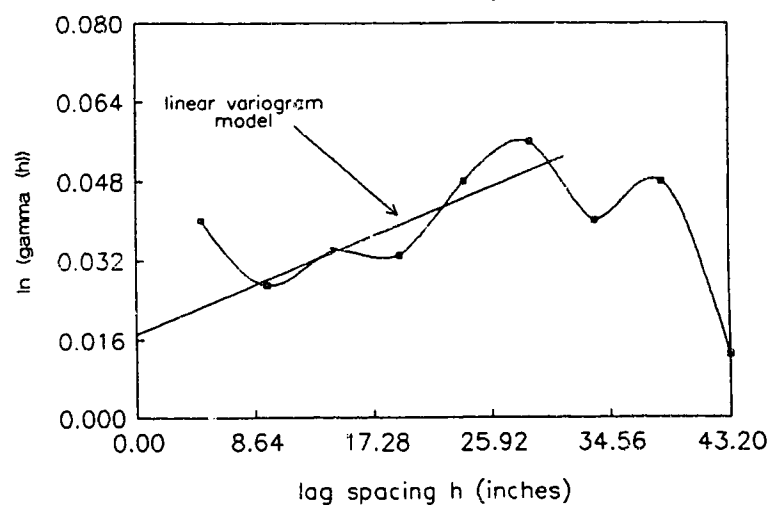
Semi-Variogram (Core G) Porosity

**Figure B-17**

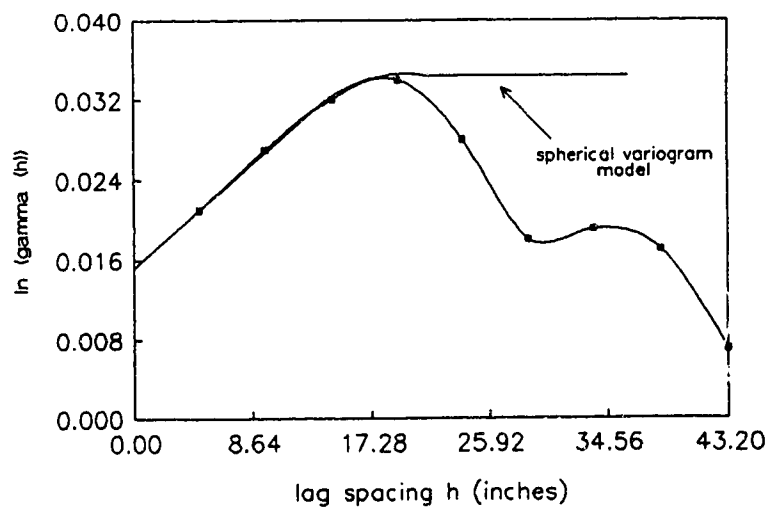
Semi-Variogram (Core H) Porosity

**Figure B-18**

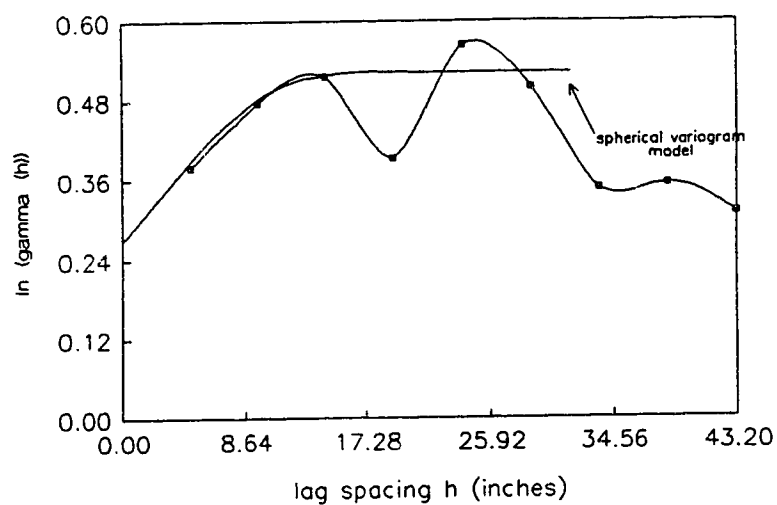
Semi-Variogram (Core I) Porosity

**Figure B-19**

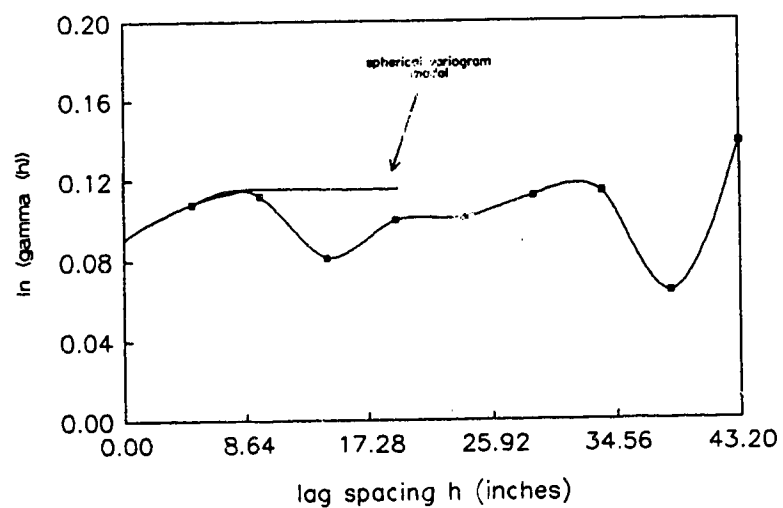
Semi-Variogram (Core J) Porosity

**Figure B-20**

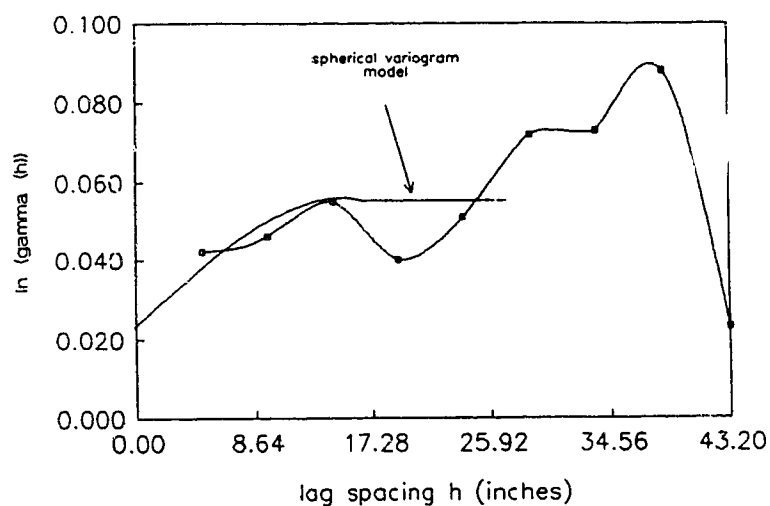
Semi-Variogram (Core A) Mean Pore Size

**Figure B-21**

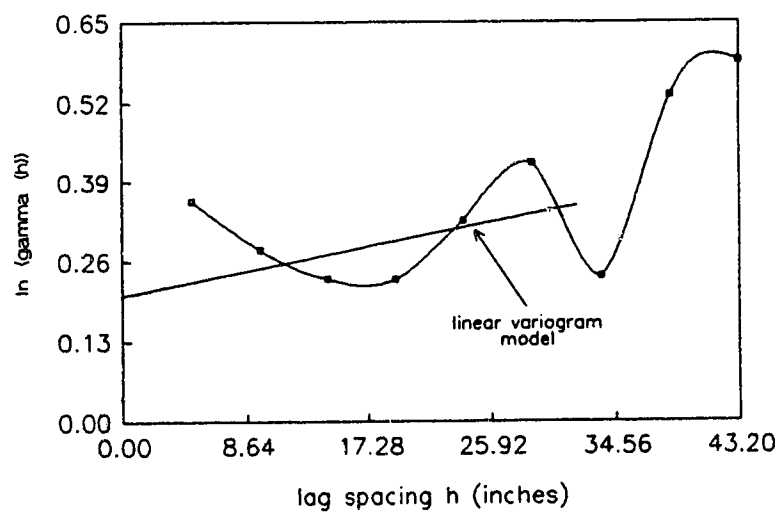
Semi-Variogram (Core B) Mean Pore Size

**Figure B-22**

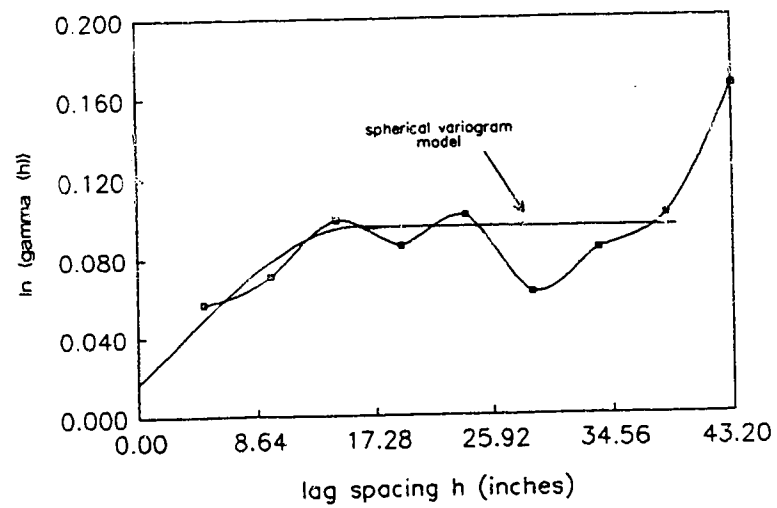
Semi-Variogram (Core C) Mean Pore Size

**Figure B-23**

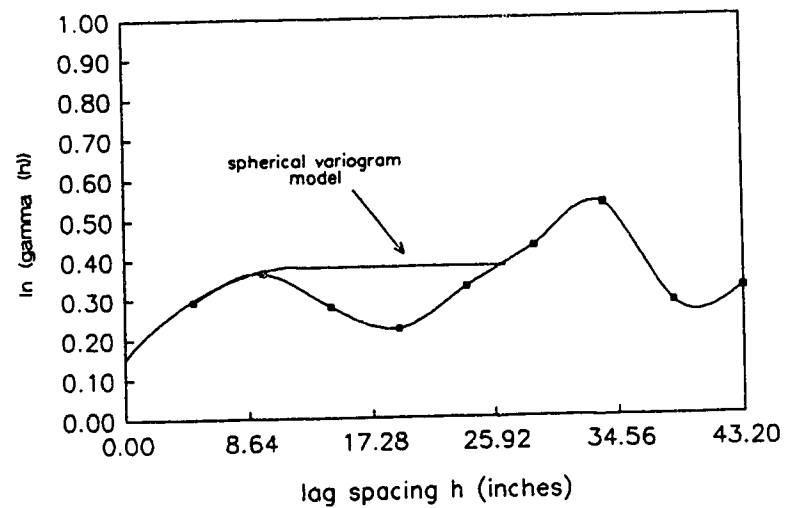
Semi-Variogram (Core D) Mean Pore Size

**Figure B-24**

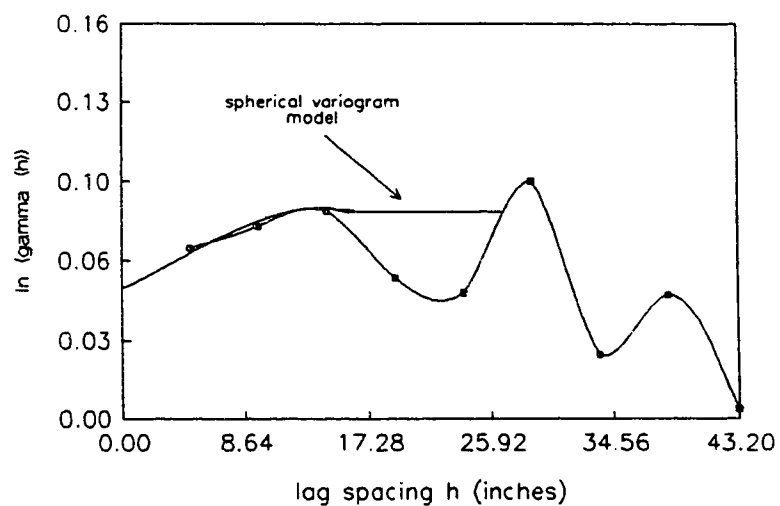
Semi-Variogram (Core E) Mean Pore Size

**Figure B-25**

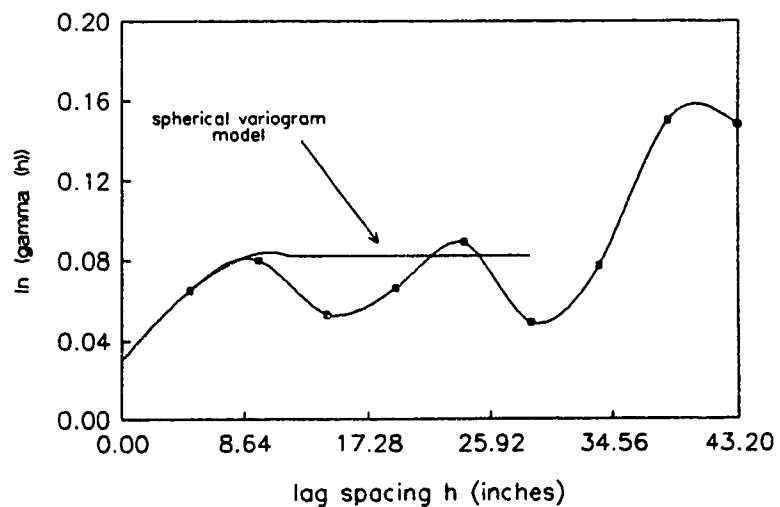
Semi-Variogram Mean Pore Size

**Figure B-26**

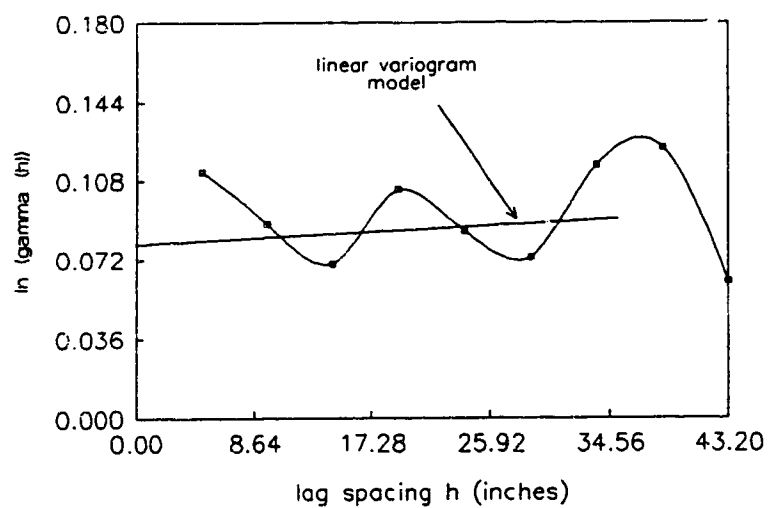
Semi-Variogram (Core G) Mean Pore Size

**Figure B-27**

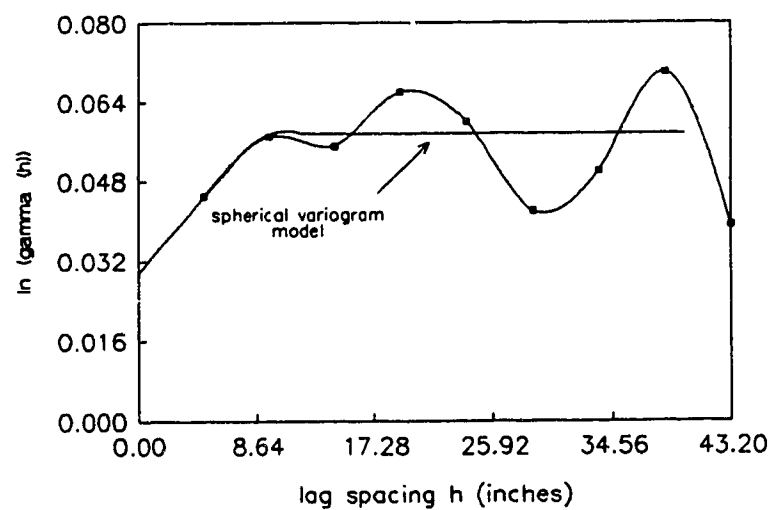
Semi-Variogram (Core H) Mean Pore Size

**Figure B-28**

Semi-Variogram (Core I) Mean Pore Size

**Figure B-29**

Semi-Variogram (Core J) Mean Pore Size

**Figure B-30**

Appendix C

1. Calculation of Property Mean and Variance

Table C-1 illustrates the calculation procedure for property variance using the data in Appendix A. This information was correlated with K , and $\log K$, in Table VII-4. The variance of the natural log of permeability $\sigma_{\ln(k)}^2$ is also listed. This parameter was calculated by program ANALYZE listed in Appendix E after the exclusion of outliers and was used in the calculation of the Dykstra-Parsons permeability variation in Table VI-1.

Note that the mean values of porosity and permeability $\bar{\mu}$ calculated here do not correspond to porosity and permeability values for the entire core shown in Table V-2. There are three reasons for this:

1. A maximum of fifty samples are averaged in this calculation procedure while the data in Table V-2 were calculated on a whole core basis.
2. Exclusion of the outliers reduces the mean value.
3. Different procedures were used in the calculation. Table V-2 porosity values were calculated from a core saturation procedure using n -hexane and permeability values were determined by flooding the core with n -hexane at four different rates and plotting differential pressures. The permeability

was then calculated from Darcy's law for linear flow. In the case of the data in Appendix A porosity and permeability were both determined by mercury porosimetry methods.

Table C-1
Property Mean and Variance Calculations

CORE A	OUTLIERS	$\bar{\mu}$	σ^2	$\sigma_{\ln(k)}^2$	DATA
POROSITY	A-1,A-3,B-4,C-5	0.138	0.00223		46
PERMEABILITY	G-3	73.11	5917.24	4.207	49
MEAN PORE SIZE		2985.6	3462742		50
CORE B	OUTLIERS	$\bar{\mu}$	σ^2	$\sigma_{\ln(k)}^2$	DATA
POROSITY		0.189	0.00138		50
PERMEABILITY	G-3	82.96	3030.66	0.309	49
MEAN PORE SIZE		5486.15	2607612		50
CORE C	OUTLIERS	$\bar{\mu}$	σ^2	$\sigma_{\ln(k)}^2$	DATA
POROSITY		0.21	0.000386		50
PERMEABILITY	I-2	76.3	1276.1	0.988	49
MEAN PORE SIZE		5385.3	1421689		50
CORE D	OUTLIERS	$\bar{\mu}$	σ^2	$\sigma_{\ln(k)}^2$	DATA
POROSITY		0.172	0.00081		50
PERMEABILITY	D-2	73.52	9057.84	3.343	49
MEAN PORE SIZE		3955.55	3290024		50

Table C-1
Property Mean and Variance Calculations
(cont'd)

CORE E	OUTLIERS	$\bar{\mu}$	σ^2	$\sigma_{\ln(k)}^2$	DATA
POROSITY		0.243	0.00069		50
PERMEABILITY		103.88	7951.4	1.181	50
MEAN PORE SIZE		5520.4	2176609		50
CORE F	OUTLIERS	$\bar{\mu}$	σ^2	$\sigma_{\ln(k)}^2$	DATA
POROSITY		0.097	0.00256		50
PERMEABILITY	E-1, J-1, I-2, A-4	80.5	18064	5.946	46
MEAN PORE SIZE		6218.44	3800035		50
CORE G	OUTLIERS	$\bar{\mu}$	σ^2	$\sigma_{\ln(k)}^2$	DATA
POROSITY		0.082	0.00124		50
PERMEABILITY	C-1, D-1, J-1 B-3, H-4, F-5	85.31	15313.22	5.854	44
MEAN PORE SIZE		6645.9	1543871		50
CORE H	OUTLIERS	$\bar{\mu}$	σ^2	$\sigma_{\ln(k)}^2$	DATA
POROSITY		0.247	0.00086		50
PERMEABILITY		65.92	1306.74	0.185	50
MEAN PORE SIZE		4375.4	1557655		50
CORE I	OUTLIERS	$\bar{\mu}$	σ^2	$\sigma_{\ln(k)}^2$	DATA
POROSITY		0.154	0.00076		50
PERMEABILITY		26.88	171.305	0.879	50
MEAN PORE SIZE		2758.6	1045225		50

Table C-1
Property Mean and Variance Calculations
(cont'd)

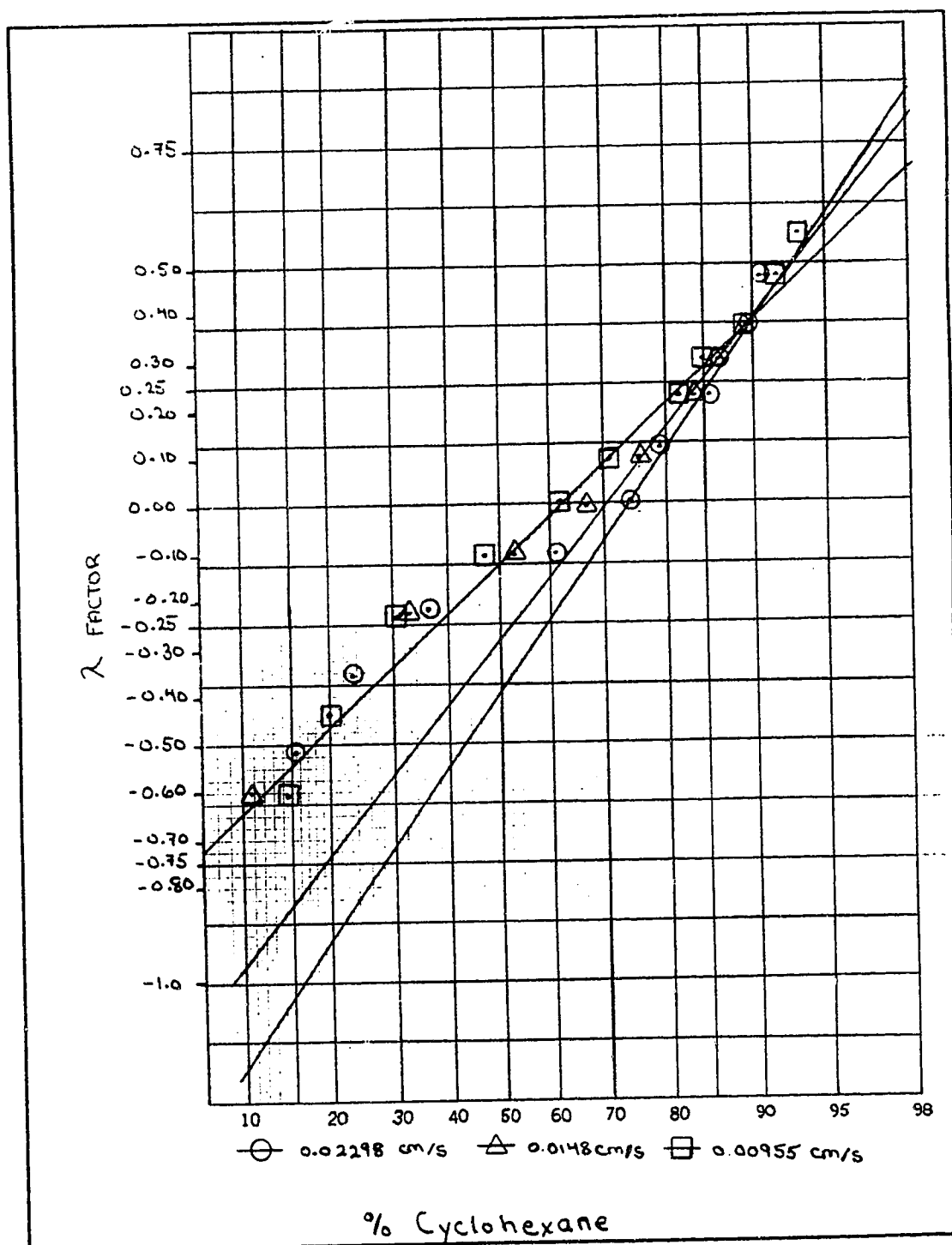
CORE J	OUTLIERS	$\bar{\mu}$	σ^2	$\sigma_{ln(k)}^2$	DATA
POROSITY		0.158	0.00064		50
PERMEABILITY		31.06	1547.68	1.405	50
MEAN PORE SIZE		2738.5	401720		50

Appendix D

This appendix contains the data used in the calculation of K , using Brigham's lambda factor method for each of the corefloods. The values for v and L used in the calculations come from Tables VII-1 through VII-3. The results of these calculations are also shown in Tables VII-1 through VII-3. Equation II-4 was used in the calculations with K , being substituted for K_1 .

1. Sample Calculation

Core J



$$\text{Rate} = 0.0222 \text{ cm/s} \quad \lambda_{90} - \lambda_{10} = 1.554$$

$$K_s = (0.02298 \text{ cm/s}) * (121.92 \text{ cm}) * \left\{ \frac{1.554}{3.625} \right\}^2 = 0.5149 \text{ cm}^2/\text{s}$$

$$\text{Rate} = 0.01528 \text{ cm/s} \quad \lambda_{90} - \lambda_{10} = 1.359$$

$$K_s = (0.0148 \text{ cm/s}) * (121.92 \text{ cm}) * \left\{ \frac{1.359}{3.625} \right\}^2 = 0.2535 \text{ cm}^2/\text{s}$$

$$\text{Rate} = 0.009722 \text{ cm/s} \quad \lambda_{90} - \lambda_{10} = 1.021$$

$$K_s = (0.00955 \text{ cm/s}) * (121.92 \text{ cm}) * \left\{ \frac{1.021}{3.625} \right\}^2 = 0.09237 \text{ cm}^2/\text{s}$$

2. Effluent Concentration Profile and λ Values

Tables D-1 through D-10 contain the effluent concentration profiles as well as the λ values calculated by program EFFPLOT for each coreflood. These λ values were plotted as shown on the previous page and K_s was calculated using the same procedure as the sample calculation.

Table D-1 Effluent Concentration Profiles (Core A)

P.V.	Rate=0.02222 cm/s		Rate=0.01528 cm/s		Rate=0.00972 cm/s	
	% C_6H_{12}	λ	% C_6H_{12}	λ	% C_6H_{12}	λ
0.050	1.786	-4.249	1.608	-4.249	0.892	-4.249
0.100	1.965	-2.846	2.500	-2.846	1.429	-2.846
0.150	1.786	-2.195	2.500	-2.195	1.429	-2.195
0.200	1.965	-1.789	2.679	-1.789	1.429	-1.789
0.250	1.786	-1.500	1.786	-1.500	1.429	-1.500
0.300	1.786	-1.278	2.500	-1.278	1.250	-1.278
0.350	1.786	-1.099	2.500	-1.099	0.715	-1.099
0.400	1.786	-0.949	2.500	-0.949	0.892	-0.949
0.450	1.071	-0.820	2.142	-0.820	1.608	-0.820
0.500	1.786	-0.707	2.858	-0.707	0.892	-0.707
0.550	2.679	-0.607	2.858	-0.607	0.892	-0.607
0.600	3.929	-0.516	3.571	-0.516	2.321	-0.516
0.650	7.142	-0.434	5.358	-0.434	3.571	-0.434
0.700	11.563	-0.359	7.321	-0.359	6.786	-0.359
0.750	17.188	-0.289	12.344	-0.289	10.626	-0.289
0.800	23.333	-0.224	18.437	-0.224	16.094	-0.224
0.850	35.319	-0.163	27.777	-0.163	25.111	-0.163
0.900	43.999	-0.105	48.665	-0.105	36.595	-0.105
0.950	53.500	-0.051	58.500	-0.051	46.222	-0.051
1.000	62.291	0.000	66.875	0.000	57.499	0.000
1.050	70.000	0.049	73.572	0.049	64.166	0.049
1.100	75.238	0.095	78.810	0.095	72.382	0.095
1.150	80.812	0.140	84.054	0.140	79.762	0.140
1.200	83.783	0.183	88.647	0.183	84.595	0.183
1.250	87.567	0.224	91.463	0.224	91.463	0.224
1.300	91.463	0.263	93.901	0.263	93.901	0.263
1.350	92.926	0.301	94.878	0.301	95.608	0.301
1.400	93.901	0.338	95.366	0.338	97.318	0.338
1.450	95.366	0.374	96.341	0.374	97.318	0.374
1.500	96.097	0.408	96.585	0.408	97.318	0.408
1.550	96.829	0.442	96.829	0.442	98.048	0.442
1.600	97.560	0.474	97.804	0.474	98.781	0.474
1.650	97.560	0.506	98.293	0.506	98.293	0.506
1.700	98.048	0.537	98.781	0.537	99.267	0.537
1.750	98.048	0.567	99.512	0.567	99.267	0.567
1.800	98.048	0.596	99.025	0.596	99.756	0.596
1.850	98.293	0.625	99.512	0.625	99.756	0.625
1.900	99.025	0.653	99.267	0.653	100.000	0.653
1.950	99.025	0.680	99.512	0.680	99.756	0.680
2.000	99.025	0.707	99.267	0.707	100.000	0.707

Table D-2 Effluent Concentration Profiles (Core B)

P.V.	Rate=0.02222 cm/s			Rate=0.01528 cm/s			Rate=0.00972 cm/s		
	% C_6H_{12}	λ		% C_6H_{12}	λ		% C_6H_{12}	λ	
0.050	1.429	-4.249		2.679	-4.249		1.250	-4.249	
0.100	3.571	-2.846		2.679	-2.846		2.500	-2.846	
0.150	4.465	-2.195		2.500	-2.195		1.786	-2.195	
0.200	4.821	-1.789		1.786	-1.789		1.965	-1.789	
0.250	4.465	-1.500		2.142	-1.500		1.786	-1.500	
0.300	4.465	-1.278		2.142	-1.278		2.321	-1.278	
0.350	4.286	-1.099		1.608	-1.099		1.786	-1.099	
0.400	3.571	-0.949		1.786	-0.949		1.786	-0.949	
0.450	2.679	-0.820		1.786	-0.820		1.429	-0.820	
0.500	3.036	-0.707		2.500	-0.707		2.679	-0.707	
0.550	3.036	-0.607		1.786	-0.607		2.500	-0.607	
0.600	1.965	-0.516		2.858	-0.516		2.679	-0.516	
0.650	2.679	-0.434		2.858	-0.434		2.142	-0.434	
0.700	2.858	-0.359		5.000	-0.359		2.679	-0.359	
0.750	3.929	-0.289		4.465	-0.289		3.929	-0.289	
0.800	7.142	-0.224		7.500	-0.224		6.250	-0.224	
0.850	10.781	-0.163		10.937	-0.163		10.156	-0.163	
0.900	18.906	-0.105		16.249	-0.105		11.407	-0.105	
0.950	35.532	-0.051		24.444	-0.051		16.406	-0.051	
1.000	50.000	0.000		39.574	0.000		30.213	0.000	
1.050	61.667	0.049		55.749	0.049		49.555	0.049	
1.100	71.905	0.095		67.916	0.095		60.624	0.095	
1.150	80.812	0.140		78.333	0.140		72.618	0.140	
1.200	87.296	0.183		81.621	0.183		80.812	0.183	
1.250	90.244	0.224		89.188	0.224		86.216	0.224	
1.300	92.926	0.263		90.730	0.263		91.463	0.263	
1.350	94.878	0.301		93.901	0.301		92.682	0.301	
1.400	96.341	0.338		95.366	0.338		92.682	0.338	
1.450	96.341	0.374		96.341	0.374		92.682	0.374	
1.500	96.585	0.408		97.318	0.408		92.926	0.408	
1.550	98.293	0.442		97.560	0.442		92.926	0.442	
1.600	98.537	0.474		98.048	0.474		93.659	0.474	
1.650	98.781	0.506		97.560	0.506		94.878	0.506	
1.700	97.804	0.537		98.781	0.537		95.853	0.537	
1.750	98.781	0.567		98.293	0.567		96.341	0.567	
1.800	99.025	0.596		99.512	0.596		96.341	0.596	
1.850	99.512	0.625		99.512	0.625		97.318	0.625	
1.900	99.512	0.653		98.781	0.653		97.074	0.653	
1.950	99.267	0.680		99.267	0.680		97.804	0.680	
2.000	99.756	0.707		99.267	0.707		98.537	0.707	

Table D-3 Effluent Concentration Profiles (Core C)

P.V.	Rate=0.02222 cm/s			Rate=0.01528 cm/s			Rate=0.00972 cm/s		
	% C_6H_{12}	λ		% C_6H_{12}	λ		% C_6H_{12}	λ	
0.050	0.892	-4.249		1.965	-4.249		1.786	-4.249	
0.100	1.071	-2.846		1.786	-2.846		1.429	-2.846	
0.150	1.965	-2.195		1.786	-2.195		1.608	-2.195	
0.200	1.786	-1.789		2.321	-1.789		1.071	-1.789	
0.250	1.608	-1.500		1.786	-1.500		1.071	-1.500	
0.300	2.500	-1.278		2.500	-1.278		1.786	-1.278	
0.350	1.786	-1.099		1.250	-1.099		0.715	-1.099	
0.400	2.679	-0.949		1.786	-0.949		1.786	-0.949	
0.450	4.465	-0.820		0.715	-0.820		1.786	-0.820	
0.500	7.142	-0.707		1.429	-0.707		1.965	-0.707	
0.550	7.858	-0.607		1.250	-0.607		1.786	-0.607	
0.600	7.858	-0.516		1.786	-0.516		1.608	-0.516	
0.650	7.500	-0.434		1.608	-0.434		1.786	-0.434	
0.700	7.142	-0.359		2.142	-0.359		1.786	-0.359	
0.750	6.071	-0.289		1.608	-0.289		1.786	-0.289	
0.800	5.358	-0.224		0.358	-0.224		1.786	-0.224	
0.850	5.358	-0.163		2.679	-0.163		2.858	-0.163	
0.900	6.786	-0.105		5.358	-0.105		5.358	-0.105	
0.950	13.438	-0.051		12.813	-0.051		14.531	-0.051	
1.000	33.829	0.000		34.255	0.000		35.319	0.000	
1.050	65.208	0.049		59.750	0.049		66.042	0.049	
1.100	79.523	0.095		78.572	0.095		79.523	0.095	
1.150	87.567	0.140		90.244	0.140		90.244	0.140	
1.200	92.926	0.183		92.926	0.183		93.901	0.183	
1.250	96.341	0.224		96.097	0.224		97.074	0.224	
1.300	97.804	0.263		97.804	0.263		98.293	0.263	
1.350	99.025	0.301		98.781	0.301		98.781	0.301	
1.400	99.756	0.338		98.781	0.338		99.512	0.338	
1.450	99.756	0.374		99.512	0.374		99.756	0.374	
1.500	98.781	0.408		99.267	0.408		99.756	0.408	
1.550	99.756	0.442		99.756	0.442		100.000	0.442	
1.600	99.756	0.474		100.000	0.474		100.000	0.474	
1.650	100.000	0.506		99.756	0.506		100.000	0.506	
1.700	100.000	0.537		100.000	0.537		99.756	0.537	
1.750	100.000	0.567		100.000	0.567		99.267	0.567	
1.800	100.000	0.596		100.000	0.596		100.000	0.596	
1.850	100.000	0.625		100.000	0.625		99.756	0.625	
1.900	100.000	0.653		100.000	0.653		100.000	0.653	
1.950	100.000	0.680		100.000	0.680		100.000	0.680	
2.000	100.000	0.707		100.000	0.707		100.000	0.707	

Table D-4 Effluent Concentration Profiles (Core D)

Rate=0.02222 cm/s			Rate=0.01528 cm/s			Rate=0.00972 cm/s		
P.V.	% C_6H_{12}	λ	% C_6H_{12}	λ	% C_6H_{12}	λ		
0.050	2.679	-4.249	0.892	-4.249	0.536	-4.249		
0.100	3.929	-2.846	3.036	-2.846	1.786	-2.846		
0.150	4.465	-2.195	2.142	-2.195	1.965	-2.195		
0.200	4.465	-1.789	1.608	-1.789	1.786	-1.789		
0.250	3.750	-1.500	1.786	-1.500	1.965	-1.500		
0.300	2.858	-1.278	1.965	-1.278	1.786	-1.278		
0.350	2.858	-1.099	1.608	-1.099	2.321	-1.099		
0.400	2.679	-0.949	2.142	-0.949	1.608	-0.949		
0.450	2.679	-0.820	1.786	-0.820	1.608	-0.820		
0.500	2.500	-0.707	0.892	-0.707	1.965	-0.707		
0.550	1.965	-0.607	1.608	-0.607	1.786	-0.607		
0.600	3.392	-0.516	2.679	-0.516	3.571	-0.516		
0.650	5.358	-0.434	3.571	-0.434	4.821	-0.434		
0.700	8.036	-0.359	7.142	-0.359	7.858	-0.359		
0.750	11.563	-0.289	10.626	-0.289	11.407	-0.289		
0.800	16.094	-0.224	23.333	-0.224	16.094	-0.224		
0.850	23.333	-0.163	32.127	-0.163	24.889	-0.163		
0.900	33.192	-0.105	39.574	-0.105	34.042	-0.105		
0.950	41.778	-0.051	50.749	-0.051	43.999	-0.051		
1.000	52.248	0.000	61.458	0.000	55.000	0.000		
1.050	60.417	0.049	67.292	0.049	64.166	0.049		
1.100	68.124	0.095	74.049	0.095	69.791	0.095		
1.150	73.572	0.140	78.810	0.140	76.667	0.140		
1.200	76.667	0.183	85.946	0.183	83.513	0.183		
1.250	82.162	0.224	88.918	0.224	88.108	0.224		
1.300	84.863	0.263	91.463	0.263	90.730	0.263		
1.350	89.729	0.301	93.415	0.301	91.707	0.301		
1.400	90.486	0.338	93.659	0.338	94.878	0.338		
1.450	93.901	0.374	94.878	0.374	96.341	0.374		
1.500	94.634	0.408	96.341	0.408	96.341	0.408		
1.550	95.853	0.442	97.560	0.442	97.560	0.442		
1.600	95.853	0.474	98.048	0.474	98.293	0.474		
1.650	97.318	0.506	98.781	0.506	99.025	0.506		
1.700	97.560	0.537	98.781	0.537	98.781	0.537		
1.750	97.560	0.567	99.025	0.567	99.267	0.567		
1.800	98.293	0.596	99.756	0.596	98.781	0.596		
1.850	98.293	0.625	100.000	0.625	99.025	0.625		
1.900	98.537	0.653	99.756	0.653	99.756	0.653		
1.950	99.025	0.680	100.000	0.680	99.512	0.680		
2.000	99.267	0.707	100.000	0.707	99.756	0.707		

Table D-5 Effluent Concentration Profiles (Core E)

Rate=0.02222 cm/s			Rate=0.01528 cm/s			Rate=0.00972 cm/s		
P.V.	% C_6H_{12}	λ	% C_6H_{12}	λ	% C_6H_{12}	λ		
0.050	1.786	-4.249	0.000	-4.249	0.000	-4.249		
0.100	2.142	-2.846	0.892	-2.846	0.892	-2.846		
0.150	2.679	-2.195	1.071	-2.195	1.071	-2.195		
0.200	2.679	-1.789	1.071	-1.789	1.608	-1.789		
0.250	0.892	-1.500	1.250	-1.500	0.892	-1.500		
0.300	2.500	-1.278	1.250	-1.278	1.071	-1.278		
0.350	1.786	-1.099	1.250	-1.099	1.608	-1.099		
0.400	2.500	-0.949	1.250	-0.949	0.892	-0.949		
0.450	1.786	-0.820	0.715	-0.820	1.071	-0.820		
0.500	1.786	-0.707	1.786	-0.707	0.892	-0.707		
0.550	2.679	-0.607	1.071	-0.607	2.500	-0.607		
0.600	6.429	-0.516	0.892	-0.516	1.786	-0.516		
0.650	10.313	-0.434	1.429	-0.434	1.965	-0.434		
0.700	9.821	-0.359	2.679	-0.359	1.608	-0.359		
0.750	8.571	-0.289	3.571	-0.289	0.715	-0.289		
0.800	8.036	-0.224	3.571	-0.224	0.892	-0.224		
0.850	8.036	-0.163	2.679	-0.163	0.715	-0.163		
0.900	8.215	-0.105	2.858	-0.105	1.071	-0.105		
0.950	27.777	-0.051	8.036	-0.051	5.358	-0.051		
1.000	69.167	0.000	40.888	0.000	33.829	0.000		
1.050	78.095	0.049	74.049	0.049	69.583	0.049		
1.100	89.459	0.095	89.459	0.095	87.567	0.095		
1.150	94.634	0.140	93.901	0.140	95.122	0.140		
1.200	96.341	0.183	94.878	0.183	95.122	0.183		
1.250	97.318	0.224	96.341	0.224	98.537	0.224		
1.300	97.804	0.263	98.781	0.263	98.781	0.263		
1.350	97.804	0.301	98.781	0.301	99.756	0.301		
1.400	98.781	0.338	99.267	0.338	99.756	0.338		
1.450	99.025	0.374	99.267	0.374	100.000	0.374		
1.500	99.756	0.408	99.756	0.408	99.756	0.408		
1.550	99.512	0.442	100.000	0.442	100.000	0.442		
1.600	99.756	0.474	100.000	0.474	100.000	0.474		
1.650	100.000	0.506	99.756	0.506	100.000	0.506		
1.700	100.000	0.537	100.000	0.537	100.000	0.537		
1.750	100.000	0.567	100.000	0.567	100.000	0.567		
1.800	100.000	0.596	100.000	0.596	100.000	0.596		
1.850	100.000	0.625	99.512	0.625	100.000	0.625		
1.900	99.756	0.653	100.000	0.653	100.000	0.653		
1.950	100.000	0.680	100.000	0.680	100.000	0.680		
2.000	99.756	0.707	99.756	0.707	99.756	0.707		

Table D-6 Effluent Concentration Profiles (Core F)

P.V.	Rate=0.02222 cm/s		Rate=0.01528 cm/s		Rate=0.00972 cm/s	
	% C_6H_{12}	λ	% C_6H_{12}	λ	% C_6H_{12}	λ
0.050	0.000	-4.249	0.715	-4.249	2.500	-4.249
0.100	0.358	-2.846	1.071	-2.846	1.786	-2.846
0.150	0.000	-2.195	1.608	-2.195	2.321	-2.195
0.200	0.892	-1.789	1.608	-1.789	1.429	-1.789
0.250	0.892	-1.500	1.250	-1.500	1.786	-1.500
0.300	0.892	-1.278	0.892	-1.278	1.071	-1.278
0.350	0.892	-1.099	1.429	-1.099	1.071	-1.099
0.400	1.071	-0.949	0.358	-0.949	1.071	-0.949
0.450	0.715	-0.820	1.071	-0.820	1.250	-0.820
0.500	1.429	-0.707	0.179	-0.707	1.429	-0.707
0.550	1.608	-0.607	0.892	-0.607	1.250	-0.607
0.600	3.392	-0.516	1.429	-0.516	1.608	-0.516
0.650	5.715	-0.434	0.892	-0.434	1.786	-0.434
0.700	9.642	-0.359	1.429	-0.359	1.786	-0.359
0.750	15.625	-0.289	1.965	-0.289	2.500	-0.289
0.800	35.319	-0.224	1.786	-0.224	2.679	-0.224
0.850	65.208	-0.163	7.142	-0.163	5.358	-0.163
0.900	83.513	-0.105	22.223	-0.105	15.782	-0.105
0.950	90.486	-0.051	55.749	-0.051	42.888	-0.051
1.000	96.097	0.000	76.667	0.000	68.959	0.000
1.050	95.853	0.049	86.755	0.049	82.972	0.049
1.100	96.097	0.095	91.463	0.095	91.463	0.095
1.150	96.341	0.140	93.901	0.140	94.145	0.140
1.200	97.560	0.183	95.608	0.183	96.097	0.183
1.250	98.293	0.224	97.560	0.224	96.585	0.224
1.300	97.318	0.263	97.560	0.263	97.560	0.263
1.350	98.781	0.301	98.781	0.301	98.781	0.301
1.400	98.781	0.338	98.781	0.338	99.025	0.338
1.450	99.267	0.374	98.781	0.374	98.781	0.374
1.500	98.781	0.408	99.267	0.408	99.025	0.408
1.550	100.000	0.442	99.512	0.442	99.025	0.442
1.600	99.756	0.474	98.537	0.474	99.267	0.474
1.650	100.000	0.506	98.293	0.506	99.756	0.506
1.700	98.781	0.537	98.781	0.537	99.512	0.537
1.750	99.512	0.567	98.537	0.567	100.000	0.567
1.800	99.025	0.596	98.048	0.596	99.756	0.596
1.850	100.000	0.625	99.025	0.625	100.000	0.625
1.900	98.781	0.653	98.293	0.653	99.756	0.653
1.950	99.512	0.680	99.025	0.680	100.000	0.680
2.000	99.756	0.707	99.267	0.707	100.000	0.707

Table D-7 Effluent Concentration Profiles (Core G)

P.V.	Rate=0.02222 cm/s			Rate=0.01528 cm/s			Rate=0.00972 cm/s		
	% C_6H_{12}	λ		% C_6H_{12}	λ		% C_6H_{12}	λ	
0.050	0.715	-4.249		0.358	-4.249		0.358	-4.249	
0.100	0.358	-2.846		0.358	-2.846		0.536	-2.846	
0.150	1.071	-2.195		0.536	-2.195		0.715	-2.195	
0.200	1.250	-1.789		0.715	-1.789		1.071	-1.789	
0.250	0.358	-1.500		1.071	-1.500		0.536	-1.500	
0.300	0.536	-1.278		0.715	-1.278		0.358	-1.278	
0.350	0.179	-1.099		0.536	-1.099		1.071	-1.099	
0.400	2.500	-0.949		0.715	-0.949		1.608	-0.949	
0.450	3.036	-0.820		1.786	-0.820		1.786	-0.820	
0.500	3.215	-0.707		2.321	-0.707		2.500	-0.707	
0.550	4.108	-0.607		2.858	-0.607		2.679	-0.607	
0.600	5.179	-0.516		3.392	-0.516		3.215	-0.516	
0.650	17.969	-0.434		4.108	-0.434		3.750	-0.434	
0.700	26.444	-0.359		11.407	-0.359		7.142	-0.359	
0.750	37.447	-0.289		17.969	-0.289		18.437	-0.289	
0.800	41.555	-0.224		29.332	-0.224		39.787	-0.224	
0.850	49.777	-0.163		32.979	-0.163		27.112	-0.163	
0.900	53.999	-0.105		38.297	-0.105		37.660	-0.105	
0.950	64.166	-0.051		45.999	-0.051		41.333	-0.051	
1.000	65.416	0.000		52.749	0.000		50.749	0.000	
1.050	69.167	0.049		58.500	0.049		53.250	0.049	
1.100	71.905	0.095		61.876	0.095		62.499	0.095	
1.150	75.238	0.140		67.292	0.140		64.792	0.140	
1.200	78.810	0.183		69.374	0.183		70.238	0.183	
1.250	81.892	0.224		74.523	0.224		73.333	0.224	
1.300	83.513	0.263		77.382	0.263		77.856	0.263	
1.350	84.595	0.301		80.541	0.301		79.523	0.301	
1.400	86.755	0.338		82.162	0.338		81.080	0.338	
1.450	88.918	0.374		83.783	0.374		83.242	0.374	
1.500	90.975	0.408		86.216	0.408		85.134	0.408	
1.550	91.463	0.442		88.108	0.442		87.026	0.442	
1.600	91.707	0.474		89.459	0.474		88.918	0.474	
1.650	91.952	0.506		90.244	0.506		90.244	0.506	
1.700	91.952	0.537		90.975	0.537		89.729	0.537	
1.750	92.438	0.567		90.730	0.567		90.000	0.567	
1.800	92.682	0.596		90.975	0.596		90.244	0.596	
1.850	92.926	0.625		91.463	0.625		90.486	0.625	
1.900	93.171	0.653		91.952	0.653		90.486	0.653	
1.950	93.415	0.680		92.194	0.680		90.730	0.680	
2.000	93.415	0.707		92.438	0.707		90.975	0.707	

Table D-8 Effluent Concentration Profiles (Core H)

Rate=0.02222 cm/s			Rate=0.01528 cm/s			Rate=0.00972 cm/s		
P.V.	% C_6H_{12}	λ	% C_6H_{12}	λ	% C_6H_{12}	λ		
0.050	0.000	-4.249	0.892	-4.249	0.892	-4.249		
0.100	0.892	-2.846	0.715	-2.846	1.429	-2.846		
0.150	1.071	-2.195	1.071	-2.195	1.250	-2.195		
0.200	0.892	-1.789	0.892	-1.789	0.892	-1.789		
0.250	1.786	-1.500	0.715	-1.500	0.892	-1.500		
0.300	0.892	-1.278	1.071	-1.278	0.892	-1.278		
0.350	1.071	-1.099	0.892	-1.099	0.892	-1.099		
0.400	1.608	-0.949	0.358	-0.949	0.715	-0.949		
0.450	1.608	-0.820	0.358	-0.820	0.715	-0.820		
0.500	0.358	-0.707	0.715	-0.707	0.892	-0.707		
0.550	0.892	-0.607	0.536	-0.607	0.892	-0.607		
0.600	1.429	-0.516	1.071	-0.516	0.715	-0.516		
0.650	2.142	-0.434	5.358	-0.434	0.000	-0.434		
0.700	1.786	-0.359	7.500	-0.359	0.715	-0.359		
0.750	1.965	-0.289	8.036	-0.289	0.892	-0.289		
0.800	16.875	-0.224	6.965	-0.224	0.892	-0.224		
0.850	52.248	-0.163	10.781	-0.163	1.429	-0.163		
0.900	78.333	-0.105	30.213	-0.105	10.000	-0.105		
0.950	89.459	-0.051	61.667	-0.051	43.999	-0.051		
1.000	92.682	0.000	80.812	0.000	75.951	0.000		
1.050	94.878	0.049	87.833	0.049	88.918	0.049		
1.100	96.585	0.095	91.707	0.095	92.438	0.095		
1.150	97.804	0.140	93.901	0.140	95.122	0.140		
1.200	97.318	0.183	95.366	0.183	96.829	0.183		
1.250	97.560	0.224	95.366	0.224	97.560	0.224		
1.300	97.560	0.263	96.585	0.263	97.560	0.263		
1.350	97.804	0.301	97.560	0.301	98.293	0.301		
1.400	98.537	0.338	98.048	0.338	98.048	0.338		
1.450	98.781	0.374	98.781	0.374	98.781	0.374		
1.500	99.267	0.408	99.025	0.408	99.025	0.408		
1.550	98.537	0.442	99.025	0.442	99.025	0.442		
1.600	98.781	0.474	99.267	0.474	99.267	0.474		
1.650	99.512	0.506	99.756	0.506	99.025	0.506		
1.700	99.267	0.537	99.512	0.537	99.512	0.537		
1.750	100.000	0.567	99.756	0.567	100.000	0.567		
1.800	99.756	0.596	100.000	0.596	100.000	0.596		
1.850	100.000	0.625	100.000	0.625	99.756	0.625		
1.900	100.000	0.653	99.756	0.653	100.000	0.653		
1.950	99.756	0.680	100.000	0.680	100.000	0.680		
2.000	100.000	0.707	100.000	0.707	99.756	0.707		

Table D-9 Effluent Concentration Profiles (Core I)

Rate=0.02222 cm/s			Rate=0.01528 cm/s			Rate=0.00972 cm/s		
P.V.	% C_6H_{12}	λ	% C_6H_{12}	λ	% C_6H_{12}	λ		
0.050	0.358	-4.249	0.358	-4.249	0.358	-4.249		
0.100	0.715	-2.846	0.358	-2.846	0.358	-2.846		
0.150	0.715	-2.195	0.892	-2.195	0.536	-2.195		
0.200	0.892	-1.789	0.892	-1.789	1.608	-1.789		
0.250	1.608	-1.500	1.608	-1.500	1.786	-1.500		
0.300	2.858	-1.278	1.786	-1.278	2.142	-1.278		
0.350	3.036	-1.099	1.608	-1.099	2.679	-1.099		
0.400	3.036	-0.949	2.679	-0.949	3.215	-0.949		
0.450	3.215	-0.820	3.571	-0.820	4.286	-0.820		
0.500	5.000	-0.707	5.358	-0.707	5.358	-0.707		
0.550	6.250	-0.607	7.858	-0.607	9.465	-0.607		
0.600	7.321	-0.516	10.626	-0.516	13.907	-0.516		
0.650	15.001	-0.434	15.782	-0.434	16.562	-0.434		
0.700	19.844	-0.359	20.223	-0.359	19.844	-0.359		
0.750	23.778	-0.289	23.111	-0.289	21.555	-0.289		
0.800	34.681	-0.224	27.332	-0.224	24.001	-0.224		
0.850	36.382	-0.163	34.042	-0.163	31.703	-0.163		
0.900	56.750	-0.105	46.222	-0.105	40.223	-0.105		
0.950	61.667	-0.051	54.499	-0.051	48.000	-0.051		
1.000	66.875	0.000	62.708	0.000	56.500	0.000		
1.050	73.572	0.049	66.875	0.049	61.041	0.049		
1.100	77.143	0.095	71.190	0.095	65.625	0.095		
1.150	79.523	0.140	75.000	0.140	71.190	0.140		
1.200	82.162	0.183	79.523	0.183	77.143	0.183		
1.250	83.242	0.224	81.351	0.224	79.523	0.224		
1.300	85.405	0.263	83.513	0.263	82.162	0.263		
1.350	86.216	0.301	84.863	0.301	83.242	0.301		
1.400	87.026	0.338	85.675	0.338	84.325	0.338		
1.450	88.379	0.374	87.567	0.374	86.755	0.374		
1.500	90.000	0.408	89.459	0.408	88.918	0.408		
1.550	90.244	0.442	90.000	0.442	90.000	0.442		
1.600	90.486	0.474	90.730	0.474	90.975	0.474		
1.650	90.730	0.506	91.219	0.506	91.463	0.506		
1.700	90.975	0.537	91.463	0.537	92.194	0.537		
1.750	92.438	0.567	92.194	0.567	92.438	0.567		
1.800	93.659	0.596	92.926	0.596	93.171	0.596		
1.850	94.389	0.625	93.659	0.625	93.659	0.625		
1.900	94.878	0.653	94.389	0.653	93.901	0.653		
1.950	95.366	0.680	94.878	0.680	94.389	0.680		
2.000	95.853	0.707	95.366	0.707	94.878	0.707		

Table D-10 Effluent Concentration Profiles (Core J)

Rate=0.02222 cm/s			Rate=0.01528 cm/s			Rate=0.00972 cm/s		
P.V.	% C_6H_{12}	λ	% C_6H_{12}	λ	% C_6H_{12}	λ		
0.050	0.536	-4.249	0.358	-4.249	0.179	-4.249		
0.100	0.715	-2.846	0.358	-2.846	0.358	-2.846		
0.150	1.071	-2.195	0.892	-2.195	0.536	-2.195		
0.200	0.892	-1.789	1.071	-1.789	1.429	-1.789		
0.250	1.965	-1.500	1.786	-1.500	1.608	-1.500		
0.300	3.215	-1.278	1.608	-1.278	1.429	-1.278		
0.350	3.215	-1.099	1.786	-1.099	1.786	-1.099		
0.400	5.179	-0.949	2.858	-0.949	3.215	-0.949		
0.450	6.608	-0.820	5.358	-0.820	5.358	-0.820		
0.500	6.429	-0.707	8.036	-0.707	9.286	-0.707		
0.550	7.500	-0.607	10.626	-0.607	14.531	-0.607		
0.600	15.312	-0.516	15.782	-0.516	16.406	-0.516		
0.650	19.687	-0.434	41.778	-0.434	20.000	-0.434		
0.700	23.778	-0.359	23.333	-0.359	21.778	-0.359		
0.750	34.892	-0.289	27.332	-0.289	23.778	-0.289		
0.800	36.382	-0.224	33.616	-0.224	31.489	-0.224		
0.850	56.500	-0.163	46.667	-0.163	39.787	-0.163		
0.900	61.458	-0.105	53.250	-0.105	47.777	-0.105		
0.950	67.292	-0.051	62.082	-0.051	56.249	-0.051		
1.000	74.049	0.000	66.251	0.000	61.041	0.000		
1.050	76.667	0.049	71.190	0.049	65.416	0.049		
1.100	79.049	0.095	75.951	0.095	70.477	0.095		
1.150	82.433	0.140	79.523	0.140	76.667	0.140		
1.200	83.242	0.183	81.080	0.183	79.762	0.183		
1.250	85.405	0.224	83.783	0.224	81.621	0.224		
1.300	86.216	0.263	84.595	0.263	83.242	0.263		
1.350	86.755	0.301	85.946	0.301	84.863	0.301		
1.400	88.379	0.338	87.296	0.338	86.755	0.338		
1.450	89.729	0.374	89.188	0.374	88.918	0.374		
1.500	90.000	0.408	90.000	0.408	90.244	0.408		
1.550	90.486	0.442	90.730	0.442	91.463	0.442		
1.600	90.730	0.474	90.975	0.474	91.952	0.474		
1.650	90.730	0.506	91.952	0.506	92.194	0.506		
1.700	91.463	0.537	92.194	0.537	92.682	0.537		
1.750	93.415	0.567	93.171	0.567	93.415	0.567		
1.800	94.145	0.596	93.901	0.596	93.901	0.596		
1.850	95.122	0.625	94.389	0.625	94.389	0.625		
1.900	95.608	0.653	94.145	0.653	94.389	0.653		
1.950	96.097	0.680	95.122	0.680	94.145	0.680		
2.000	96.585	0.707	96.341	0.707	94.878	0.707		

Appendix E

1. Program EFFPLOT

Sample Data File:

The following is a complete data file used for program EFFPLOT.

1.3770,1.3826,1.3890,1.3935,1.3982,1.4027,	<div style="border-left: 1px solid black; border-right: 1px solid black; height: 20px; margin: 0 auto; width: 20px;"></div>	CALIBRATION
1.4067,1.4115,1.4157,1.4194,1.4235,		CURVE DATA
0.00,0.05,0.10,0.15,0.20,0.25,0.30,0.35,	<div style="border-left: 1px solid black; border-right: 1px solid black; height: 20px; margin: 0 auto; width: 20px;"></div>	PORE VOLUME
0.40,0.45,0.50,0.55,0.60,0.65,0.70,0.75,		INCREMENTS
0.80,0.85,0.90,0.95,1.00,1.05,1.10,1.15,	<div style="border-left: 1px solid black; border-right: 1px solid black; height: 20px; margin: 0 auto; width: 20px;"></div>	R.I. VALUES
1.20,1.25,1.30,1.35,1.40,1.45,1.50,1.55,		FOR EACH INCREMENT
1.60,1.65,1.70,1.75,1.80,1.85,1.90,1.95,	<div style="border-left: 1px solid black; border-right: 1px solid black; height: 20px; margin: 0 auto; width: 20px;"></div>	<div style="border-left: 1px solid black; border-right: 1px solid black; height: 20px; margin: 0 auto; width: 20px;"></div>
2.00,		
1.3771,1.3780,1.3781,1.3780,1.3781,1.3780,1.3780,1.3780,	<div style="border-left: 1px solid black; border-right: 1px solid black; height: 20px; margin: 0 auto; width: 20px;"></div>	<div style="border-left: 1px solid black; border-right: 1px solid black; height: 20px; margin: 0 auto; width: 20px;"></div>
1.3780,1.3776,1.3780,1.3785,1.3792,1.3810,1.3836,1.3872,		
1.3905,1.3960,1.4000,1.4041,1.4078,1.4115,1.4137,1.4160,	<div style="border-left: 1px solid black; border-right: 1px solid black; height: 20px; margin: 0 auto; width: 20px;"></div>	<div style="border-left: 1px solid black; border-right: 1px solid black; height: 20px; margin: 0 auto; width: 20px;"></div>
1.4171,1.4185,1.4200,1.4206,1.4210,1.4216,1.4219,1.4222,		
1.4225,1.4225,1.4227,1.4227,1.4227,1.4228,1.4231,1.4231,	<div style="border-left: 1px solid black; border-right: 1px solid black; height: 20px; margin: 0 auto; width: 20px;"></div>	<div style="border-left: 1px solid black; border-right: 1px solid black; height: 20px; margin: 0 auto; width: 20px;"></div>
1.4231		
CORE A - RUN #1 RATE=263.57 CM3/HR		


```

*****
*      PROGRAM EFFPLOT      *
*      *
* THIS PROGRAM APPLIES THE EXPERIMENTAL *
* CALIBRATION CURVE TO THE RAW EFFLUENT *
* CONCENTRATION DATA IN ORDER TO OBTAIN *
* A PROFILE OF CYCLOHEXANE CONCENTRATION *
* VS PORE VOLUMES OF CYCLOHEXANE INJECTED *
* THIS PROFILE IS THEN USED TO          *
* CALCULATE VALUES FOR HEXANE RECOVERY *
* AFTER INJECTION OF 1.0, 1.5 AND 2.0 PV *
* OF CYCLOHEXANE.              *
*****

      REAL A(41),B(11),C(41),D(41),PV(41),U(41),NUMB
      REAL AAREA1,AAREA2,AAREA3
      INTEGER I,J,K

      READ(5,*) (B(J),J=1,11)
      READ(5,*) (PV(I),I=1,41)
      READ(5,*) (A(I),I=1,41)

      DO 10 I=1,41
        IF (PV(I).GT.0.0) THEN
          U(I)=((PV(I)-1.0)/SQRT(PV(I)))
        ENDIF
        DO 20 J=1,10
          IF (A(I).LE.B(J)) THEN
            C(I)=0.0
            D(I)=C(I)/100.0
            GO TO 10
          ELSEIF (A(I).GT.B(J).AND.A(I).LE.B(J+1)) THEN
            NUMB=A(I)-B(J)
            RATIO=NUMB/(B(J+1)-B(J))
            C(I)=RATIO*10.0+(10.0*(J-1))
            D(I)=C(I)/100.0
            GO TO 10
          ELSEIF (A(I).GT.B(11)) THEN
            C(I)=100.0
            D(I)=C(I)/100.0
            GO TO 10
          ELSE
            GO TO 20
          ENDIF
        ENDIF
      CONTINUE
20    CONTINUE
10    CONTINUE

```

```

      WRITE(6,4)
4      FORMAT('1','EFFLUENT CONCENTRATION PROFILE')
      WRITE(6,5)
5      FORMAT('CORE J - RATE=116.20 CM3/HR (RUN #3)')
      WRITE(6,6)
6      FORMAT('PV',8X,'PERCENT C6H12',8X,'LAMBDA')

      DO 30 K=1,41
        PRINT 25, PV(K),C(K),U(K)
30     CONTINUE
25     FORMAT(' ',F6.3,6X,F8.3,7X,F6.3)

```

```

*****
* CALCULATE AREAS UNDER      *
* EFFLUENT CONCENTRATION     *
* PROFILES USING SIMPSON'S    *
* 1/3 RULE                    *
*****

```

```

*****
* AREA TO 1.0 PV *
*****

```

```

AAREA1=C(1)+4.0*C(2)+2.0*C(3)+4.0*C(4)+2.0*C(5)+4.0*C(6)
+
+2.0*C(7)+4.0*C(8)+2.0*C(9)+4.0*C(10)+2.0*C(11)+4.0*C(12)
+
+2.0*C(13)+4.0*C(14)+2.0*C(15)+4.0*C(16)+2.0*C(17)
+      +4.0*C(18)+2.0*C(19)+4.0*C(20)

```

```

AFREA1=AAREA1+C(21)

```

```

*****
* AREA TO 1.5 PV *
*****

```

```

AAREA2=AAREA1+2.0*C(21)+4.0*C(22)+2.0*C(23)+4.0*C(24)
+      +2.0*C(25)+4.0*C(26)+2.0*C(27)+4.0*C(28)
+      +2.0*C(29)+4.0*C(30)

```

```

AFREA2=AAREA2+C(31)

```

```

*****
* AREA TO 2.0 PV *
*****

```

```

AAREA3=AAREA2+2.0*C(31)+4.0*C(32)+2.0*C(33)+4.0*C(34)
+      +2.0*C(35)+4.0*C(36)+2.0*C(37)+4.0*C(38)
+      +2.0*C(39)+4.0*C(40)

```

```

AFREA3=AAREA3+C(41)

```

```

*****
* CALCULATE % HEXANE RECOVERY *
*****

```

```

HEX1=100.0-(0.05/3.0*AFREA1)
HEX2=150.0-(0.05/3.0*AFREA2)
HEX3=200.0-(0.05/3.0*AFREA3)

```

```

IF (HEX2 .GT. 100.000) HEX2=100.00
IF (HEX3 .GT. 100.000) HEX3=100.00

```

```

WRITE(6,7) HEX1
7  FORMAT(/'HEXANE RECOVERY @ 1.0 PV = ',F8.3,'%')
   WRITE(6,8) HEX2
8  FORMAT('HEXANE RECOVERY @ 1.5 PV = ',F8.3,'%')
   WRITE(6,9) HEX3
9  FORMAT('HEXANE RECOVERY @ 2.0 PV = ',F8.3,'%')
   STOP
   END

```

2. Program ANALYZE

Sample Data File:

The following is a sample of the data input format required for program ANALYZE. The data shown is for the first 3 samples only. Additional data may be added up to a maximum of 50 samples per computer run. Processing of greater than 50 samples per computer run will require modification of the source code. The data which starts with 1.000 in each line corresponds to HG injection readings at the following pressures: 20, 30, 40, 50, 60, 80, 100, 125, 150, 175, 200, 300, 400, 500, 600, 700, 800, 900 and 1000 psi.

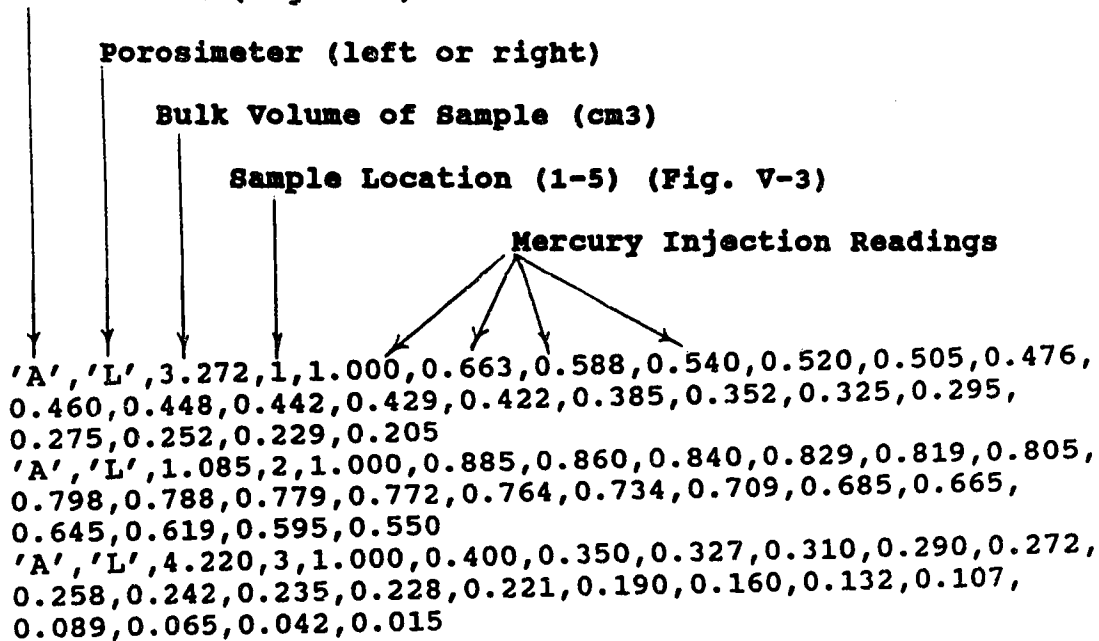
Core Level (Fig. V-3)

Porosimeter (left or right)

Bulk Volume of Sample (cm3)

Sample Location (1-5) (Fig. V-3)

Mercury Injection Readings



```
'A','L',3.272,1,1.000,0.663,0.588,0.540,0.520,0.505,0.476,
0.460,0.448,0.442,0.429,0.422,0.385,0.352,0.325,0.295,
0.275,0.252,0.229,0.205
'A','L',1.085,2,1.000,0.885,0.860,0.840,0.829,0.819,0.805,
0.798,0.788,0.779,0.772,0.764,0.734,0.709,0.685,0.665,
0.645,0.619,0.595,0.550
'A','L',4.220,3,1.000,0.400,0.350,0.327,0.310,0.290,0.272,
0.258,0.242,0.235,0.228,0.221,0.190,0.160,0.132,0.107,
0.089,0.065,0.042,0.015
```

PROGRAM ANALYZ

```

*****
*   ANALYZE
*
*   THIS PROGRAM PERFORMS DATA ANALYSIS UPON
*   CAPILLARY PRESSURE DATA OBTAINED ON A CORE
*   BY CORE BASIS. THE MAIN PORTION OF THE PROGRAM
*   READS IN THE MERCURY INJECTION DATA AND
*   SUBTRACTS THE APPROPRIATE CALIBRATION CURVE.
*   THE CORRECTED DATA IS THEN PASSED ON TO OTHER
*   SUBROUTINES WHERE FURTHER DATA PROCESSING
*   OCCURS.
*
*   SUBROUTINES:
*
*   AREA  - CALCULATES THE AREA UNDER THE
*           CAPILLARY PRESSURE CURVE. ALSO
*           CALCULATES POROSITY, PERMEABILITY AND
*           THE MEAN PORE THROAT DIAMETER FOR EACH
*           SAMPLE.
*
*   VARIO - CALCULATES EXPERIMENTAL SEMI-VARIOGRAM
*           FOR THE CORE BASED UPON THE LOGARITHM
*           LOGARITHM OF THE DATA VALUES
*           CALCULATED BY SUBROUTINE AREA. ALSO
*           CALCULATES THE AUTOCORRELATION FUNCTION
*           AND FRACTAL DIMENSION.
*****

```

```

REAL
CALA(50), CALB(50), CAL3(50), CAL4(50), BV(50), CU(50), CV(50)
REAL
MI(50,20), MIC(50,20), PRES(50), POR(50), PERM(50), D50(50)
REAL
PORS(50), PERMS(50), D50S(50), VRR(50), MVRR(50), XVAR(50)
REAL CMU, CMV
CHARACTER
LEVEL(50)*1, LEVELS(50)*1, PTYPE(50)*1, ALPHA(50)*1
INTEGER I, J, LOC(50), LOCS(50), COUNT, IX, VARBLE

```

```

*****
* DATA FOR THE CALIBRATION CURVES
* AND CORRESPONDING PRESSURES ARE
* READ INTO 1-D ARRAYS USING DATA
* STATEMENTS.
*****

```

```

DATA CALA
/1.000,0.965,0.964,0.963,0.962,0.960,0.959,0.954,
+ 0.949,0.945,0.942,0.939,0.925,0.910,0.895,0.881,
+ 0.866,0.852,0.836,31*0.821/

```

```

DATA CALB
/1.000,0.910,0.904,0.900,0.896,0.893,0.886,0.882,
+ 0.876,0.871,0.865,0.861,0.839,0.811,0.788,0.760,
+ 0.732,0.704,0.678,31*0.654/

```

```

DATA PRES
/0.0,20.0,30.0,40.0,50.0,60.0,80.0,100.0,125.0,
+ 150.0,175.0,200.0,300.0,400.0,500.0,600.0,700.0,
+ 800.0,900.0,31*1000.0/

```

```

DATA
ALPHA/'A','B','C','D','E','F','G','H','I',41*'J'/

```

```

DO 10 I=1,50
  READ(5,*)
LEVEL(I),PTYPE(I),BV(I),LOC(I),(MI(I,J),J=1,20)
10 CONTINUE

```

```

CAL3(1)=0.000
CAL4(1)=0.000

```

```

DO 20 J=1,19

```

```

  CAL3(J+1)=CALA(J)-CALA(J+1)
  CAL4(J+1)=CALB(J)-CALB(J+1)
20 CONTINUE

```

```

DO 30 I=1,50
  MIC(I,1)=0.000
  DO 40 J=1,19
    MIC(I,J+1)=MI(I,J)-MI(I,J+1)
  40 CONTINUE
30 CONTINUE

```

```

DO 50 I=1,50
  IF (PTYPE(I).EQ.'L') THEN
DO 60 J=1,20
  MI(I,J)=MIC(I,J)-CAL3(J)
60 CONTINUE
  ELSE
DO 70 J=1,20
  MI(I,J)=MIC(I,J)-CAL4(J)
70 CONTINUE

```

```

70  CONTINUE
    ENDIF
50  CONTINUE

```

```

    DO 80 I=1,50
      DO 90 J=1,20
        MIC(I,J)=MI(I,J)
        IF(MIC(I,J).LE.0.000) THEN
          MIC(I,J)=0.000
        ENDIF
      90  CONTINUE
    80  CONTINUE

```

```

*****
* CALL SUBROUTINE AREA FOR THE          *
* CALCULATION OF POROSITY, PERMEABILITY *
* AND MEAN PORE THROAT SIZE FOR EACH   *
* SAMPLE.                               *
*****

```

```

      CALL AREA(BV,PRES,MIC,POR,PERM,D50)

```

```

*****
* SORT ARRAYS BY LOCATION              *
*****

```

```

      COUNT=0
      DO 250 I=1,5
        DO 260 J=1,50
          IF(LOC(J).EQ.I) THEN
            COUNT=COUNT+1
            LOCS(COUNT)=LOC(J)
            LEVELS(COUNT)=LEVEL(J)
            PORS(COUNT)=POR(J)
            PERMS(COUNT)=PERM(J)
            D50S(COUNT)=D50(J)
          ENDIF
        260  CONTINUE
      250  CONTINUE

```

```

*****
* SORT ARRAYS BY LEVEL                *
*****

```

```

      DO 270 I=1,10
        COUNT=I
        DO 280 J=1,50
          IF(LEVELS(J).EQ.ALPHA(I)) THEN
            LEVEL(COUNT)=LEVELS(J)

```

```

        LOC(COUNT)=LOCS(J)
        POR(COUNT)=PORS(J)
        PERM(COUNT)=PERMS(J)
        D50(COUNT)=D50S(J)
        COUNT=COUNT+10
    ENDIF
280  CONTINUE
270  CONTINUE

*****
* PRINT OUT RESULTS FROM          *
* SUBROUTINE AREA.                *
*****

    WRITE(6,200)
    200  FORMAT(T20,'DATA SUMMARY-CORE
J'//,T10,'LEVEL',T17,'LOCATION',
+      T27,'POROSITY',T37,'PERMEABILITY',T51,'MEAN PORE
THROAT'/,
+      T42,'md',T57,'nM'/,60('-'))
    DO 210 I=1,50
        WRITE(6,220) LEVEL(I),LOC(I),POR(I),PERM(I),D50(I)
    220  FORMAT(T12,A2,T20,I2,T30,F6.3,T42,F11.3,T55,F8.3)
    210  CONTINUE

*****
* CALL SUBROUTINE VARIO THREE TIMES USING      *
* THE DATA CALCULATED IN SUBROUTINE AREA.      *
*****

    VARBLE=1
    CALL VARIO(PERM,VARBLE)

    VARBLE=2
    CALL VARIO(POR,VARBLE)

    VARBLE=3
    CALL VARIO(D50,VARBLE)

    STOP
    END

*-----
SUBROUTINE AREA(BVOL,PRESS,MICOR,P,PM,DIA)

```



```

      REAL
      BVOL(50),PRESS(50),PC(50),MICOR(50,20),HG(50,20),Y(50)
      REAL
      P(50),PM(50),DIA(50),TOTAL,PC50(50),NUMB,RATIO,RES
      REAL
      BPAR(4),INT,S1,S2,S3,S4,IFT,ANGLE,LFAC,C(19,3),X(50)
      INTEGER I,J,IC,NX,IER

```

```

      TOTAL=0.000

```

```

*****
* CONVERT PRESSURE VECTOR TO      *
* UNITS OF ATM E-2 AND CALCULATE *
* HG SATURATION VS PRESSURE      *
*****

```

```

      DO 100 J=1,20
        PC(J)=(1.0/((PRESS(J)/14.7)+1.0422))**2
100    CONTINUE

```

```

      DO 110 I=1,50
        DO 120 J=1,20
          TOTAL=MICOR(I,J)+TOTAL
          HG(I,J)=TOTAL
120    CONTINUE
          P(I)=TOTAL/BVOL(I)
          TOTAL=0.000
110    CONTINUE

```

```

      DO 130 I=1,50
        DO 140 J=1,20
          MICOR(I,J)=HG(I,J)/(P(I)*BVOL(I))
140    CONTINUE
130    CONTINUE

```

```

*****
* FIND CAPILLARY PRESSURE      *
* CORRESPONDING TO 50% HG      *
* SATURATION WITHIN THE SAMPLE. *
* USE THIS VALUE TO CALCULATE  *
* THE MEAN PORE THROAT DIAMETER. *
*****

```

```

      DO 150 I=1,50
        DO 160 J=1,19
          IF(0.50.GT.MICOR(I,J).AND.0.50.LE.MICOR(I,J+1))
THEN
          NUMB=0.50-MICOR(I,J)
          RATIO=NUMB/(MICOR(I,J+1)-MICOR(I,J))

```

```
PC50(I)=(PRESS(J)+RATIO*(PRESS(J+1)-PRESS(J)))+15.3204
```

```
GO TO 150
```

```
ENDIF
```

```
160 CONTINUE
```

```
150 CONTINUE
```

```
*****
* CALCULATION OF MEAN PORE THROAT      *
* SIZE USING PRESSURE VALUES FROM     *
* ARRAY PC50.                          *
*****
```

```
*****
* THE MEAN PORE DIAMETER IN nm IS CALCULATED. *
* THE CONTACT ANGLE IS CONVERTED TO RADIANS  *
* AND THE MEAN PRESSURE TO MPA.              *
*****
```

```
DO 200 I=1,50
```

```
DIA(I)=-4.0*480.0*COS(140.0*0.01745329)/(PC50(I)*0.0067708)
```

```
200 CONTINUE
```

```
IC=19
```

```
NX=20
```

```
*****
* INITIALIZE END CONDITIONS *
* PARAMETERS FOR NATURAL   *
* SPLINE FUNCTION.         *
*****
```

```
BPAR(1)=0.0
```

```
BPAR(2)=0.0
```

```
BPAR(3)=0.0
```

```
BPAR(4)=0.0
```

```
*****
* CALL IMSL SUBROUTINE      *
* ICSICU WHICH CALCULATES   *
* THE SPLINE COEFFICIENTS   *
*****
```

```
DO 170 I=1,50
```

```
X(1)=MICOR(I,1)
```

```
Y(1)=PC(1)
```

```
DO 180 J=1,19
```

```
IF(MICOR(I,J).GE.MICOR(I,J+1)) THEN
```

```
RES=(MICOR(I,J)-MICOR(I,J+1))+0.001
```

```

        MICOR(I,J+1)=MICOR(I,J+1)+RES
        X(J+1)=MICOR(I,J+1)
    ELSE
        X(J+1)=MICOR(I,J+1)
    ENDIF
        Y(J+1)=PC(J+1)
180  CONTINUE

```

```

    CALL ICSICU(X,Y,NX,BPAR,C,IC,IER)

```

```

*****
* USING THE CALCULATED SPLINE *
* COEFFICIENTS THE AREA UNDER *
* THE CAPILLARY PRESSURE      *
* CURVE MAY BE FOUND BY      *
* NUMERICAL INTEGRATION.      *
*****

```

```

    INT=0.0
    DO 190 J=1,19
        S1=(X(J+1)-X(J))
        S2=S1**2
        S3=S1**3
        S4=S1**4

```

```

INT=INT+C(J,3)/4.0*S4+C(J,2)/3.0*S3+C(J,1)/2.0*S2+Y(J)*S1
190 CONTINUE

```

```

*****
* CALCULATE PERMEABILITY FROM *
* PURCELL'S EQUATION. FOR OUR *
* CASE:                        *
*                               *
* INTERFACIAL TENSION=480 DYNES/CM *
* CONTACT ANGLE=140 DEGREES *
* LITHOLOGY FACTOR=0.216 *
*                               *
* WHEN K IS LOW, THE SPLINE *
* FUNCTION MAY OCCASIONALLY RESULT *
* IN A NEGATIVE AREA CALCULATION. *
* SINCE THIS IS PHYSICALLY *
* IMPOSSIBLE, ANY OCCURENCES *
* RESULTING IN A NEGATIVE K VALUE *
* ARE ARBITRARILY SET TO 0.10 MD. *
*****

```

```

    ANGLE=140.0
    IFT=480.0
    LFAC=0.216

    RAD=ANGLE*0.01745329

    PM(I)=10.24*((IFT*COS(RAD))**2)*LFAC*P(I)*(INT/14.7**2)
    IF(PM(I).LE.0.000) THEN
        PM(I)=0.10
    ENDIF
170 CONTINUE
    RETURN
    END

```

```

*-----
      SUBROUTINE VARIO(VAR,VARBLE)

```

```

*****
* THIS SUBROUTINE CALCULATES THE VARIOGRAM      *
* FOR THE DATA IN QUESTION BASED UPON THE      *
* LOGARITHM OF THE DATA VALUES CALCULATED    *
* IN SUBROUTINE AREA. THE AUTOCORRELATION      *
* FUNCTION IS THEN CALCULATED AND CONVERTED    *
* TO A FRACTAL DIMENSION.                      *
*****

```

```

      REAL VAR(50),VR(50),LAGV(50),ARRAY(50,50)
      REAL LAG,AC,ACM,ACV,FDIM
      INTEGER I,J,K,NPR,LG,NX,VARBLE

      PARAMETER (LAG=4.8,NX=10.0)

      IF (VARBLE .EQ. 1) THEN
        WRITE(6,398)
      ELSEIF (VARBLE .EQ. 2) THEN
        WRITE(6,399)
      ELSE
        WRITE(6,400)
      ENDIF
398 FORMAT('1','VARIOGRAM SUMMARY ',
+        '(PERMEABILITY)',/)
399 FORMAT('1','VARIOGRAM SUMMARY ',
+        '(POROSITY)',/)
400 FORMAT('1','VARIOGRAM SUMMARY ',
+        '(PORE THROAT DIAMETER)',/)
      WRITE(6,401)
401 FORMAT('X VALUE',6X,'Y VALUE',/)

```

```

      DO 402 I=1,50
        VAR(I)=LOG(VAR(I))
402  CONTINUE

```

```

      LG=NX-1

```

```

*****
* THE VECTOR VAR IS CONVERTED INTO A      *
* TWO DIMENSIONAL ARRAY TO FACILITATE     *
* THE CALCULATION OF THE SEMI-VARIANCES.  *
*****

```

```

      DO 403 J=1,5
        DO 404 I=1,NX
          ARRAY(I,J)=VAR((J-1)*10+I)
404  CONTINUE
403  CONTINUE

      DO 405 K=1,LG
        VR(K)=0.0
        DO 406 J=1,5
          DO 407 I=1,NX-K
            VR(K)=VR(K)+(ARRAY(I+K,J)-ARRAY(I,J))**2
407  CONTINUE
406  CONTINUE
        NPR=5*(NX-K)
        VR(K)=0.5*VR(K)/FLOAT(NPR)
        LAGV(K)=FLOAT(K)*LAG
        WRITE(6,408) LAGV(K),VR(K)
408  FORMAT(F8.2,5X,F12.3)
405  CONTINUE

```

```

*****
* CALCULATE AUTOCORRELATION FUNCTION      *
* AND ASSOCIATED FRACTAL DIMENSION.      *
*****

```

```

      ACM=0.0
      ACV=0.0
      AC=0.0

      DO 409 I=1,50
        VAR(I)=EXP(VAR(I))
        ACM=ACM+VAR(I)
409  CONTINUE
      ACM=ACM/50
      DO 410 I=1,50
        ACV=ACV+(VAR(I)-ACM)**2
410  CONTINUE

```

```

      ACV=ACV/50
      DO 411 I=1,49
        AC=AC+((VAR(I)-ACM)*(VAR(I+1)-ACM))
411 CONTINUE
      AC=.5*AC
      FDIM=(2.0*AC+2.0)/(2.0*LOG(2.0))
      WRITE(6,*)ACM,ACV
412 FORMAT('ACM VALUE = ',F9.3,/'MEAN VARIANCE = ',F14.3)
      WRITE(6,*)AC,FDIM
413 FORMAT('AUTOCORRELATION FUNCTION =',F7.3,
+        /'FRACTAL DIMENSION =',F7.3)
      RETURN
      END

```